THERMOLUMINESCENCE PROCESSES IN CaF_2 DOPED WITH Ce AND Mn.

By

BAHAEDDIN JASSEMNEJAD

Bachelor of Science
Central State University
Edmond, Oklahoma
1981

Master of Science
Central State University
Edmond, Oklahoma
1984

Submitted to the Faculty of the Graduate College
of the Oklahoma State University
in partial fulfillment of the requirements
for the degree of
DOCTOR OF PHILOSOPHY
May, 1987

THERMOLUMINESCENCE PROCESSES

IN CaF_2 DOPED WITH Ce

AND Mn.

Thesis Approved

Thesis Adviser

Dean of the Graduate College

ACKNOWLEDGEMENTS

I would like to take this opportunity to express my appreciation to all the people responsible for my graduate education at Oklahoma State University. Special thanks to Dr. S.W.S. McKeever for being an excellent advisor, committee chairman, and mostly for being a friend ("boss, whatever you said turned out to be the best for me!"). I am grateful to other members on my committee, Drs. G. Dixon, G.J. Martin and Z. Al-Shaieb. I also thank Drs. P. Westhaus and T. Wilson for their discussions. I would like to thank Mrs. J. McKeever for her kindness to type this thesis.

I would like to thank my wife, Soheila for her encouragement and moral support. Without her patience the endless hours of work would have been impossible. Finally I thank my family in Kurdistan, Iran and my mother-in-law Mrs. F. Ballazadeh for their support. I dedicate this thesis to peace and understanding.

TABLE OF CONTENTS

LIST OF TABLES

LIST OF FIGURES

CHAPTER I

INTRODUCTION

The CaF_2 lattice can be visualized as a cubic array of F^- ions with a Ca^{2+} at every alternate body center position. Owing to their similarity in ionic size rare earth (RE^{3+}) and Mn^{2+} ions can readily substitute for Ca^{2+} in this lattice. In the case of RE^{3+} ion substitution the interstitial F^- ion charge compensator, which preserves charge neutrality, is located either in nearest neighbor (nn) or in next nearest neighbor (nnn) positions. This respectively leaves these dipolar (RE^{3+}-F^-) complexes with the tetragonal (C_{4v}) and the trigonal (C_{3v}) symmetry.[1] RE^{3+} ions which are nonlocally charge compensated can also exist, these possess cubic (O_h) symmetry.[2]

The spectroscopic behavior of rare earth ions has made RE-doped CaF_2 a suitable material for applications such as infrared up-converters; photochromic, information-storage materials; optically pumped microwave masers; and acoustic spectrometers.[2] In recent years, rare-earth-doped CaF_2 has also been used successfully in thermoluminescence (TL) dosimetry where the luminescence properties of the rare-earth ions have made these materials sensitive radiation dosimeters,[3] and this thesis will concentrate on this particular application.

Traces of rare-earth impurities, particularly Ce, even in so-called "pure" CaF_2 can dominate the response of this material to ionizing radiation.[4,5] The investigation by Sunta[6] of the mineral

CaF_2 containing Ce^{3+} impurities, of Ce^{3+} ion implantation in synthetic CaF_2 by Bangert et al[5], and the charge conversion of irradiated rare-earth ions, also in synthetic CaF_2, by Merz and Pershan[7] are some examples of studies of the TL behavior of CaF_2:Ce.

The investigation of RE^{3+} ions in general as efficient sensitisers for Mn^{2+} luminescence has revealed that those RE^{3+} ions which by themselves are poor luminescence emitters are the efficient sensitiser for Mn^{2+} and conversley those which strongly produce their own luminescence are poor sensitisers.[8] Ginther[9] and Sen and Bose[10] suggest that Ce^{3+} is an efficient sensitiser for the Mn^{2+} emission. In his recent model for TL production in CaF_2:Mn, Sunta suggests that the 495nm TL emission from Mn is the result of non-radiative energy transfer from traces of rare-earth Ce^{3+} ions to Mn^{2+} ions.[8]

The use of both CaF_2:RE and CaF_2:Mn in TL dosimetry is widespread and in order to overcome problems such as a lack of reproducibility and of reusability when using the dosimeter materials, a knowledge of the precise TL mechanism (i.e. the identification of the defects involved in the production of TL) would prove useful. Although there has been considerable research effort into the TL properties of CaF_2:Ce and CaF_2:Mn, the exact TL mechanisms in these materials are still uncertain.[5,6,7,8,11,12,13] For example, Sunta's model for TL from CaF_2:Mn[8] suggests that the electrons which are produced along with holes during ionizing radiation are trapped by traces of RE^{3+} ion impurities forming RE^{2+} ions. Holes are trapped elsewhere (at unknown sites). Heating releases the holes which recombine with electrons to form RE^{3+*} (RE^{3+} ion in an excited state). The non-radiative de-

excitation energy from RE^{3+*} to RE^{3+} is then transfered to Mn^{2+} ions located in the close vicinity. This produces Mn^{2+*} (Mn^{2+} in an excited state) followed by the relaxation to Mn^{2+} and the emission of 495nm light. He suggests that the $\underline{Ce}^{3+}$ ion is acting as a <u>sensitizer</u> for emission from Mn during TL production in this material.

In view of the importance of Ce in CaF_2 it is the purpose of this research to study, by the application of several solid state techniques (TL, optical absorption, photoluminescence and Thermally Stimulated Depolarization Currents (TSDC)) the role of Ce in the TL production from CaF_2:Ce, both with and without Mn, and possible TL mechanisms in these materials are presented.

In the following paragraphs we briefly describe each of the above techniques and discuss the type of information that can be gleaned from each of them.

TL provides useful information on the properties of the various types of defect present within an insulator or semiconductor. The sensitivity of this technique is unrivalled and this makes it a valuable tool for the detection of trace impurities. Even in the most "pure" materials the presence of impurities is considered essential for the TL to occur.[3] However application of this technique on its own, does not describe the defect structure of a solid. It is when it is used in conjunction with other experimental methods that the information gained can be very useful.

By the application of the optical absorption technique information such as the concentration of defects, the presence of which results in light absorption in the UV-IR region, is gained. From the correlation between thermal "step annealing" measurements of optical

absorption (i.e. samples heated to a specific temperature) and TL, information about the types of the defect involved in the TL production may be gained.

From photoluminescence measurements information such as the excitation and luminescence of the defect centers responsible for TL emission can be earned. Using this technique one can also study the process of the energy transfer from sensitizers to activators which may result in TL emission. Photo-induced charge transfer dynamics can also be examined.

The TSDC technique is a sensitive method for monitoring the concentration of dipolar defects within a material. Using this technique one can study the interactions, for example, between dipolar defects and other dipolar defects, or between dipoles and clusters of impurities within the material. The interactions may manifest themselves in a distribution of the activation enthalpy for dipole rotation.

By way of an extended abstract we shall now describe the main features of our experimental results, to be presented in greater depth in the chapters to follow.

The TL of CaF_2:Ce contains two main glow peaks, one at approximately $100^{o}C$ and the other at approximately $300^{o}C$. The photoreversible charge transfer processes which take place in this material are a strong influence on the ~ $100^{o}C$ peak. The ~ $300^{o}C$ glow peak is associated with the annealing of the photochromic (PC) centers.

The work presented in this thesis suggests that the presence of Ce in CaF_2:Mn has a strong influence in the TL response of this material. The data suggest that even the presence of trace amounts of

Ce will be enough to reduce the sensitivity of CaF_2:Mn to ionizing radiation.

The TL glow curve of CaF_2 intentionally doped with both Ce and Mn is akin to that of Ce-only doped samples rather than of the Mn-only doped samples. However the presence of Mn emission (495nm) as a component of the TL emission in the TL glow curves of this material is the main and obvious difference between the TL emission from this material and that from CaF_2:Ce. The TL mechanism in CaF_2:Ce;Mn can be envisioned as being essentially the same as for CaF_2:Ce, as discussed above.

We suggest that the presence of Mn emission in the TL from CaF_2:Ce;Mn may be the result of energy transfer from Ce to Mn (chapter 6 section D). Alternatively, it may be due to re-absorption of light (290nm) from V_k+e recombination by Mn/radiation-induced defect complex(es) (for example, a Mn/F-center)(chapter 6 section D). In the spirit of the latter mechanism, it should be noted that as the Ce content increased, the 495nm Mn emission decreased.

The TL for Mn-only doped CaF_2 shows two major glow peaks for low Mn concentrations. As the Mn content is increased the peak at higher temperature becomes larger and shifts to higher temperature with respect to the lower temperature peak. For high Mn contents (3%) the TL glow peak appears at approximately 300°C as a single, composite peak. We found that the presence of trace rare-earth impurities influences the TL and optical absorption from CaF_2:Mn. This thus affects the thermal stability and sensitivity of TL from these materials (chapter 7 section A).

At high Mn concentration we suggest that the TL mechanism is

dominated by the F-H type recombination processes at Mn^{2+}-F complex(es)(chapter 7 section B). However, it should be emphasised that it is important to provide more-direct experimental and theoretical evidence for the formation of Mn^{2+}-F complex(es) in CaF_2:Mn rather than the indirect evidence presented in this work.

Based on the results presented here we find that rare-earth ions do not play a sensitizing role in producing the 300°C TL peak in dosimetry-grade CaF_2:Mn. Thus, the model presented by Sunta[8], suggesting that non-radiative energy transfer from RE^{3+} to Mn^{2+} is the dominant process in TL emission from CaF_2:Mn, is rejected.

Finally, the thesis will report on measurements of TSDC peaks in CaF_2:Ce and CaF_2:Ce;Mn. Using this technique, Ce^{3+}-$F_{int}(C_{4v})$ dipolar centers, in both CaF_2:Ce and CaF_2:Ce;Mn, have been investigated. The major reasons for this study stem from two sources. First it has been suggested that the C_{4v} centers are the precursers to the photochromic centers in CaF_2:Ce.[14] Second it has been reported that, in order for energy transfer from C_{4v} centers to Mn to take place, the distance between these two centers should be at least~ 40 lattice constants.[9] In our TSDC measurements we were able to observe the influence of Mn on the dipole rotation. Our data do not support the contention that C_{4v} centers are the precursers to photochromic centers. Additionally in our samples the concentrations calculated by using the TSDC method do not represent the actual dipole concentration.

CHAPTER II

THEORETICAL BACKGROUND

Section A

CaF_2

CaF_2, with its naturally-occuring form known as fluorite, belongs to the chemical compounds with the formula RX_2. In a compound RX_2 each ion of species R is surrounded by eight equivalent nearest-neighbor ions of species X forming the corners of a cube of which R is the center (the site of R ion has O_h symmetry). Each ion of species X is surrounded by a tetrahedron of four equivalent R ions (the site of X ion has T_d symmetry). The structure has a face-centered-cubic translational group and a space lattice of symmetry O_h[5] (figure 1).

Some physical properties of a CaF_2 crystal are listed below:

a) molecular weight is 78.08;

b) lattice constant is 5.4629Å;

c) approximate melting point is 1360°C;

d) the band gap is 12.2eV;

CaF_2 containing rare-earth impurities is a suitable material for applications such as infrared up-converters, photochromic, information storage materials; optically pumped microwave masers; and acoustic spectrometers.[2] Rare-earth-doped CaF_2 and CaF_2 doped with Mn have

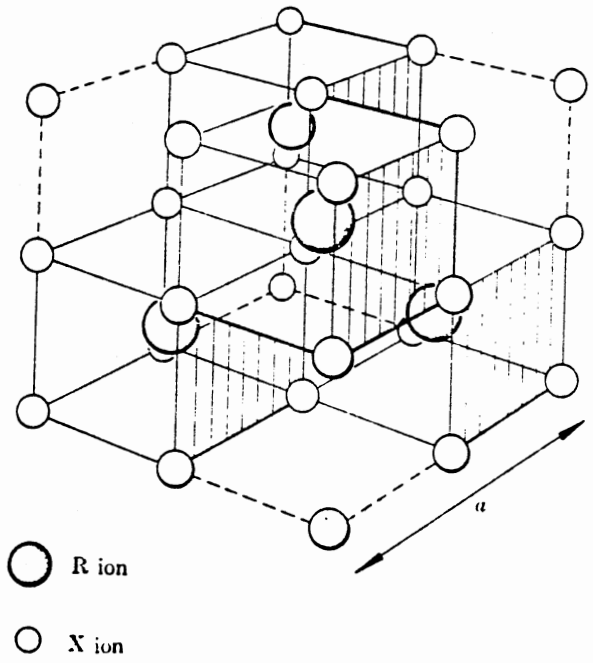

Figure 1. The structure of the fluorite RX_2 lattice. "a" is the lattice parameter of the conventional cubic unit cell. For clarity, the X ions are drawn smaller than the R ions. (After Hobby[19]).

also been successfully used in thermoluminescence dosimetry.[3]

Section B

Color Centers in CaF_2

The importance of color centers in ionic crystals during the thermoluminescence process necessitates a discussion at this stage about such centers (structure and optical properties) in CaF_2. We will do so by first giving the methods by which color centers are produced.

Pure crystals are transparent throughout the visible region of the spectrum. The crystals may be colored in a number of ways, viz:

1. by the introduction of chemical impurities;
2. by additive coloration i.e. baking the the crystal in the vapor of the alkali metal and then cooling it quickly;
3. by ionizing radiation (x-ray, γ-ray, neutron, proton and electron bombardment); and
4. by electrolysis.

Chemical impurities such as trivalent rare-earth RE^{3+} ions and divalent Mn^{2+} ions can substitute for Ca^{2+} in this lattice. The interstitial F^- ion charge compensator, which preserves charge neutrality during RE^{3+} substitution, is located in either a nearest neighbor (nn) position along $\langle 001 \rangle$ or a next nearest neighbor (nnn) position along $\langle 111 \rangle$, thus respectively leaving this dipolar complex (RE^{3+}-F^-) with C_{4v} or C_{3v} symmetry[1]. RE^{3+} ions which are nonlocally charge compensated can also exist; these possess O_h symmetry[2]. Clustering of C_{4v} and C_{3v} centers can readily occur in CaF_2.[1]

The presence of Mn^{2+} in the CaF_2 lattice results in optical

absorption bands, as shown in figure (2). As illustrated, the absorption bands are assigned to transitions from ground state ^6S to the excited ^4G, ^4D, ^4P and ^4F states.[15] The luminescence at 495nm in CaF_2 is attributed to the de-excitation from the ^4G level to the ^6S level of the Mn^{2+} ion (figure 3).[15,16] An absorption band at 450nm has been observed in CaF_2:Mn^{2+} irradiated at 77K.[12,15] It has been suggested that this absorption band is due to transitions from the ^7S ($3d^5$) level to the $^7P(3d^54p)$ energy state of Mn^+ (figure 4).[12]

The optical absorption from CaF_2 doped with low Ce concentrations (.01 mole%) reveals absorption bands characteristic of 4f to 5d electronic transitions within the Ce^{3+} ions (figure 5). Refering to figure (5), the bands indicated as B and E have been assigned to transitions from the ground state to the excited 5d energy levels split by the C_{4v} crystal field and by the spin-orbit interaction (i.e. transitions within Ce^{3+} ion within the Ce^{3+}-F^- center (C_{4v}); see figure 6).[17,18,19] The bands labelled C and D have been suggested to be due to the 4f-5d transitions within Ce^{3+} ions within clusters of the C_{4v} centers (as the Ce content is increased these bands grow more rapidly than the B and E bands). It has been suggested that the Ce^{3+} in C_{3v} sites results in two very closely spaced absorption bands near 311.85nm (figure 7).[17]

The strong doublet fluorescence emission (320 and 340nm) of Ce^{3+} is attributed to the de-excitation from the lowest levels of the 5d to the $^2F_{5/2}$ and $^2F_{7/2}$ energy levels of the 4f electronic configuration split by the spin-orbit interaction (figure 8).[17]

Ce^{2+} absorption bands are shown in figure (9). These bands are assigned to transitions from states of 4f5d to the $4f^2$ electronic

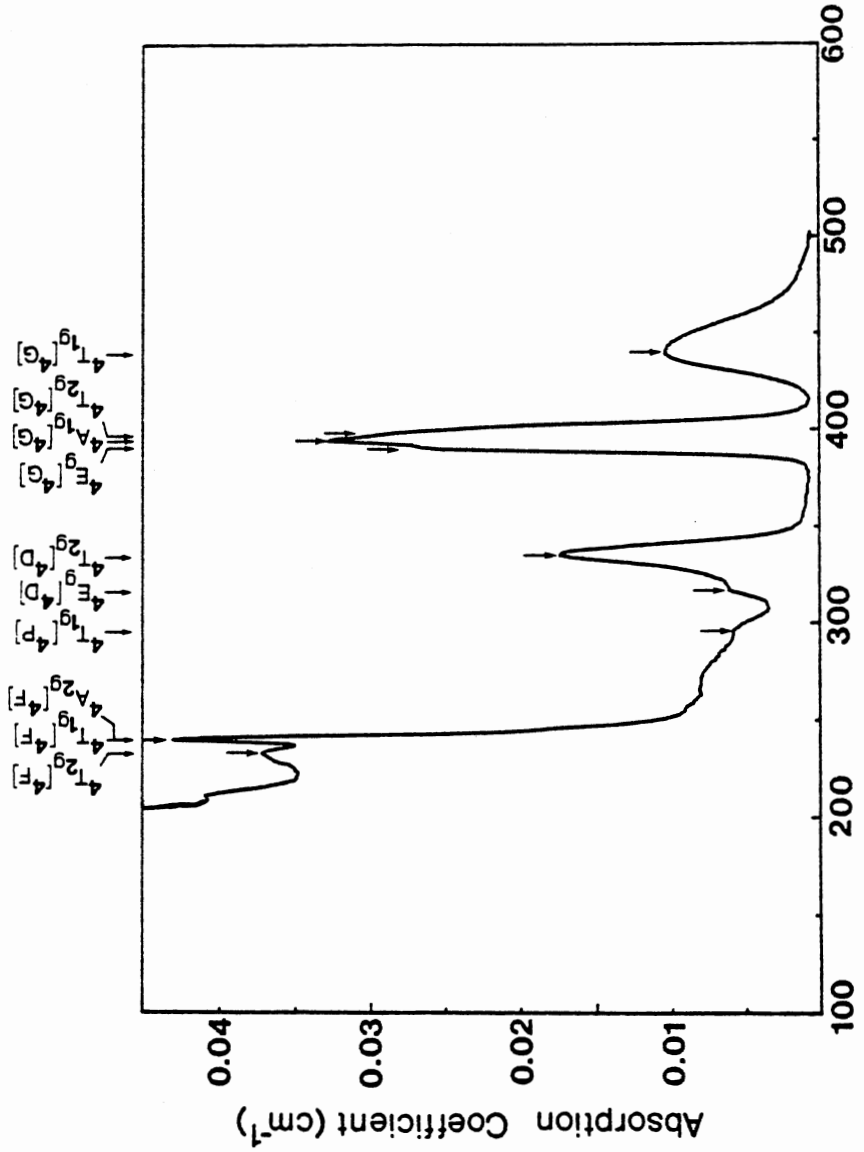

Figure 2. Optical absorption of CaF_2:Mn (3%). The optical transitions within Mn^{2+} ions are labelled on the diagram. (After McKeever et al(15)).

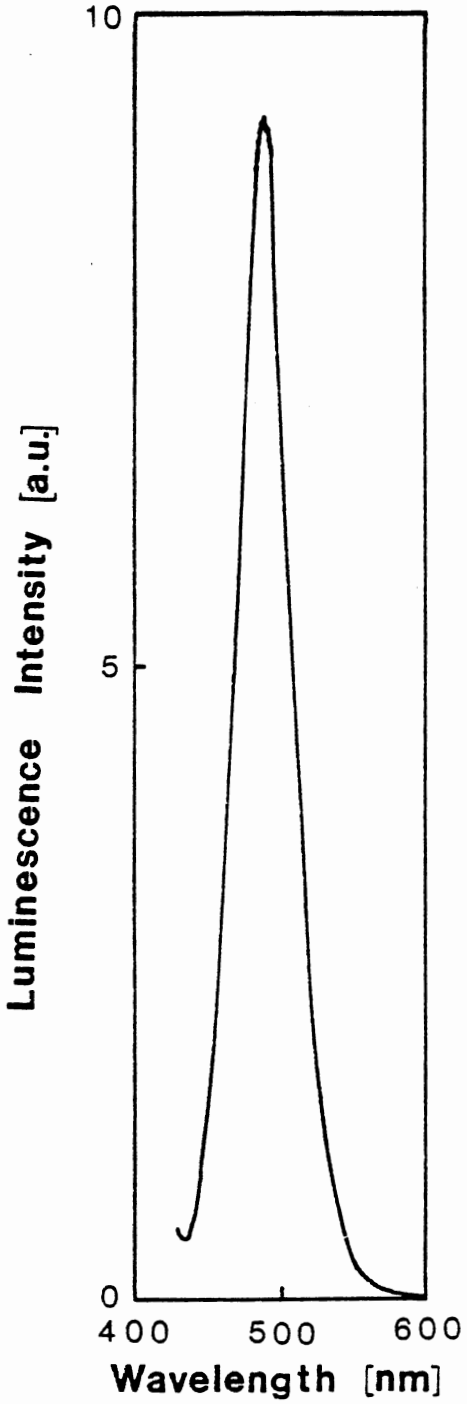

Figure 3. Emission spectrum of CaF_2:Mn (0.5%). Excitation wavelength is 395nm.

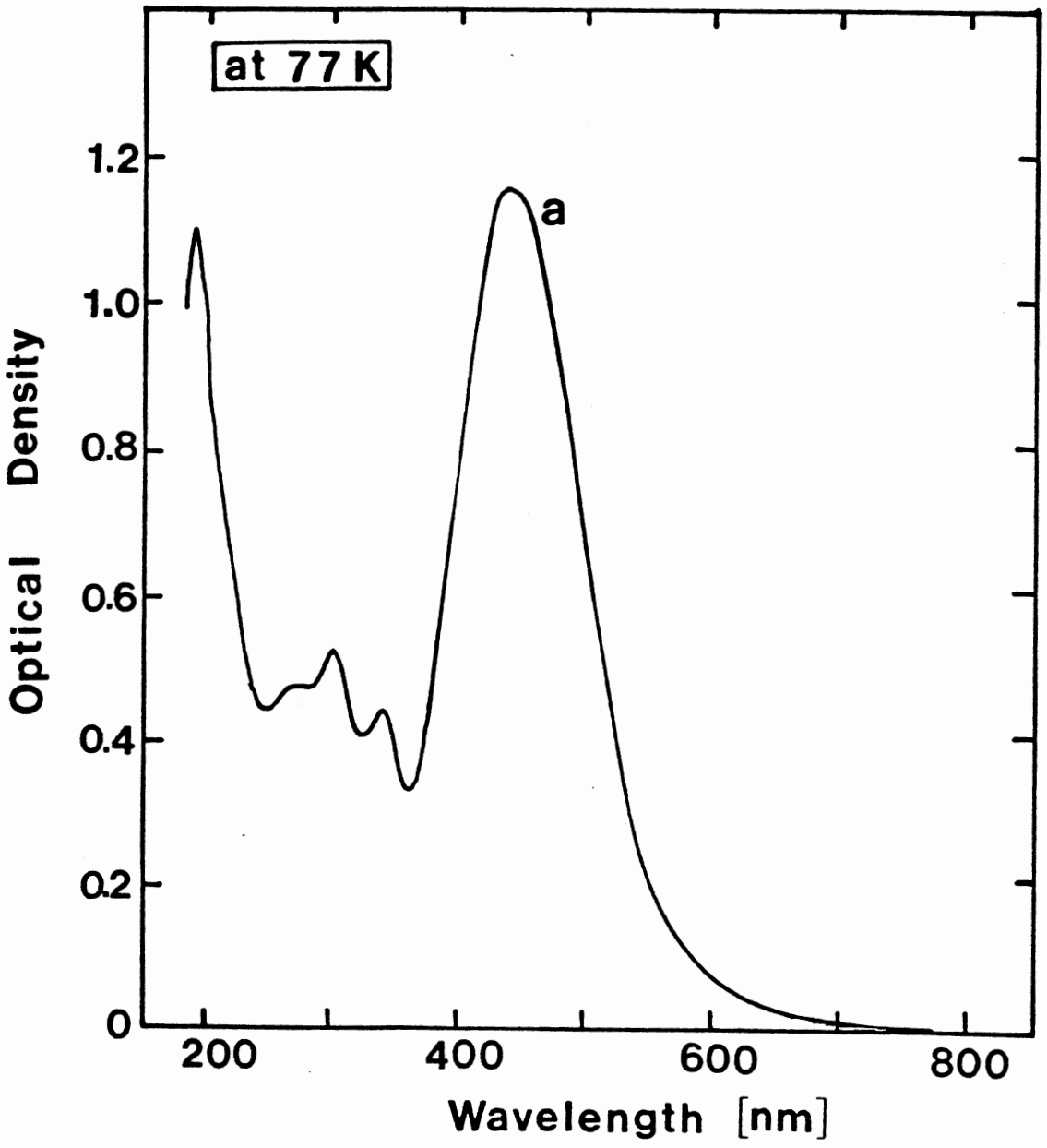

Figure 4. Optical absorption of CaF_2:Mn (3%) at 77K following irradiation with 2MeV electrons (0.5μA) at L.N.T. (After McKeever et al [17]).

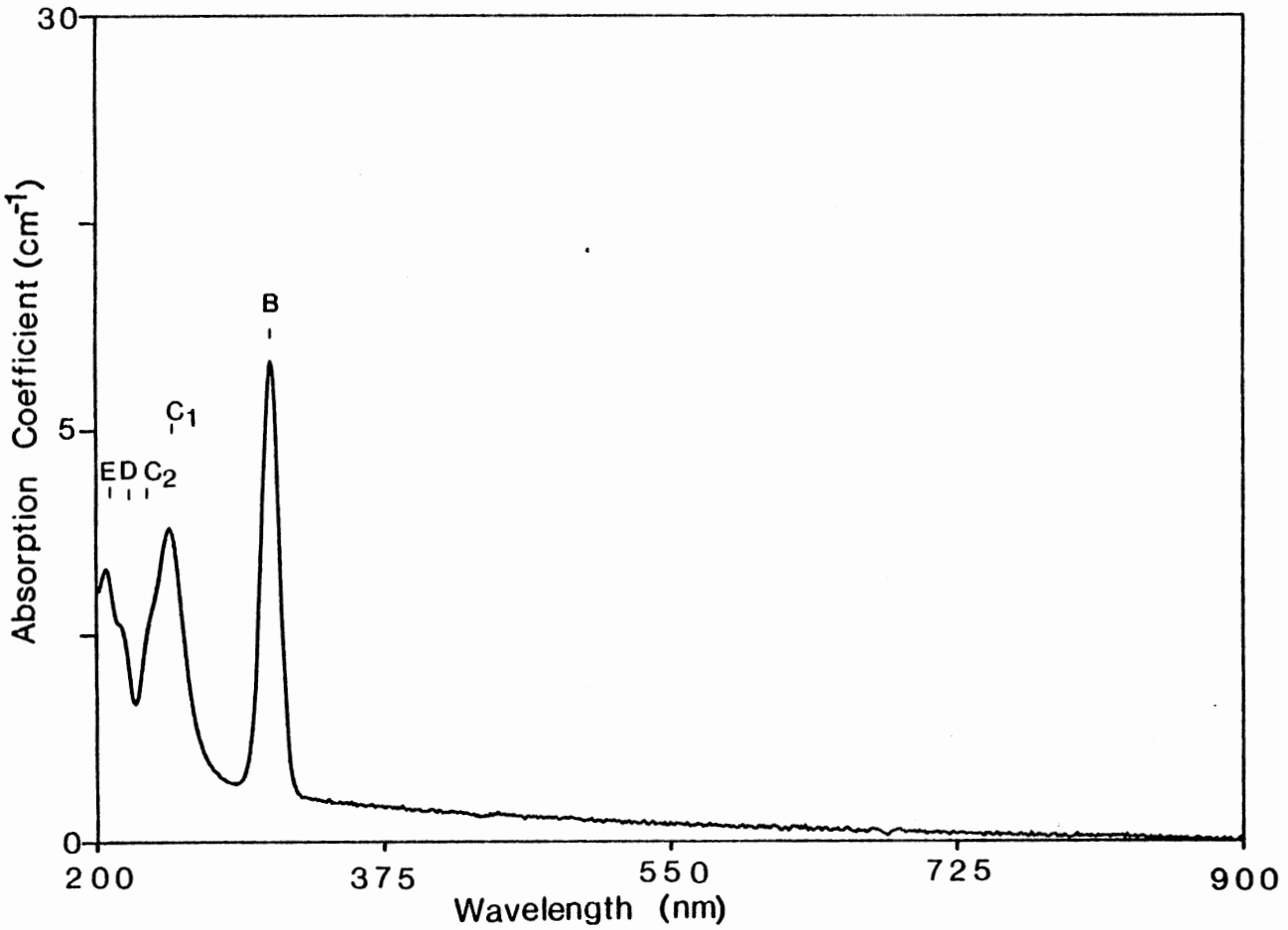

Figure 5. Optical absorption of CaF_2:Ce (0.01%) at room temperature.

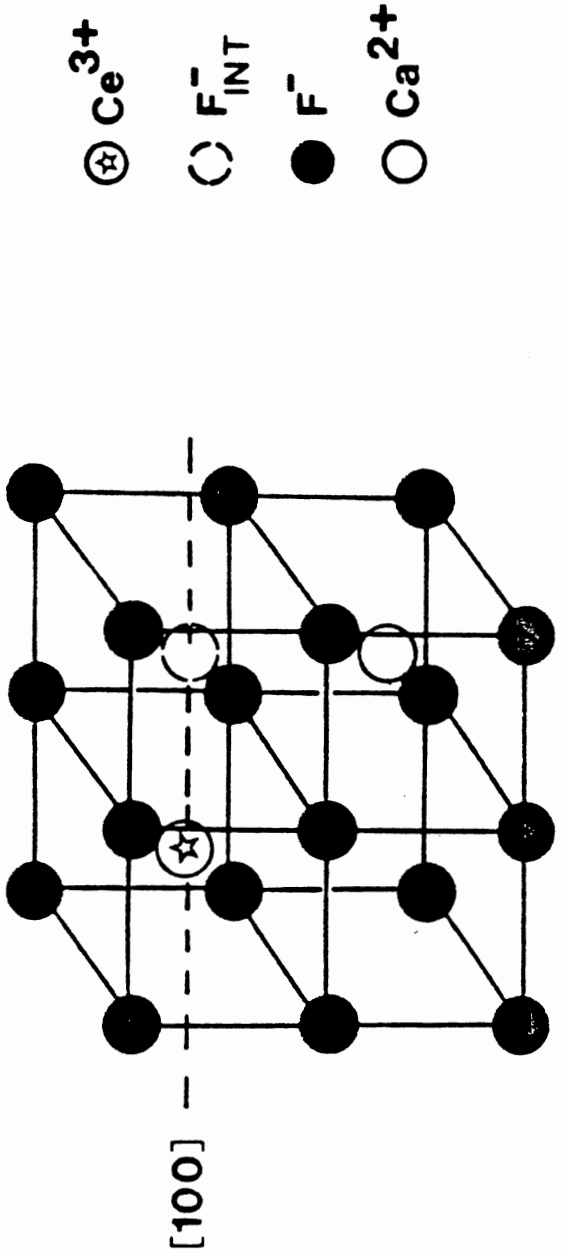

Figure 6. The Ce C_{4v} center.

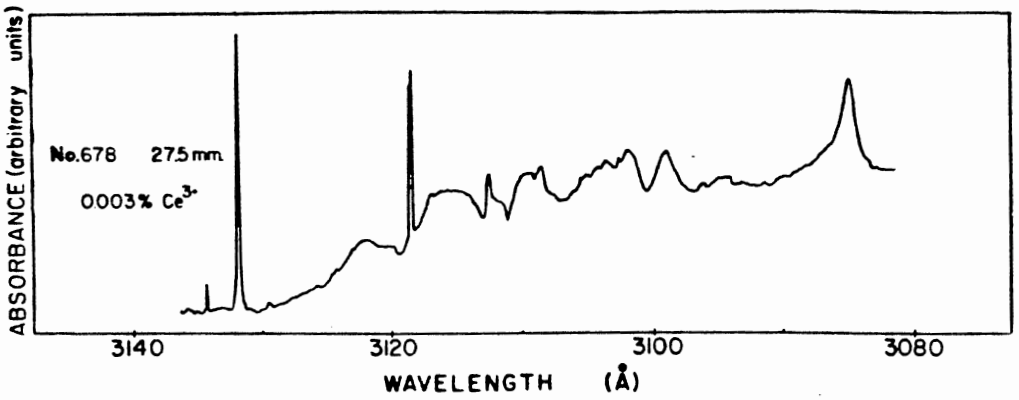

Figure 7. Absorption spectra of CaF_2:Ce (0.003%) showing closely spaced pair of lines attributed to the $C_{3v}(F_i)$ center. (After Manthy[37]).

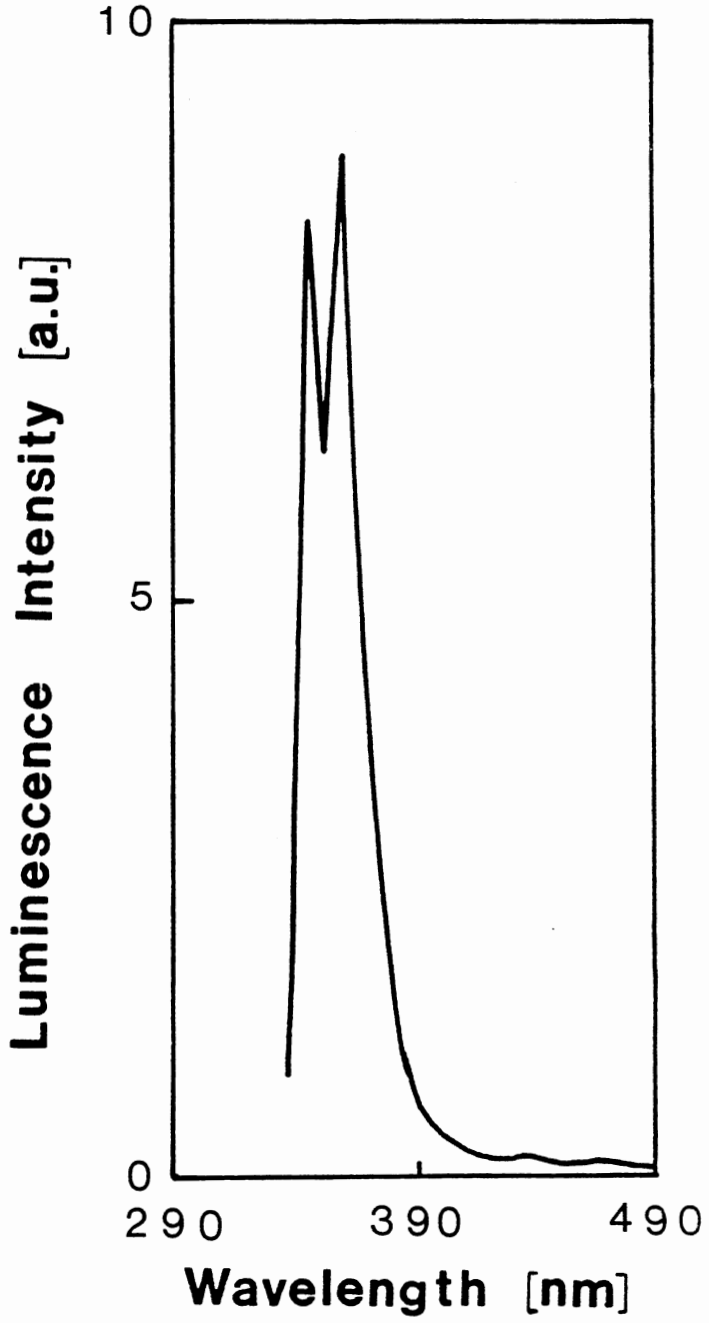

Figure 8. Emission spectrum of CaF_2:Ce (0.01%) at room temperature.

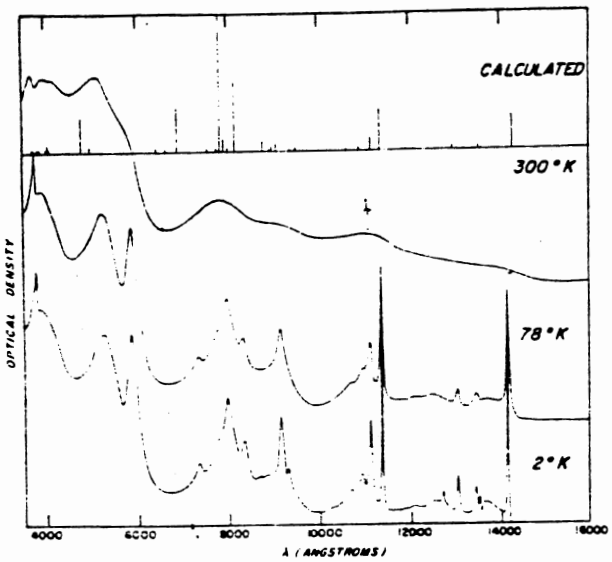

Figure 9. Absorption spectrum of $CaF_2:Ce^{2+}$ at three different temperatures (2, 78 and 300K). (After Alig et al[20]).

configuration.[20]

As mentioned before, one of the methods by which a defect can be formed is by the absorption of ionizing radiation. Before discussing radiation-induced centers in CaF_2, a brief discussion of the mechanism responsible for the creation of such centers in alkali halides is relevant.

Exposure of ionic crystals to ionizing radiation results in the creation of electrons and holes, from which might be followed the formation of defects. The mechanism by which defects are created, during irradiation, in alkali halides has been well understood.[21,22,23,24] After the creation of free electrons and holes by the ionizing radiation, the holes become self trapped to form V_k centers (a hole trapped by two halogen ions along the <110> direction, displaced with respect to their normal sites and forming an X_2^- molecule). The capture of an electron by a V_k center forms a self-trapped exciton (V_k + e) in an excited state (i.e. either the electron and hole are both excited, or the electron alone is excited, or the hole alone is excited).[25]

The electron and hole recombination (i.e. annealing of the self-trapped exciton) can take place either radiatively or nonradiatively. It is the nonradiative recombination that can result in defect production.[25] In KCl, for example, nonradiative recombination of the electron and the hole when only the hole is in an excited state produces an F-center (a halogen ion vacancy with a trapped electron) and an H-center (a halogen atom in an interstitial position).[25] The separation of the F and the H center is the consequence of a collision sequence among the host Cl ions along <110>. This is due to the kinetic

energy transfer to them from the nonradiative electron-hole recombination (figure 10).

Although there have been extensive studies aimed at understanding the defect production mechanisms during ionizing irradiation in alkaline earth fluorides, the exact mechanisms involved are still uncertain.[23,26,27,28,29,30] It has been suggested that the photochemical processes in these materials are very analogous to those in alkali halides.[23] It has been reported, however, that the self trapped exciton in fluorites is not equivalent to a V_k center plus an electron (V_k + e), but is closer to an F and H pair.[31,32] Four possible configurations for F and H pairs in fluorite-structure compounds are shown in figure (11). The self-trapped hole (V_k) in CaF_2 is located primarily on two equivalent nearest-neighbor fluorine ions forming an F_2^- molecule with its axis along the close-packed <100> (figure 11). The H center consists of a hole shared between two F^- ions with the proportion of 2/3 on the interstitial F^- ion and 1/3 on a substitutional F^- ion, along <111>. The collision sequence as occurs in alkali halides along <110> during F-H pair production, has not been observed in fluorites.[25] Thus, fluorite compounds are difficult to color in their pure state.

The F center in CaF_2 is a single electron trapped in a fluorine ion vacancy (figure 12). The M center is composed of two nearest F centers either along the <110> or <100> directions. The R center is formed from three F centers along <100>. The N center consists of four F centers in the (100) plane. The F center and several of its aggregates (M,R, and N) in CaF_2 have been produced by electron and X-irradiation at 77K.[27,28,33] The F and M centers result, respectively,

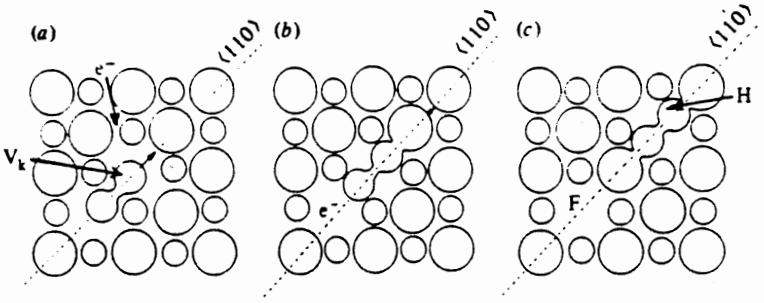

Figure 10. (a) Self-trapped hole (V_k-center) and free electron after irradiation. (b) Dissociation of self-trapped exciton. X_2 molecule departs in a <110> direction following the non-radiative recombination of e^- and V_k. (c) H-center forms some distance from the F center. (After McKeever[3]).

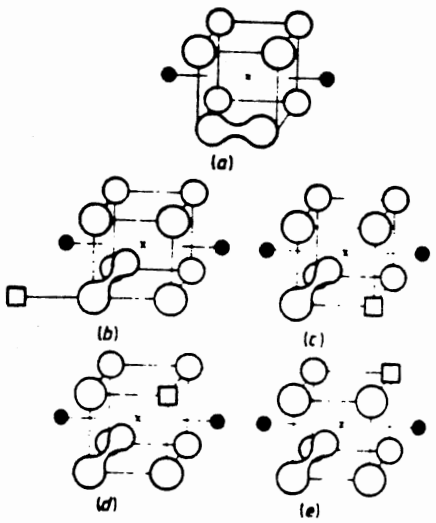

Figure 11. Possible configurations of F-H pairs in CaF_2. (a) The V_k center, aligned along <010>, before it captures an electron. (b), (c), (d), (e) configurations 1, 2, 3, and 4 respectively. Ca^{2+} is represented by filled circles, while the dumb-bell shape indicates the H center, aligned along <$\bar{1}$11>. Open squares represent the F center. (After Adair et al[31]).

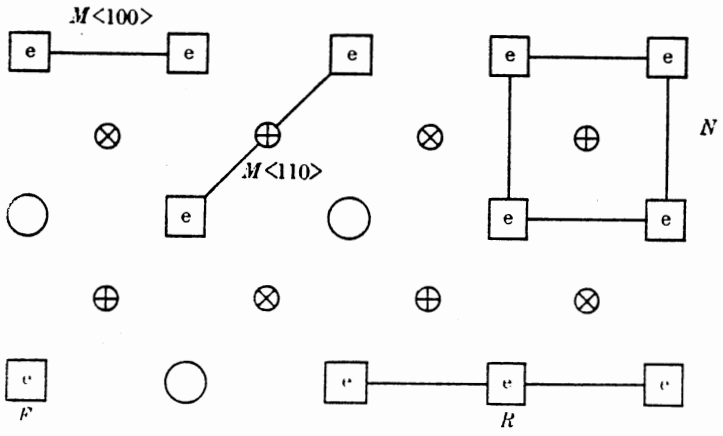

Figure 12. Schematic representation of the structure of F, M, R and N centers in fluorites. and are cations above and below the plane of the paper. O are anions. (After Hayes et al[34]).

in optical absorption at 376 and 521nm.[27,33,34] Excitation in either the F or M band regions produces a broad emission band with the peak at 585nm.[34]

The self-trapped hole (V_k) in CaF_2 may be produced by X-irradiation of undoped CaF_2 at 77K,[25,34,35,36] but the presence of trivalent rare-earth impurity ions can enhance the initial rate of production of these centers.[34] The V_k center in CaF_2 results in strong optical absorption in the ultraviolet region (~310nm).[7,37] Electron and V_k recombination produces an emission at 279nm.[37] It has been suggested that 50% of the holes created by X-irradiating CaF_2:Tm at 77K exist in a nonparamagnetic state at room temperature.[37]

Because H centers are formed as a consequence of F-center formation H centers, in undoped CaF_2, are also not easily formed. However, vacancy and interstitial centers are more easily produced in doped fluorites. For example these centers are produced in small amounts by irradiation at 77K of trivalent rare-earth doped CaF_2.[35,36,37] Upon warming the crystal the V_k centers already formed during irradiation become mobile and after capture by the charge-compensating F^- interstitials H centers are produced.[35,36,37] H centers in CaF_2 result in a broad absorption band peaking at ~308nm.[38]

Finally we will bring this section to an end by introducing the rare-earth/defect complex in CaF_2.

Optical absorption of additively colored crystals of CaF_2 doped with La, Ce, Gd, Tb, Y or Lu show a spectrum known as the "four-band spectrum" (figure 13).[39,40]

UV irradiation of these materials at room temperature results in

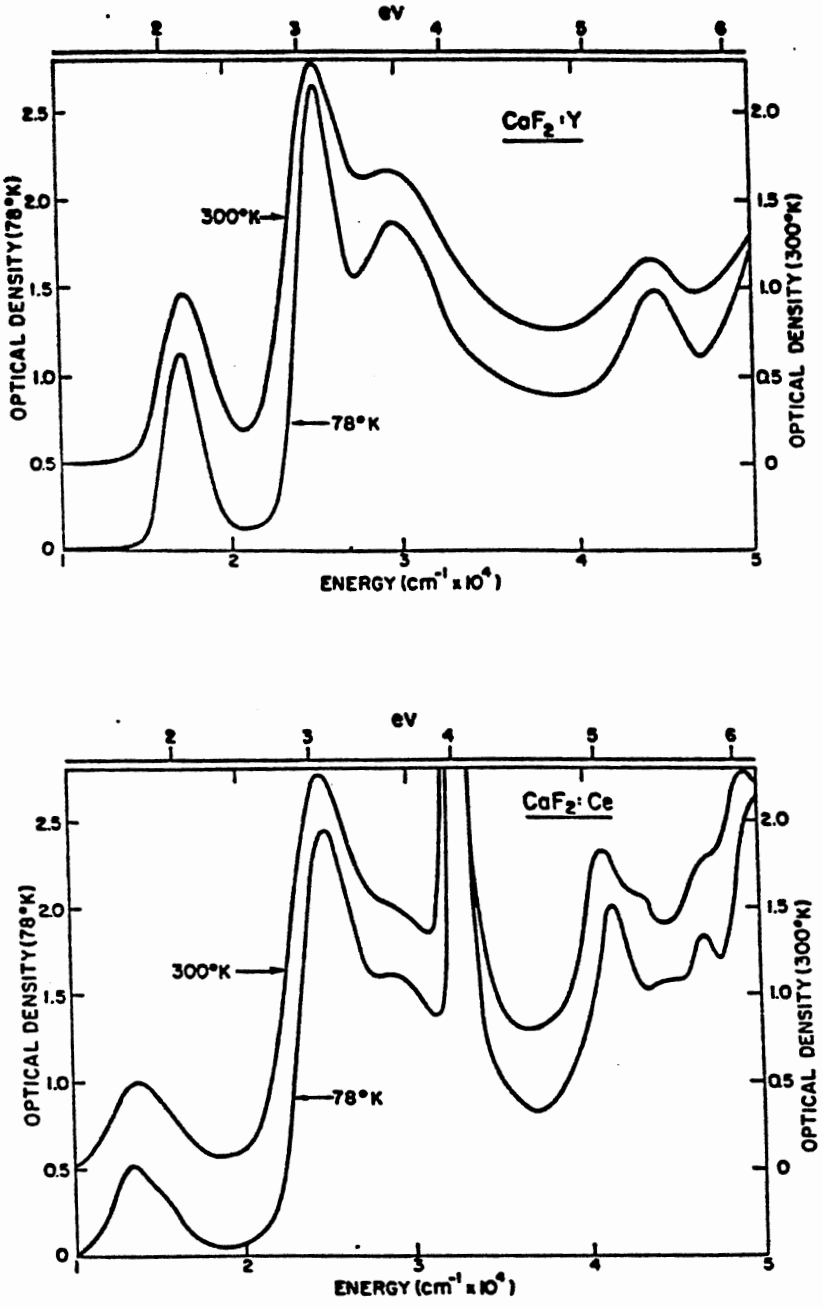

Figure 13. (a) P.C. spectrum of CaF_2 with 0.3% of Y, 1.0mm thickness. (b) P.C. spectrum of CaF_2 with 0.05% Ce, 2.1mm thickness. (After Staebler[39]).

a reduction of the four-band spectrum and a growth of new absorption bands in the visible region, with a consequent change in the color of the crystal. Exposure of the crystal then to visible light, or to heat, results in the reverse process, and the material returns to the original state. Materials of this type are known as "photochromic" and they have important practical applications in information storage and display.

It has been observed, using EPR techniques and a combination of linear- and circular-dichroism measurements, that the center responsible for the four-band spectrum consists of a trivalent rare-earth impurity ion associated with a nearest F^- vacancy with two trapped electrons (the defect thus posseses C_{3v} symmetry).[4] This center is called the "photochromic" (PC) center. Theoretical work[41] suggests that the orbitals describing the PC center are the same as those of a perturbed F center. The unperturbed F center in CaF_2 has T_d symmetry with respect to the Ca^{2+} ions; the introduction of Ce^{3+} along $\langle 111 \rangle$ in a body-center position reduces the symmetry to C_{3v}. The consequent energy states and the allowed transitions between them are shown in figure (14).

Gamma-irradiation of CaF_2:Ce at 77K results in the conversion of Ce^{3+} to Ce^{2+} ions in sites with O_h symmetry and no PC centers are formed.[39] Irradiation at room temperature, however, produces Ce^{2+} in cubic sites and PC centers but not PC^+ centers (ionizing PC centers; the absorption spectrum of the PC^+ center looks like that of the PC centers but shifted slightly to higher energy).[39] Wagner and Mascarenhas[14] claim that PC centers are formed at the expense of the C_{4v} centers (four C_{4v} centers form one PC center) during X-irradiation

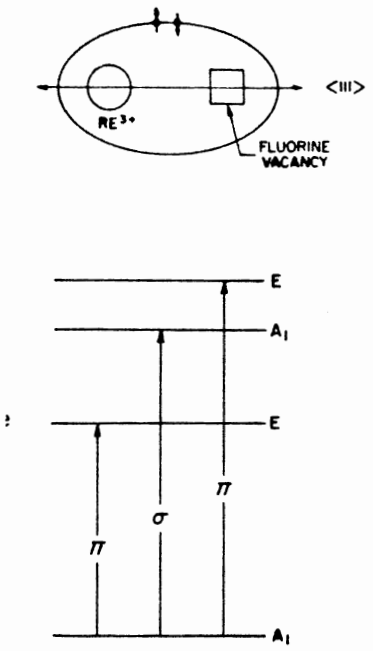

Figure 14. (a) Schematic model of PC center. (b) Energy levels occupied by the two electrons. Labels refer to the appropriate irreducible representations in C_{3v} point symmetry. (After Alig[41]).

at room temperature. However, there is no justification given by these authors as to why four C_{4v} centers are required to form one PC center. There is also no mention of the fate of the F^- interstitial ions after the PC centers are formed.

Section C

Thermoluminescence

We presented in the previous section a somewhat detailed review of the color centers in CaF_2, in particular the defects relevant to this work. For the remainder of this chapter we discuss various experimental methods employed in this work. In doing so we begin with thermoluminescence.

Luminescence phenomena are generally described by utilizing energy band theory. The luminescence appearing in solids during thermoluminescence processes can be explained by the same fundamental principles as applied to luminescence in general. Thus, in the following subsections we will first briefly look at the energy band model of solids and introduce the concept of localized energy levels (traps and recombination centers). Then we will examine the position of thermoluminescence in the context of luminescence phenomena in general.

Band theory of solids

Every solid contains electrons. The band theory of solids is based on a one-electron approximation. In this model it is assumed that the electron interacts with both the field of the fixed atomic cores (nuclei and inner shell electrons) and an average field arising from the charge distribution of all the other outer-shell electrons.

For the perfect crystal the total crystal potential energy $V(\vec{r})$ must have the periodicity of the crystal lattice. From the solution of the Schrödinger equation

$$(\hbar^2/2m)\nabla^2\Psi + [\varepsilon - V(\vec{r})]\Psi = 0 \qquad (2.1)$$

which suffices for the above model, it is deduced that the electrons in solids are arranged in energy bands (closely spaced energy levels) separated by regions in energy for which no wavelike electron orbitals exist. These regions are called energy gaps (band gaps or forbidden gaps).

The density of occupied energy states N(E) in each band is given by

$$N(E) = Z(E)f(E) \qquad (2.2)$$

where Z(E) is the density of available energy states, and

$$f(E) = 1/\exp[(E-E_f)/kT + 1] \qquad (2.3)$$

is the Fermi-Dirac distribution function for the electrons (i.e. the probability that an energy state E will be occupied in an ideal electron gas in thermal equilibrium). E_f denotes the Fermi energy (i.e. the energy of the topmost filled states in the ground states).

Traps and recombination centers

In an insulator all the allowed energy bands are either filled or empty. Thus there are no states immediately above the highest filled band (valence band). The nearest available state is at the bottom of the next allowed band (conduction band). The Fermi level at absolute zero is halfway between, i.e. in the middle of the forbidden gap. The presence of lattice defects (impurities, radiation damage centers, vacancies, interstitials, etc.) which disturb the translational

symmetry of the crystalline structure results in localized energy states which might fall within the band gap.

The localized energy states, upon capturing free charge carriers may act as traps or as recombination centers (figure 15). Differentiation between traps and recombination centers is based upon the relative probabilities of thermal release and recombination. The probability of thermal excitation from a localized state at a given temperature T is given by:

$$p = s \exp(-\Delta E/kT) \qquad (2.4)$$

where ΔE is the energy depth, or trap depth (i.e. energy difference between the localized state and the bottom of the conduction band for the electron centers, or the top of the valence band for the hole centers); k is Boltzmann's constant; and s is a constant. (This last constant will be discussed more in the next subsection.) It can easily be seen from equation (2.4) that for the localized states with small ΔE the probability for the release of the charge carrier is higher than the ones with large ΔE. Thus, the localized states with small ΔE are more likely to act as traps than recombination centers. Based upon this one could locate the traps toward the bottom of the conduction and towards the top of the valence band, whereas the recombination centers will be located near the middle of the band gap (figure 15). However, it should be noted that a trap at one temperature may act as a recombination center at lower temperature and vice versa.[3] There might also exist a delocalized level of the energy depth D for which the relative probabilities of trapping and recombination are equal. Such a level designates a demarcation between the traps and the recombination centers. In other words localized states with $E<D$ would

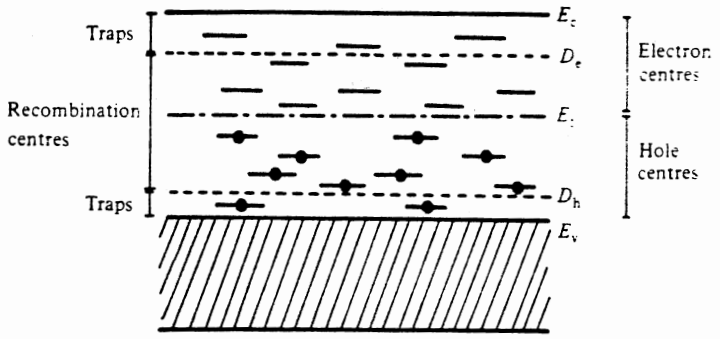

Figure 15. Energy levels in an insulator in equilibrium at absolute zero. The levels below E_f are full of electrons, while those above are empty. (After McKeever[3]).

act as a trap whereas if E>D it would be a recombination center[3] (figure 15). It should be mentioned that discrimination between traps and recombination centers is not solely dependent on the trap depth (ΔE). For a given concentration of trapped charge, the probability of the recombination is governed by the value of the capture cross-section (the value of capture cross-section depends upon the potential distribution in the region of the defect; figure (16). The recombination probability has the following form

$$A = v\sigma \tag{2.5}$$

where v is the carrier thermal velocity ($\alpha T^{1/2}$) and σ is the capture cross-section.

Luminescence

Luminescence is the emisssion of optical radiation (UV-IR) from a material by means other than heating it to incandescence. During the luminescence process some of the energy input into the material may be absorbed (excitation) and then released in the visible radiation form (emission). The various luminescence phenomena are named according to the means with which the material receives its excitation energy. Thus we have photoluminescence (optical radiation energy), radioluminescence (X-ray, γ, β particles, etc.), cathodoluminescence (electron beam), electroluminescence (electrical energy), chemiluminescence (chemical energy), sonoluminescence (acoustic energy).[3]

Luminescence phenomena are usually described by utilizing energy band theory. In the energy level diagram shown in figure 17a an electron, after aquiring sufficient excitation energy, makes a transition from the ground state g to the excited state e. Deexcitation

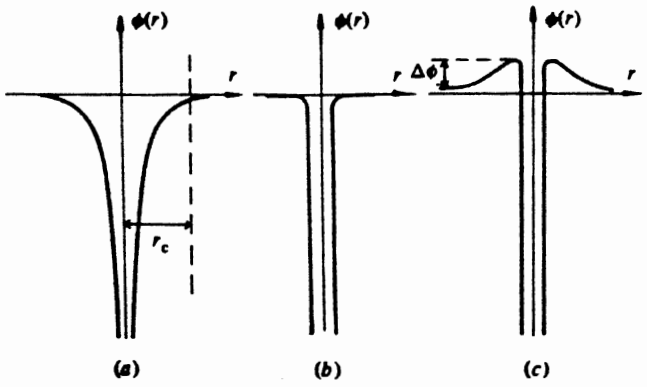

Figure 16. Schematic representation of the potential distribution $\phi(r)$ around defect center. (a) Coulombic attractive; (b) neutral; (c) coulombic repulsive. Typical values for the capture cross-section are $10^{-6}m^2$, $10^{-19}m^2$ and $10^{-26}m^2$, respectively. (After McKeever[3]).

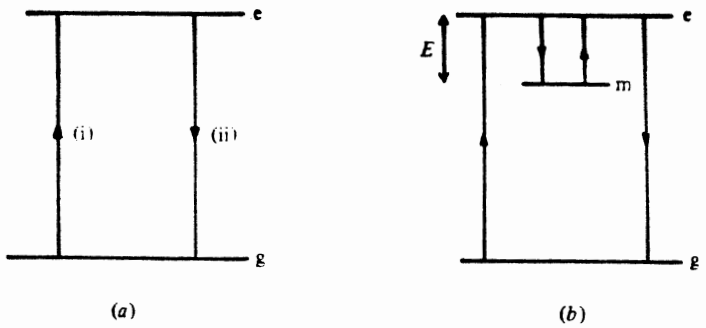

Figure 17. Energy transitions involved in the production of (a) fluorescence and (b) phosphorescence. Symbols defined in text.

from e to g is followed by emission. The average time between excitation and emission (lifetime) can be between 10^{-3} to 10^{-8} sec. The luminescence phenomena which is described by figure 17a is called "fluorescence".

There are some luminescence processes that cannot be described by figure 17a. Instead, as shown in figure 17b the charges become trapped in a localized state m (a metastable state). If the charge now aquires an energy equal to ΔE (E_e-E_m) it will be released to the e state with the consequent relaxation to the g state resulting in the emission of light. Thus this trapping phenomenon results in a longer delay (seconds to years) between excitation and emission. The average time spent by the charge inside the trap is given by

$$\tau = s^{-1}\exp(\Delta E/kT) \qquad (2.6)$$

where the term assignments remains as before. This process of luminescence is called "phosphorescence". Energy ΔE can be supplied either thermally or optically. The former is called Thermally Stimulated Luminescence (or thermoluminescence, TL) whereas the latter is named Optically Stimulated Luminescence (or OSL).

Thermoluminescence model

By using a simple energy band scheme, i.e. a "two level model", an attempt is now made to introduce many of the essential features of thermoluminescence. However every material has its own energy band scheme which may be much more complex than that described below.

In the "two level model" as shown in figure (18) there are just two localized levels. One acts as a trap (T) center (located between E_c and D_c) and the other acts as a recombination (R) center located

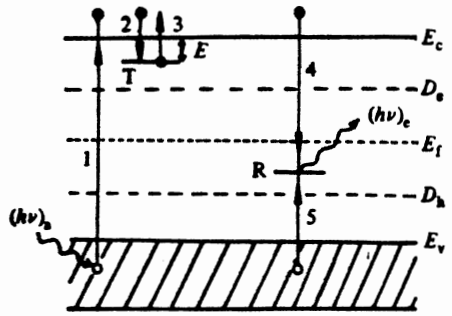

Figure 18. Simple two-level model for thermoluminescence. Allowed transitions: (1) ionization; (2) and (5) trapping; (3) thermal release; (4) radiative recombination and the emission of light. Electrons are the active carriers, but an exactly analagous situation arises for holes. Electrons, solid circles; electron transitions, solid arrows; holes, open circles; hole transitions, open arrows. (After McKeever[3]).

somewhere between D_e and D_h). During ionizing radiation electrons are trapped at T whereas the holes are trapped at R. By assuming that the probability of thermal release (transition 3) is zero (i.e. irradiation is performed at a low enough temperature such that no detrapping takes place) then the trap filling process may be described by the following four equations

$$dn_c/dt = f - n_c A_r n_h - n_c(N - n)A, \tag{2.7a}$$

$$dn/dt = n_c(N - n)A, \tag{2.7b}$$

$$dn_v/dt = f - n_v(N_h - n_h)A_h, \tag{2.7c}$$

$$dn_h/dt = n_v(N_h - n_h)A_h - n_c n_h A_r. \tag{2.7d}$$

During this process charge neutrality should be maintained, namely:

$$n_c + n = n_v + n_h \tag{2.8}$$

where in the above equations:

$n_c \equiv$ concentration of electrons in the conduction band (per unit volume); $n_v \equiv$ concentration of holes in the valence band (per unit volume); $n \equiv$ concentration of electrons in traps (per unit volume); $N \equiv$ concentration of available electron traps of depth ΔE below the conduction band (per unit volume); $n_h \equiv$ concentration of holes in recombination centers (per unit volume); $N_h \equiv$ concentration of available hole centers (per unit volume); $A \equiv$ transition coefficient for electrons in the conduction band becoming trapped (per unit time, transition 2 in figure 18); $A_h \equiv$ transition coefficient for holes in the valence band becoming trapped in the hole centers (volume per unit time; transition 5); $A_r \equiv$ recombination transition coefficient for electrons in the conduction band with holes in centers (transition 4); $f \equiv$ the electron-hole production rate (volume per unit time; transition 1). In the above equations it is also further assumed that due to its

small probability no band to band transitions take place.

After the radiation has ceased the system (crystal) which is in a nonequilibrium state (charge carriers are trapped at the trapping centers thus both the entropy and the energy of the system have changed) tends to regain its equilibrium state (original state of the crystal before irradiation). This results in the flow of charges among different centers and this can be speeded up by raising the temperature of the crystal. The rate equations describing this charge traffic are given below.

$$dn_c/dt = np - n_c(N - n)A - n_c n_h A_r, \tag{2.9a}$$

$$dn/dt = n_c(N - n)A - np, \tag{2.9b}$$

$$dn_h/dt = -n_c n_h A_r \tag{2.9c}$$

where p has already been defined in equation (2.4). Since the transitions to or from the valence band are not considered in this case, the charge neutrality becomes

$$n_c + n = n_h. \tag{2.10}$$

The thermal release probability (p) has an important role in the discrimination between the above two sets of equations (i.e. the trap filling and trap emptying processes). It is considered to be zero during the trap filling process, but large during trap emptying. As shown in equation (2.4) it is exponentially related to temperature. The $\exp(-\Delta E/kT)$ factor in this equation is the probability of the release of the electron via its interaction with phonons (thermal energy), where ΔE is defined as the energy difference between the trap and the bottom of the conduction band (trap depth); s is called the "frequency factor" or "attempt to escape frequency". Since during the trap emptying process the rate of release of the electrons is given by the

Arrhenius equation, written as:

$$p = \nu K \exp(-\Delta G/kT) \tag{2.11}$$

where G is Gibbs free energy, given by G = H - TS where H is enthalpy (H = E + PV) and S is entropy. Thus we can write

$$p = \nu K \exp(\Delta S/k)\exp(-\Delta H/kT)$$

$$p = \nu K \exp(\Delta S/k)\exp(\Delta PV/kT)\exp(-\Delta E/kT). \tag{2.12}$$

Assuming that the change in P (pressure) and V (volume) are negligible then

$$p = \nu K \exp(\Delta S/k)\exp(-\Delta E/kT). \tag{2.13}$$

By comparing equations (2.13) and (2.4) we see that s can be identified with $\nu K \exp(\Delta S/k)$. It is interpreted as the number of times per second, ν, that a bound electron interacts with the lattice phonons times a transition probability K, and an exponential entropy term. The maximum value that s takes is 10^{12}-$10^{14} s^{-1}$ (lattice vibration frequency). s has a small temperature dependency which can be ignored when it is compared with the strong exponential temperature dependence of the Arrhenius term.

After the electrons that are detrapped radiatively recombine with the holes then visible light is produced. The intensity at any time during the heating (with a constant heating rate) is given as

$$I(t) = - dn_h/dt. \tag{2.14}$$

Equation (2.14) is shown schematically in figure (19). As shown in this figure application of a linear heating such as

$$T = T_o + \beta t \tag{2.15}$$

where β is defined as heating rate (i.e. dT/dt), causes the temperature to increase and this results in the detrapping of the electrons with the consequent recombination with holes. Thus the

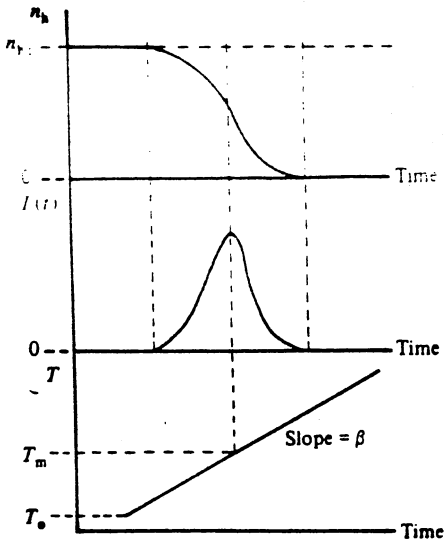

Figure 19. Relationship between thermoluminescence intensity I(t) and the number of trapped holes n_h at the recombination centers. Also shown is the linear relationship between time and temperature during heating. (After McKeever[3]).

thermoluminescence intensity increases. Further increase in temperature causes the release of more electrons; and since at this stage the number of available recombination sites are less than before the rate of recombination decreases and thus thermoluminescence intensity decreases. The intensity of this TL light versus temperature is called a TL "glow curve".

Thermoluminescence analysis

The experimental data obtained for a TL glow curve or a series of glow curves may be used to calculate various parameters such as the trap depth (ΔE), the frequency factors (s), the capture cross-sections and the densities of the various traps and recombination centers taking part in the thermoluminescence emission.

Theoretical expressions to which the experimental data is fitted may be derived by selecting the rate equations appropriate to a particular model (viz. equations 2.9a-c) and introducing simplifying assumptions into them. The important asumptions introduced are:

(1) $n_c << n$; i.e. the free carrier concentration in the conduction band is much less than the trapped carrier concentration.

(2) $dn_c/dt << dn/dt$ i.e. the rate of change of the free carrier concentration is always very much less than the rate of change of the trapped carrier concentration (this means that n_c is approximately constant).

(3) The probability of retrapping is negligible compared with the probability of recombination (Randall-Wilkins model).[42,43]

Using these assumptions we get:[3]

$$I(t) = n_o s \exp(-\Delta E/kT) \exp\{-(s/\beta) \int_{T_o}^{T} \exp(-\Delta E/kT) dT\} \qquad (2.16)$$

which is called the "first-order (monomolecular) kinetics equation". In equation (2.16) T_o and n_o refer, respectively, to the value of T and n at time $t = \phi$. However if it is assumed that there is strong retrapping of the released charge (i.e. the Garlick-Gibson model[44] we get:[3]

$$I(t) = \frac{(n_o^2 s/RN)\exp(-\Delta E/kT)}{\{1+(n_o s/RN\beta)\int_{T_o}^{T}\exp(-\Delta E/kT)dT\}^2} \qquad (2.17)$$

where $R = A/A_r$. This is called the "second-order (bimolecular) kinetics equation". In those cases where neither the Randall-Wilkins nor the Garlick-Gibson model is true use is made of the following empirical form (known as "the general-order kinetics" equation)[3]:

$$I(t) = \frac{(n_o^2 s/RN)\exp(-\Delta E/kT)}{\{1+[(b-1)n_o s/RN\beta]\int_{T_o}^{T}\exp(-\Delta E/kT)dT\}^{(b/(b-1))}} \qquad (2.18)$$

where b is the kinetic order and is neither 1 nor 2.

An example of an application of such an analysis has been recently given for CaF_2:Mn. It has been suggested that the TL glow curve at 80-300K is described by 1.4-order kinetics with $s = 2.74\times10^4 s^{-1}$, $\Delta E = 0.234$eV, and $\beta = 0.079 Ks^{-1}$.[45] It has also been proposed that the ~280°C TL dosimetry peak cannot be described by first or second-order kinetics but is well described by the more general-order kinetics.[46]

To avoid approximations in the analytical solutions to the rate equations (2.9a-c) one can solve the equations numerically. Bräunlich and Scharmann[47] and McKeever et al[48] did so and concluded that a fit to an experimental glow curve to the first, second or general order formalisms cannot be used to indicate that the simple model is necessarily valid. Thus there will be an ambiguity in the results obtained from application of the type of analyses mentioned above. Due

to the uncertainty in the nature of the TL process in CaF_2:Mn, CaF_2:Ce,Mn and CaF_2:Ce, we did not perform such analysis in this work.

Application of thermoluminescence

The various applications of TL were first suggested by Farrington Daniels and his co-workers in the 1950's.[3]

One of these applications is in radiation dosimetry. Exposure of a thermoluminescence dosimeter (TLD) to ionizing radiation results in the absorption of energy (via electron-hole pair production and filling of the localized energy levels). The intensity of the TL is then proportional to the energy stored in the specimen. The first material to be used as a TL dosimeter was LiF following an atomic weapon test in the 1950's.[3] Since then the application of TL in radiation dosimetry has been very widespread.

The application of TL in solid state physics can provide useful information on the properties of the various types of defect present within an insulator or semiconductor. Its sensitivity is supreme, thus it could be a valuable tool for the detection of trace impurities. Even in most "pure" materials the presence of impurities is considered essential for the TL to occur. However, application of this technique on its own, does not describe the defect structure of a solid. It is only when used in conjunction with other experimental methods that the information gained can be very useful.

Some other applications of TL are in age determination, geology, and biology (see reference (3)).

Thermoluminescence processes in CaF_2

Research in thermoluminescence at the Naval Research Laboratory[49] resulted in the development of CaF_2:Mn, a synthetic CaF_2 phosphor suitable for TLD. This phosphor has a high radiation sensitivity. However, it has a surprisingly high fading rate. In recent years rare-earth doped CaF_2 has also been used successfully in thermoluminescence dosimetry where the luminescence properties of the rare-earth ions has made these materials sensitive radiation dosimeters.

Due to the widespread usage of both CaF_2:RE and CaF_2:Mn in TL dosimetry and in order to overcome problems such as the lack of reproducibility (batch-to-batch variation) and of reusability when using these dosimeter materials, a knowledge of the TL mechanisms (i.e. the identification of the defects involved in the production of TL) would prove useful. Although there has been considerable research effort into the TL properties of CaF_2:Ce and CaF_2:Mn, the exact TL mechanisms in these materials are still uncertain.[5,6,7,8,11,12]

For example Sunta[8] suggests that the TL mechanism in CaF_2:Mn is as follows. The electrons which are produced along with holes during ionizing radiation are trapped by traces of RE^{3+} ions. Holes are trapped elsewhere (at unspecified sites). Heating releases holes which recombine to form RE^{3+*} (RE^{3+} ion in an excited state). The nonradiative de-excitation energy from RE^{3+*} to RE^{3+} is then transferred to Mn^{2+} ions located in the close vicinity. This produces Mn^{2+*} (Mn^{2+} in an excited state) followed by the relaxation to Mn^{2+} and the emission of 495nm light. He claims that the Ce^{3+} ion is acting as a sensitizer for emission from Mn during TL production in this material. This author[6] also suggests that in the natural mineral, fluorite,

electrons are trapped at Ce^{3+} during irradiation reducing it to Ce^{2+}. Holes are trapped at F^-_{int}, lattice F^- or at O^{2-}_{sub} sites. Thus forming hole centers with different thermal stabilities. Heating releases the holes which recombine with Ce^{2+} leaving it in Ce^{3+*} followed by deexcitation to the ground state Ce^{3+} and production of TL light (317, 338 and 380nm). In these mentioned models, there is no evidence regarding the energy transfer, the nature of both the hole and the electron sites and the recombination mechanisms (these are the main ingredients of a TL model). Obviously there is no basis for suggesting a possible TL mechanism in these materials, thus they are pure speculation.

Section D

Absorption and emission of electromagnetic radiation

Since a major part of our study involves optical measurements i.e. absorption (excitation), and emission, some background concerning the processes and parameters involved is needed at this point.

Since absorption and emission are primarily concerned with transitions between different energy levels, focus should be centered upon those time-varying operators that can induce the transitions. In doing so one applies time dependent perturbation theory which addresses the following problem. Initially the unperturbed system is in an eigenstate of $\hat{H}_o$ (Hamiltonian of the system). Then the perturbation, $\hat{H}_1(t)$, i.e. an electromagnetic field (oscilating or harmonic function) is "turned on". What is the probability, after time t, that a transition to another state (of H_o) occurs?

This problem is solved in many quantum mechanics and spectroscopy books.[50,51] We give here only the results. The interaction between the electrons and the radiation field introduces simultaneous transitions between electron states and the photons in the radiation field. The transition probability per unit time is

$$P = (4\pi^2/h)\left|\int \psi_f^* H_1 \psi_i d\tau\right|^2 \rho(E) \tag{2.19}$$

where $\rho(E)$ is the density of states, and h is Plank's Constant.

For electric-dipole allowed transitions we have for the probability of emission per second

$$P_{emission} = (N+1)(64\pi^4\nu^3/3hc^3)\left|\mu_{if}\right|^2 \tag{2.20}$$

N being the mean number of photons of energy $h\nu$ (if N=0 we have spontaneous emission), c is the speed of light and

$$\vec{\mu}_{if} = e\vec{r}_{if} \; ; \; \vec{r}_{if} = \int \psi_f^* \vec{r} \psi_i d\tau. \tag{2.21}$$

where $\vec{\mu}$ is the dipole moment operator and ψ_i and ψ_f respectively refer to the initial and final states. The absorption probability rate is

$$P_{abs} = (N64\pi^4\nu^4/3hc^3)\left|\vec{\mu}_{if}\right|^2. \tag{2.22}$$

The luminous emission intensity per second from an atomic emitter (photon energy $E=h\nu$ multiplied by the transition probability), is

$$I(h\nu) = (64\pi^4\nu^4/3c^3)\left|\vec{\mu}_{if}\right|^2. \tag{2.23}$$

The absorption coefficient $\alpha(E)cm^{-1}$ is given by

$$\alpha(E) = \sigma(\nu) \times N_c \tag{2.24}$$

where $\sigma(\nu)$, the effective cross-section, is by definition

$\sigma(\nu)$ = absorption transition probability rate/ photon flux per sec.

$$= 8\pi^3\nu\left|\vec{\mu}_{if}\right|^2/3hcd\nu, \tag{2.25}$$

where the effective cross section is obtained in practice over all the possible neighboring energies to $h\nu$ for the absorbed photons

$$\int\sigma(\nu)d\nu = (8\pi^3\nu/3hc)|\vec{\mu}_{if}|^2 \qquad (2.26)$$

and N_c, the defect concentration of the absorbing impurity is given by Smakula's formula.[52]

$$N_c(cm^{-3}) = [0.87\times10^{17}n/(n^2+2)^2f_{nm}]\alpha_{max}(\nu)(cm^{-1})\gamma(eV) \qquad (2.27)$$

where $\gamma(eV)$ is the full-width-at half-maximum of the absorption intensity assuming a Gaussian shape; n is the index of refraction and f_{nm} is the oscilator strength.

The quantum yield is defined as a ratio of the number of photons emitted from a given level to the number of photons absorbed by a given or overlying levels, namely:

$$\zeta = \Sigma A_{mn}/\Sigma A_{mn}+\Sigma C_{mn} \qquad (2.28)$$

where A_{mn} is the transition probability from level m to the level n. C_{mn} is the probability of radiationless transition from level m to level n.

Sensitized luminescence

Sensitized luminescence refers to "the process whereby an impurity atom (activator) having no appreciable absorption band in a given region of the (visible or UV) spectrum is made to emit radiation upon excitation in this region as a result of absorption by, and transfer from, another impurity atom (sensitizer) or from the host lattice."[53]

There are two basic mechanisms of energy transfer:[53]

(1) Radiative energy transfer-absorption by an activator (A) of those photons which are emitted by a sensitizer (S). It is essential that the sensitizer posesses strong fluorescence in a region over which the activator has strong absorption.

(2) Non-radiative (resonance) energy transfer. Excitation of the activator ion via a mutipole-mutipole or exchange interaction with the sensitizer ion. In this case no real photons are involved. An overlap between the sensitizer emission spectrum and the activator absorption spectrum is essential in all types of energy transfer in order for the transfer to occur.

The process of energy transfer can be broken into five steps:[53]
(1) absorption of excitation energy E_1 by the S ion which is raised to an excited state,
(2) relaxation of the legand ions surrounding the S ion leaving the S ion with the energy $E_2 (E_2 < E_1)$,
(3) transfer of energy E_2 to the A ion,
(4) relaxation of the lattice surrounding A, making the available energy $E_3 < E_2$,
(5) the transition on A to the ground state and the emission of a photon of energy E_3.

The pioneer work on the formalism of energy transfer via a resonant interaction was done by Föster[54,55] and Dexter.[53] The equations presented here are the ones developed by Dexter.[53]

If the sensitizer and the activator both have allowed electric-dipole transitions then the transition rate for the dipole-dipole interaction with absorption data for S and emission data for A is given as

$$P_{SA}(dd) = (3\hbar^4 C^4 Q_A / 4\pi n^4 K^2 R^6 \tau_S)(\varepsilon/\varepsilon_c)^4 \int (f_S(E) F_A(E)/E^4) dE. \quad (2.29)$$

which can be simplified as

$$P_{SA}(dd) = (1/\tau_S^o)(R_o/R)^6 \quad (2.30)$$

where

$$R_o^6 = (3\phi_S Q_A \hbar^4 c^4 / 4\pi K^2 n^4)(\varepsilon/\varepsilon_c)^4 \int (f_S(E) F_A(E)/E^4) dE, \qquad (2.31)$$

where τ_S^o is the lifetime of the sensitizer in the absence of activators, ϕ_S is the quantum efficiency of the sensitizers with activator present, $(\varepsilon_c/\varepsilon)$ is the ratio of the field within the crystal to that of an isolated atom, n is the index of refraction, R is the separation of the nuclei A and S, $f_S(E)$ is the normalized function representing the shape of the emission band, $F_a(E)$ is the absorption normalized function such that $\sigma(E) = QF_A(E)$ where $\sigma(E)$ is the absorption cross-section, E is the energy of the photon.

The energy transfer rate due to the exchange interaction can be written as

$$P_{SA}(ex) = (1/\tau_S^o)\exp[\gamma(1-R/R_o)] \qquad (2.32)$$

where $\gamma = 2R_o/r_b$ and

$$\exp(\gamma)/\tau_S^o = (2\pi K^2/\hbar) \int f_S(E) F_A'(E) dE.$$

where r_b is an effective Bohr radius, R_o is the critical transfer distance and K is a constant with the dimensions of energy. The exchange mechanism will allow transfer to, and excitation of, A by all types of allowed and forbidden transitions, including for example, L=0 to L=0 transitions. From equation (2.32) it can be seen that the exchange energy transfer rate will vary as the exponential of the sensitizer-activator separation as compared to the R^{-6} dependence of the dipole-dipole rate.

The phenomena of energy transfer (the mechanism and the centers involved) in CaF_2:Ce,Mn has been investigated by several researchers.[9,10,56,57] Ginther[9] suggests that Ce ions and aggregates of Ce ions in CaF_2:Ce,Mn act as sensitizers for Mn. He believes that the distance between Ce and Mn, in order for energy

transfer to take place, should be from 30 to 80 lattice sites. He further believes that this variation in distance is due to the competition between the two types of sensitizing centers. Leach[56] proposes that the energy transfer from Ce to Mn is via an exchange interaction in which the excitation energy is transfered by a "spin flip" transition. Sen and Bose[10] claim that in CaF_2:Ce,Mn energy transfer occurs not only from Ce to Mn centers but also from Ce to Ce and Ce to perturbed levels of the lattice (F^- ions). McKeever et al[57] suggest that, during photoluminescence efficient energy transfer from Ce^{3+} ions in tetragonal sites to Mn^{2+} takes place. They further believe that during X-ray induced luminescence and thermoluminescence, Ce in cubic sites and in PC centers dominate these processes and energy transfer to Mn is not of major importance.

Section E

Thermally stimulated depolarization currents

TSDC is the generating of currents due to the release of a polarized state within a solid dielectric. The net polarization of a solid dielectric in the presence of an external electric field may be the result of the contributions from the major sources listed below:

(I) Electric polarization i.e. the deformation of the electronic shell. The time required for this process is about 10^{-15}s.

(II) Atomic polarization i.e. the atomic displacement (deformation effect) in molecules with heteropolar bonds. The time required for this process is about 10^{-14} to 10^{-12}s.

(III) Orientational or dipolar polarization i.e. alignment of the permanent molecular or ionic dipoles with the applied electric field.

The time required for this process can be as low as 10^{-12}s or long enough that no relaxation is observed under the conditions of observation.

(IV) Translational or space-charge polarization, i.e. free charges (ions or electrons or both) are moved toward the electrodes. The time required can vary from milliseconds to years.

All of the above mentioned internal polarizations lead to surface charges which have the opposite polarity to those of the polarizing electrode.

Here we focus only on dipolar and space charge polarization. The former is the result of the polarization of point defect dipoles in ionic crystals.

The principle of the TSDC method as shown in figure (20) consists of three steps:

(1) application of a dc bias at temperature T_p, i.e. polarization of the dipoles;

(2) cooling under this bias to some lower temperature T_o (e.g. liquid nitrogen temperature) and removal of the field, i.e. "freezing" the dipoles in their polarized positions;

(3) heating (at a constant heating rate β) the polarized sample up to or above the polarization temperature (T_p). Current discharge becomes measurable and gives rise in the external circuit (short circuit condition) to a current. The current is normally displayed as a function of temperature known as a TSDC spectrum.

The first consistent theory of TSDC was introduced in 1964 by Bucci and Fieschi.[58] The dipolar polarization at any time and temperature is governed by the competition between the orienting action

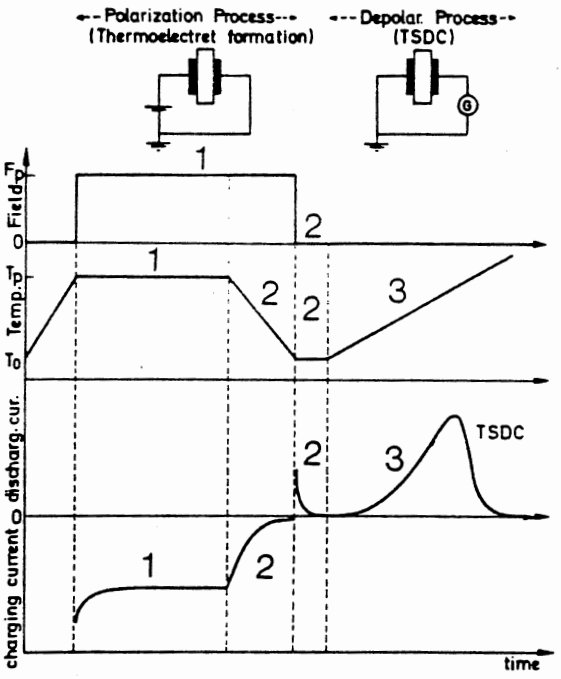

Figure 20. Principle of TSDC method. (After Vanderschern et al[59]).

of the field and the randomizing action of the thermal motions. Assuming "a symmetrical two site barrier" model (the Frölich model) for creating polarization, the build up of polarization P in a unit volume of the material at time t, subject to an electric field F_p at temperature T_p is:

$$P(t) = P_e[1+\exp(-t/\tau)], \tag{2.33}$$

where P_e (frozen-in polarization) is the equilibrium or steady state polarization. At very high field and for all but the lowest temperature this has been shown by Langevin to be

$$P_e = N_D\mu^2F_p/3kT_p \tag{2.34}$$

where N_D is the concentration of dipoles; μ is the electric dipole moment; k is Boltzmann's constant; F_p is the local electric field operating on the dipoles; and τ, the relaxation time, is given by an Arrhenius-type equation,[59] viz:

$$\tau(T) = \tau_o\exp(E_o/kT). \tag{2.35}$$

Here, τ_o^{-1} is called the characteristic frequency factor. A discussion about the form of τ_o^{-1} was given in section (B) and E_o is the activation energy for the dipole rotation (assuming that the volume and pressure do not change during the experiment, otherwise activation enthalpy (H = E+PV) is to be used).

If the relaxation times for polarizing and depolarizing the dielectric can be considered identical, the decay of polarization after removal of the field at $t=\infty$ is given by[59]

$$P(t) = P_e\exp(-t/\tau) \tag{2.36}$$

and the corresponding depolarization current density can be written

$$J(t) = -dP(t)/dT = P(t)/\tau. \tag{2.37}$$

Assuming a temperature increasing linearly with time from a value T_o at

a rate β so that

$$T = T_o + \beta t \tag{2.38}$$

and rewriting equation (2.36) to be

$$P(t) = P_e[\exp(-\int_o^t dt/\tau)] \tag{2.39}$$

then the current density J_D during a TSDC experiment is

$$J_D(T) = (P_e(T_p)/\tau_o)\exp(-E/kT)\exp[-(1/\beta\tau_o)\int_{T_o}^{T}\exp(-E/kT')dT'] \tag{2.40}$$

TSDC analysis

The experimental data obtained for $J_D(T)$ is fitted into the Bucci-Fieschi equation (equation(2.40)) , in order to calculate parameters such as E and τ_o. By using the following equation the dipole concentration can be calculated

$$N_D = 3P_e kT_{eff}/\mu^2 F_p \tag{2.41}$$

where T_{eff} (the effective polarization temperature) is given by

$$T_{eff} = E_o/k\ln(\tau_o). \tag{2.42}$$

Expression (2.40) is valid only for single-valued relaxation times or activation energies. In the cases where the relaxation processes occuring in solids deviate considerably from the "two barrier model" given by equation (2.33), the expression (2.40) should be modified by some empirical parameters characteristic of some kind of distribution function of relaxation times or activation energies. Physically the existance of a spectrum of relaxation times or activation energies can be explained by several mechanisms, e.g. dipole-dipole interactions, variations in the size and shape of the rotating dipolar entities, clustering of dipoles, and anisotropy of the crystal structure in which the dipoles are located.

For example in materials with a high dipole concentration the

interactions among the dipoles lead to a broadening of the dipole reorientation curve. For increasing concentrations, the half-width of the TSDC peak increases. The position of maximum depolarization current, on the other hand, is not affected by dipole-dipole interactions. This feature has been explained to be due to the fact that the dipole-dipole interaction results in activation energy not being single-valued but instead having a distribution of values scattered about a mean value E_o.[60-64]

As an example of the effect of dipole-dipole interactions on a TSDC curve, Den Hartog and his group,[60] from an investigation of the effect of the Ce^{3+} concentration on the reorientation of dipoles in SrF_2:Ce^{3+}, observed that the shape of the dipole reorientation curve changes with the concentration of dipoles even for fairly dilute systems. They propose that this is due to dipole-dipole interactions. The activation energy is not single-valued, but is distributed about the mean value E_o; and consequently the width of the distribution p will increase with increasing dipole concentrations. Figure (21) shows an example of the improvement in the experimental fit when a Gaussian distribution of the activation energy about E_o is considered. The Bucci-Fieschi equation now has the following form:

$$J_D^*(T) = J_D(T)F(E_o,\tau_o,p,T), \tag{2.43}$$

where F is a correction term given by:

$$F(E_o,\tau_o,p,T) = (1/p\sqrt{\pi})\int_0^\infty dE \exp\{-((E-E_o)/kT)-((E-E_o)^2/p^2)\}$$
$$-\int_0^T (a dT'/\tau_o)[\exp(-E/kT')-\exp(-E_o/kT')] \tag{2.44}$$

where a is a constant and p is the width of the distribution.

Wagner and Mascarenhas[65] report that the rotational energies of the RE-F^- complexes (C_{4v} centers) in CaF_2 increase when the ionic

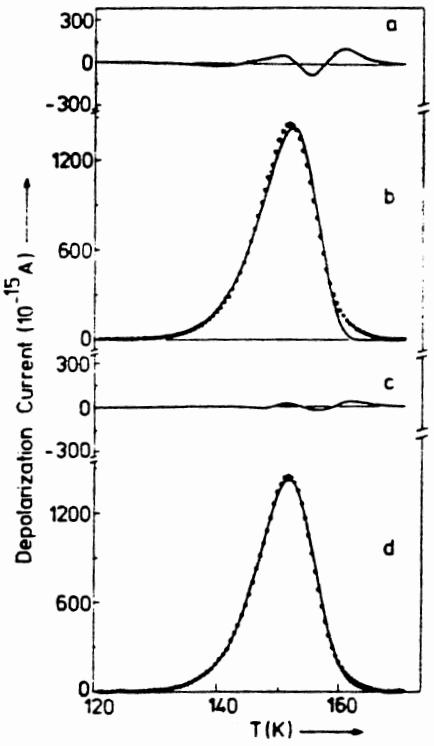

Figure 21. Example of the improvement that is achieved when dipole-dipole interactions are taken into account. (b) Experimental and the best-fit by a three parameter TSDC formula (i.e. equation (40)); results: E=0.42eV, $\tau_o=10^{12}$ sec. (d) Same points fitted by a four parameter formula (equation (43); results: E_o=0.48eV; p=0.007eV, $\tau_o=10^{-14}$ sec. (a) and (c) give the vertical distance between the experimental points and the fitted curve. (After Weperen et al[60]).

radius of the RE ions increases. Royce and Mascarenhas[66] from an investigation of CaF_2:Ce report that, for crystals having a nominal concentration of Ce between 0.01 and 0.05 mole percent, E=0.46±0.02eV with $\tau_o = (6\pm4)\times10^{-15}$sec. They also report that for higher Ce concentration (0.1%) the activation energy and τ_o were dependent upon the fractional number of free dipoles. The smallest number of free dipoles resulted in the activation energy being lowest (0.36eV) and τ_o having the largest value (10^{-12}sec). These reported parameters by Wagner and Mascarenhas[66] are obtained by fitting TSDC data into Bucci-Fieschi equation (2.40). It has also been suggested by Wagner and Mascarenhas[14] that X-irradiation reduces the size of the TSDC peak in CaF_2:Ce (i.e. a reduction in the C_{4v} dipole concentration), and, furthermore, they conclude that for each four dipoles destroyed one photochromic center is formed (see section B).

CHAPTER III

EXPERIMENTAL DETAILS

Section A

Sample preparation

The samples used in this work were all purchased from Optovac Inc. They were grown using Optovac's double crucible technique to minimize oxygen contamination. Neither optical absorption nor luminescence due to oxygen were observed in this work. The samples used had nominal impurity (mole%) concentrations as follows:

(i) CaF_2:Mn-0.001%; 0.01%; 0.1%; 0.5%; 1.0% and 3.0%.

(ii) CaF_2:Ce-0.01%; 0.1%; 0.5%; 1.0%; 1.5% and 2%.

(iii) CaF_2:Mn,Ce-0.5%, 0.01%; 0.5%, 0.1%; 0.5%, 0.5%; and 0.5%, 2.0%.

(iv) CaF_2:Ce,Mn-0.5%, 0.001%; 0.5%, 0.01%; 0.5%, 0.1%; 0.5%, 0.5%; and 0.5%, 2.0%.

The samples used in the thermoluminescence measurements were in powder form. Tribothermoluminescence signals were very small compared to radiation-induced TL signals. The crystals were cut and polished along the (001) plane, with the thickness ~ 1mm, for optical measurements. The thicknesses of the samples used for the TSDC measurements were about 1 to 3mm with gold coating on the faces of the (001) plane.

Section B

Experimental configuration

Thermoluminescence

The schematic layout of the apparatus used to collect the thermoluminescence data is shown in figure (22). It consists of:

1. Cryostat. This houses the heater and it is connected to a vacuum pump (600 torr) and a N_2 gas tank.
2. Temperature controller (EUROTHERM). This device maintains a constant heating rate (usually chosen as $2.08^{o}s^{-1}$ in this work).
3. Photomultiplier tube (EMI9635QB) operating in the integral current mode. This device was used to measure the intensity of the thermoluminescence light.
4. High voltage DC power supply (BERTAN MODEL 215) for P.M.T.
5. Digital multimeter (KEITHLEY 195). This device was used to read the sample temperature through a Chromel-Alumel thermocouple.
6. Picoammeter (KEITHLEY 480). This device was used to read the current from the P.M.T.
7. Chart recorder (Omniscribe). This was used to record the thermoluminescence data, as intensity versus time.
8. Computer (HP 86 P.C.). This device was used to store the thermoluminescence data for subsequent data analysis.

Thermally Stimulated Depolarization Currents

Figure (23) displays the experimental configuration used to record the thermally stimulated depolarization current data. It

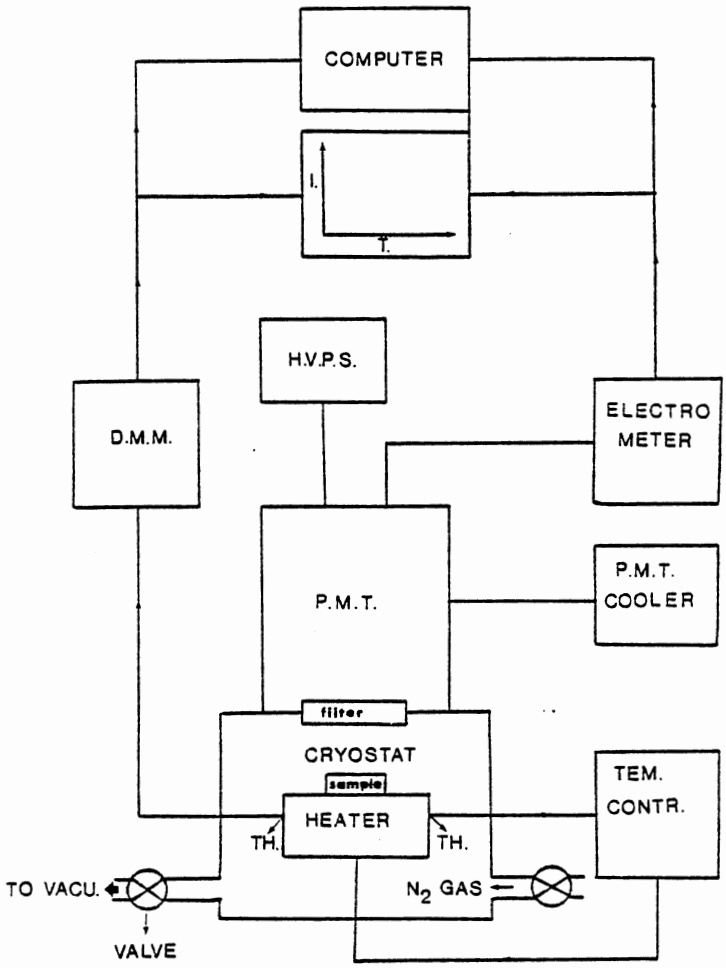

Figure 22. Schematic layout of the TL equipment as described in text.

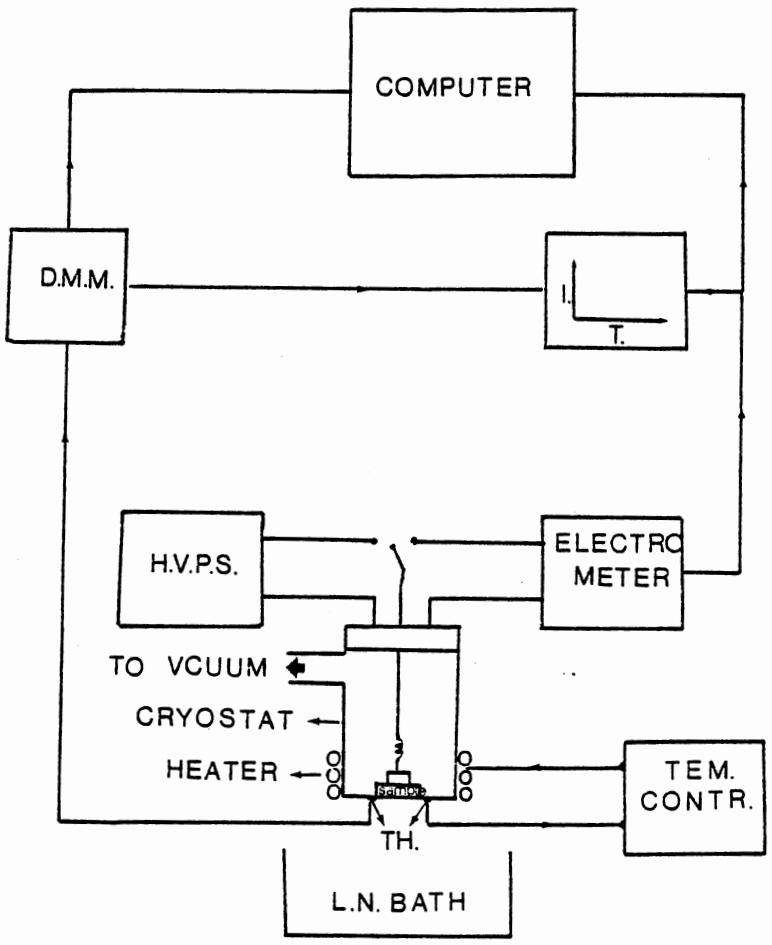

Figure 23. Schematic layout of the TSDC equipment as described in text.

consists of:

1. Liquid nitrogen cryostat. This houses the sample and it is connected to a vacuum pump for maintaining a vacuum of ~ 4×10^{-6}mbar.

2.Temperature controller (EUROTHERM) to maintain a constant heating rate (0.1 to $0.2^{o}s^{-1}$).

3. High voltage power supply (HP6515A DC) to polarize the sample (usually V_p=1000V).

4. Digital multimeter (KEITHLEY 195) to read the temperature of the sample through a copper-constantan thermocouple.

5. Electrometer (KEITHLEY 616). This device was used to measure the current.

6. Chart recorder (HP 2035B). This device was used to record the TSDC spectra.

7. Computer (HP 86 P.C.) This device was used to store the data. Curve fitting of the TSDC curves was also performed on this machine using a nonlinear, least square fitting routine.

Photoluminescence

The experimental configuration used to collect photoluminescence data is shown in figure (24) and consists of:

1. Oriel monochromator. This device was used to select the excitation wavelength from a 150W Xenon lamp. The grating blazed at 280nm with 1200 lines/mm. The slit widths were 1-2mm.

2. Spex monochromator. This device was used as the selector of the emission wavelength The gratings used were blazed at 300nm and 500nm with 1200 lines/mm. The slit widths were 1-2mm.

3. Photomultiplier tube (EMI9635 QB). This device was used to detect

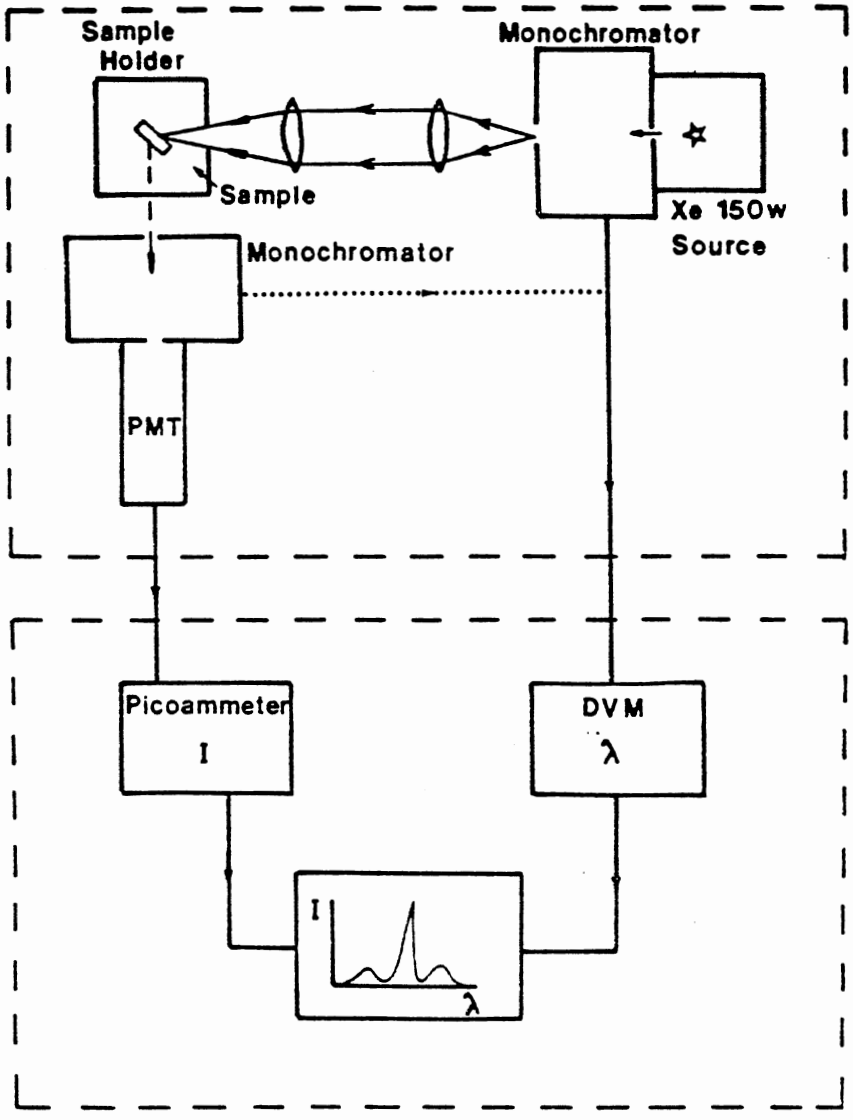

Figure 24. Schematic layout of the photoluminescence equipment as described in text.

the emission.

4. CaF_2 lenses for focusing the excitation beam on the sample.

5.X-Y chart recorder (HOUSTON INST. 200): used to record the excitation spectrum.

6. Omniscribe chart recorder: for recording the emission spectrum.

7. High voltage DC power supply (ORTEC) for maintaining DC voltage to the P.M.T.

8. Digital multimeter (KEITHLEY 195) for reading the wavelength.

9. Picoammeter (KEITHLEY 480) for reading the current from P.M.T.

Optical absorption

The optical absorption measurements were carried out on an IBM 9430 UV-visible spectrometer, with an accompanying IBM PC data station, and a PERKIN ELMER 330 spectrometer, with a 3600 Data Station.

The Xenon lamp and Oriel monochromator were also used as an optical bleaching source. Thermal bleaching was carried out in the TL oven as in the TL measurements. The samples were γ-irradiated by exposure to ^{60}Co source with a dose rate of $\sim 0.053 Gys^{-1}$. The photoluminescence data have not been corrected for the P.M.T. detection response or the emission response of the Xenon excitation source.

CHAPTER IV

THERMALLY STIMULATED DEPOLARIZATION CURRENTS

There were two major reasons which motivated us to investigate TSDC in CaF_2:Ce and CaF_2:Ce,Mn. First it has been suggested that the PC centers (figure 14) are formed from dipolar C_{4v} centers (figure 6) during irradiation. Thus this should result in the reduction of the number of dipolar C_{4v} centers which contribute to the TSDC peak.[14] Second it has also been reported that in order for energy transfer from C_{4v} centers to Mn to take place, the distance between these two centers should be at least ~40 lattice constants.[9] Thus we wished to examine, by using the TSDC method, whether we could detect the presence of the Mn ions possibly manifesting themselves via a change in the behavior of the relaxation of these dipoles.

In the sections to follow we report on the results that we obtained in our measurements concerning the above suggestions. And furthermore we present the results of calculations regarding other related informative features such as the closeness of two dipoles i.e. how close the two dipoles can be situated in order that their interaction affect their contribution to the size of the TSDC peak, but not to affect their optical absorption bands; and the order of the aggregation reactions for these dipoles.

We have obtained data from CaF_2 samples with nominal Ce concentrations of 0.01, 0.1, 0.5, 1.0, 1.5 and 2.0 mole percent and also from fixed Ce (0.5 mole percent) with variable Mn concentration

(0.001, 0.1, 0.5 and 2.0 mole percent). The TSDC peak for the dipolar C_{4v} center relaxation appears at ~158K (figures 25 and 26). These curves were "thermally cleaned" of undesired peaks in their lower and higher temperature regions for the purpose of proper data analysis. The "thermal cleaning" procedure consists of polarizing the sample at ~155K, cooling to L.N.T., and then heating to 145K. The parameters, activation energy E_B and relaxation time τ_B, were calculated by fitting the collected data into the Bucci-Fieschi equation (equation 2.40). The calculated values are listed in tables 1 and 2. Assuming the presence of dipole-dipole interactions which results in the broadening of the TSDC peak (chapter 2 section C) the data were also fitted into the modified Bucci-Fieschi equation (equation 2.43) which contains a correction term accounting for such a broadening effect (equation 2.44). The new calculated parameters E_I, τ_I and p, which reflects the width of the energy distribution about the mean value E_I are listed in tables 1 and 2. In all cases better fits were obtained with the modified Bucci-Fieschi equation. For example, compare figures (27) and (28). The sum-square which is the sum of the squares of the differences between the experimental and theoretical data for these fits (i.e. the Bucci-Fieschi and modified Bucci-Fieschi) are, respectively, 852 and 223. Clearly the lower value of 223 for the modified Bucci-Fieschi fit indicates a better fit.

By using the obtained values for the parameters E_I and τ_I and by application of equations (2.41), where $\mu = 4.0\ 10^{-29}$cm, the "apparent" dipole concentration, N_d^t (to be explained in section A), was calculated. The "actual" dipole concentration, N_d^o (to be explained in section A), is calculated by the application of Smakula's formula

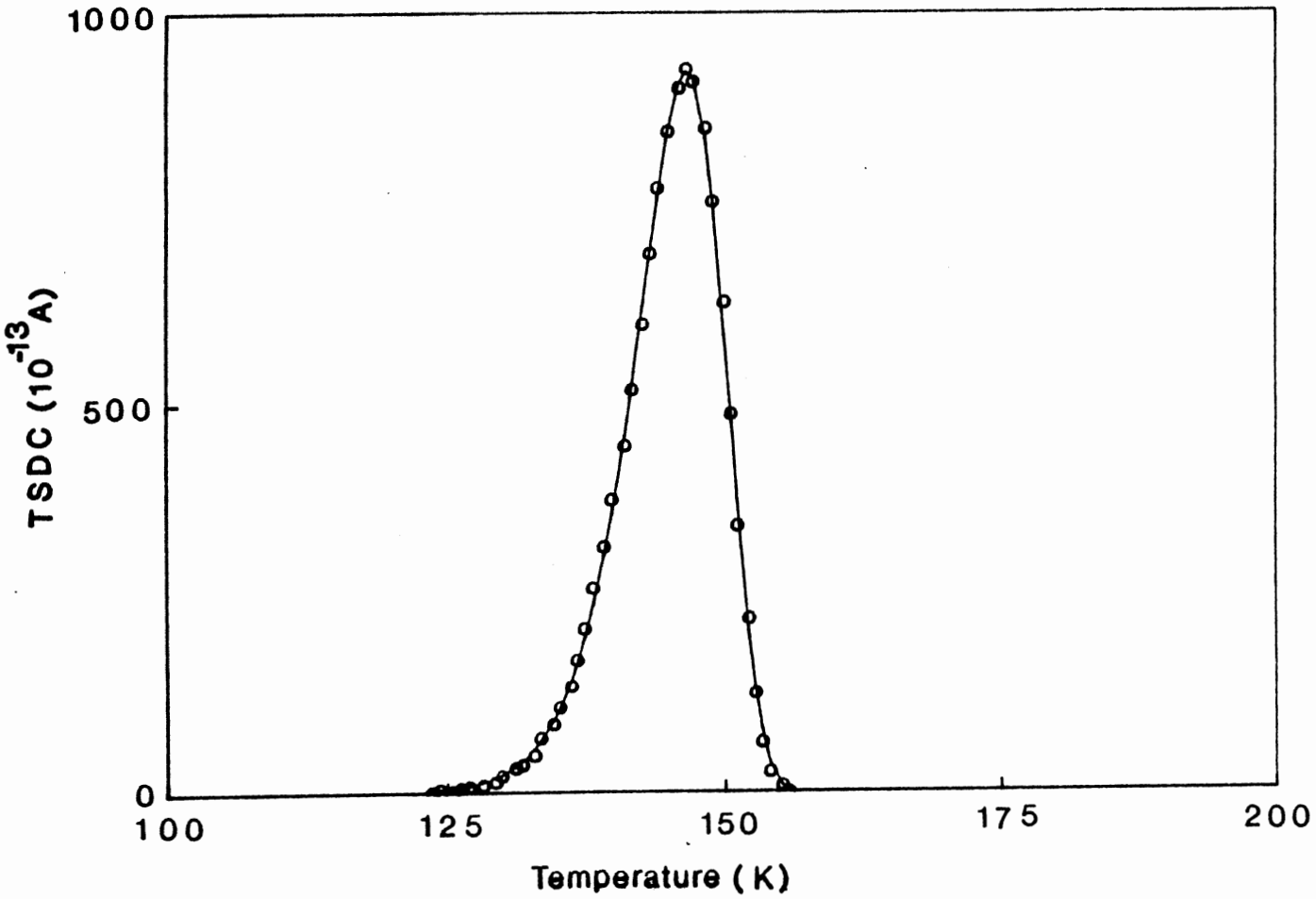

Figure 25. The TSDC spectrum from CaF_2:Ce (0.01%). Circles indicate experimental data, the solid line is the modified TSDC theoretical fit.

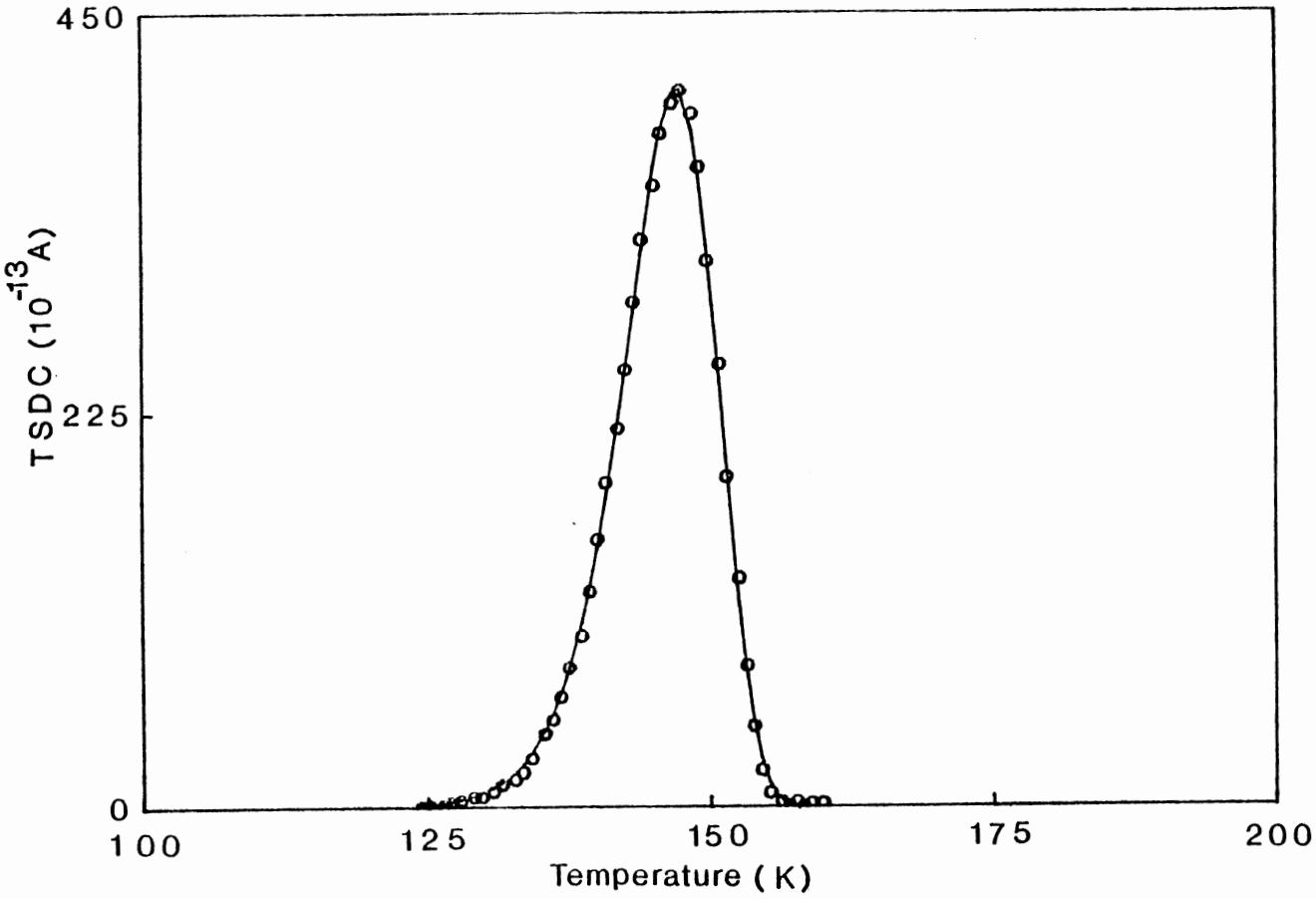

Figure 26. The TSDC spectrum from CaF_2:Ce,Mn (0.5%, 0.01%). Circles indicate experimental data; the solid line is the modified TSDC theoretical fit.

TABLE I

Values of the Ce melt concentration (mole %), N_d^t (apparent C_{4v} dipole concentration), N_d^o (actual C_{4v} dipole concentration), activation energies (E_B, E_I), relaxation times (τ_B, τ_I) and width parameters (p) for CaF_2:Ce.

Ce (mole %)	N_d^t (Cm^{-3})	N_d^o (Cm^{-3})	E_I (eV)	E_B (eV)	τ_I (s)	τ_B (s)	p (eV)
.01	3.14E18	5.16E18	.452	.452	6.33E-15	6.33E-15	-6.29E-5
0.1	3.66E18	8.45E18	.459	.459	3.63E-15	3.62E-15	6.17E-5
0.5	2.19E18	12.0E18	.459	.454	4.54E-15	6.67E-15	2.47E-3
1.0	1.24E18	14.4E18	.452	.433	8.58E-15	3.69E-14	4.84E-3
1.5	0.67E18	20.5E18	.453	.397	4.96E-15	4.64E-13	9.27E-3
2.0	0.48E18	20.6E18	.423	.368	5.34E-14	4.60E-12	9.55E-3

TABLE II

Values of the Ce and Mn melt concentrations (mole %), N_d^t (apparent C_{4v} dipole concentration), N_d^o (actual C_{4v} dipole concentration), activation energies (E_B, E_I), relaxation times (τ_B, τ_I), and width parameters (p) for CaF_2:Ce,Mn.

Ce,Mn (mole %)	N_d^t (Cm^{-3})	N_d^o (Cm^{-3})	E_I (eV)	E_B (eV)	τ_I (s)	τ_B (s)	p (eV)
.5,.001	1.74E18	7.54E18	.449	.436	4.95E-15	1.80E-14	4.45E-3
.5,.01	2.00E18	7.54E18	.465	.447	2.56E15	1.05E-14	4.62E-3
.5,.1	1.66E18	7.54E18	.466	.462	2.88E-15	4.19E-15	2.39E-3
.5,.5	1.30E18	7.54E18	.449	.449	10.5E-15	10.47E-15	7.0E-5
0.5,2.0	1.04E18	7.54E18	.439	.424	2.51E-14	8.17E-15	4.53E-3

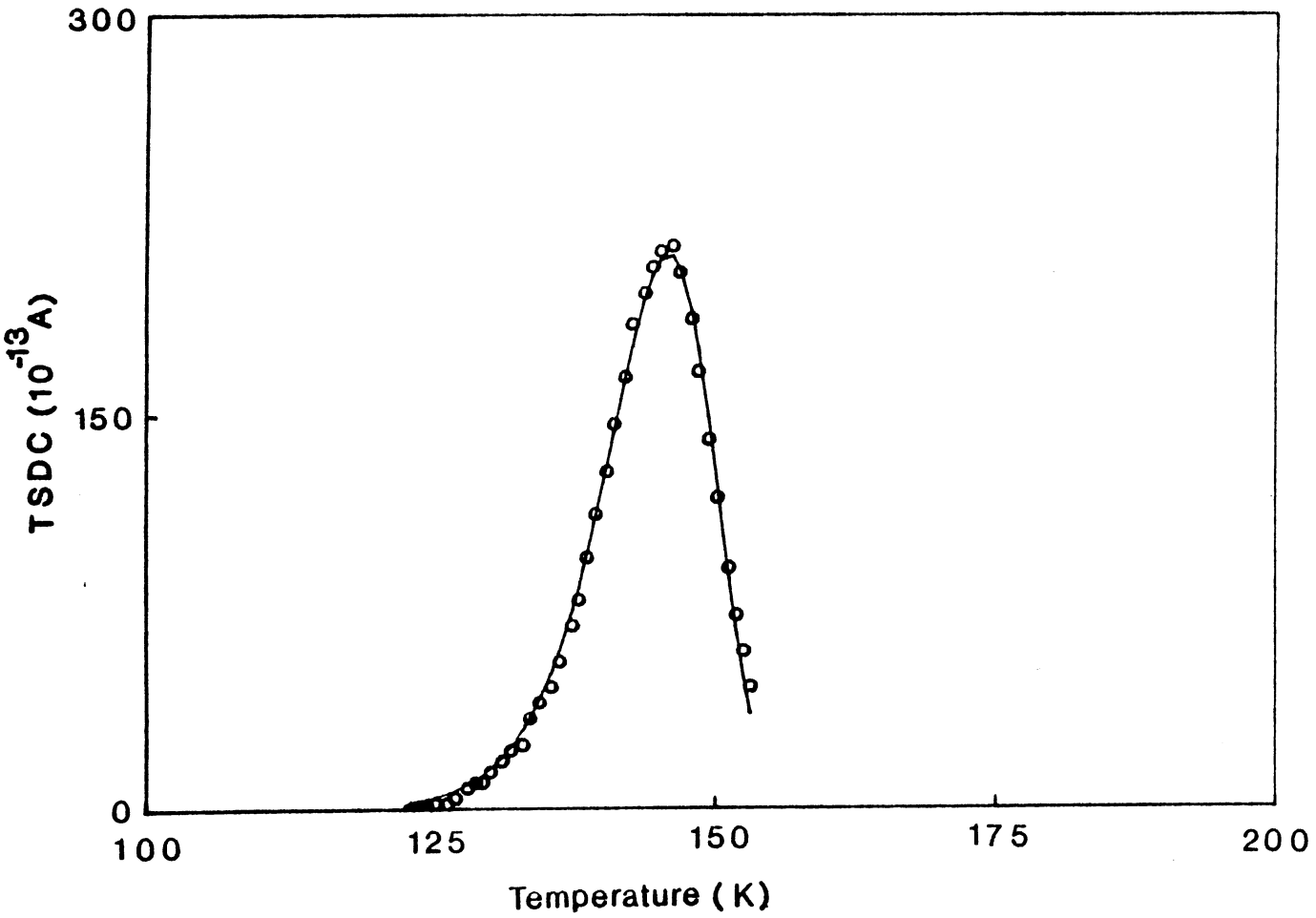

Figure 27. The TSDC spectrum from CaF_2:Ce (2.0%). Circles indicate experimental data, solid line is the Bucci-Fieschi TSDC theoretical fit. The sum square as defined in the text is 852.

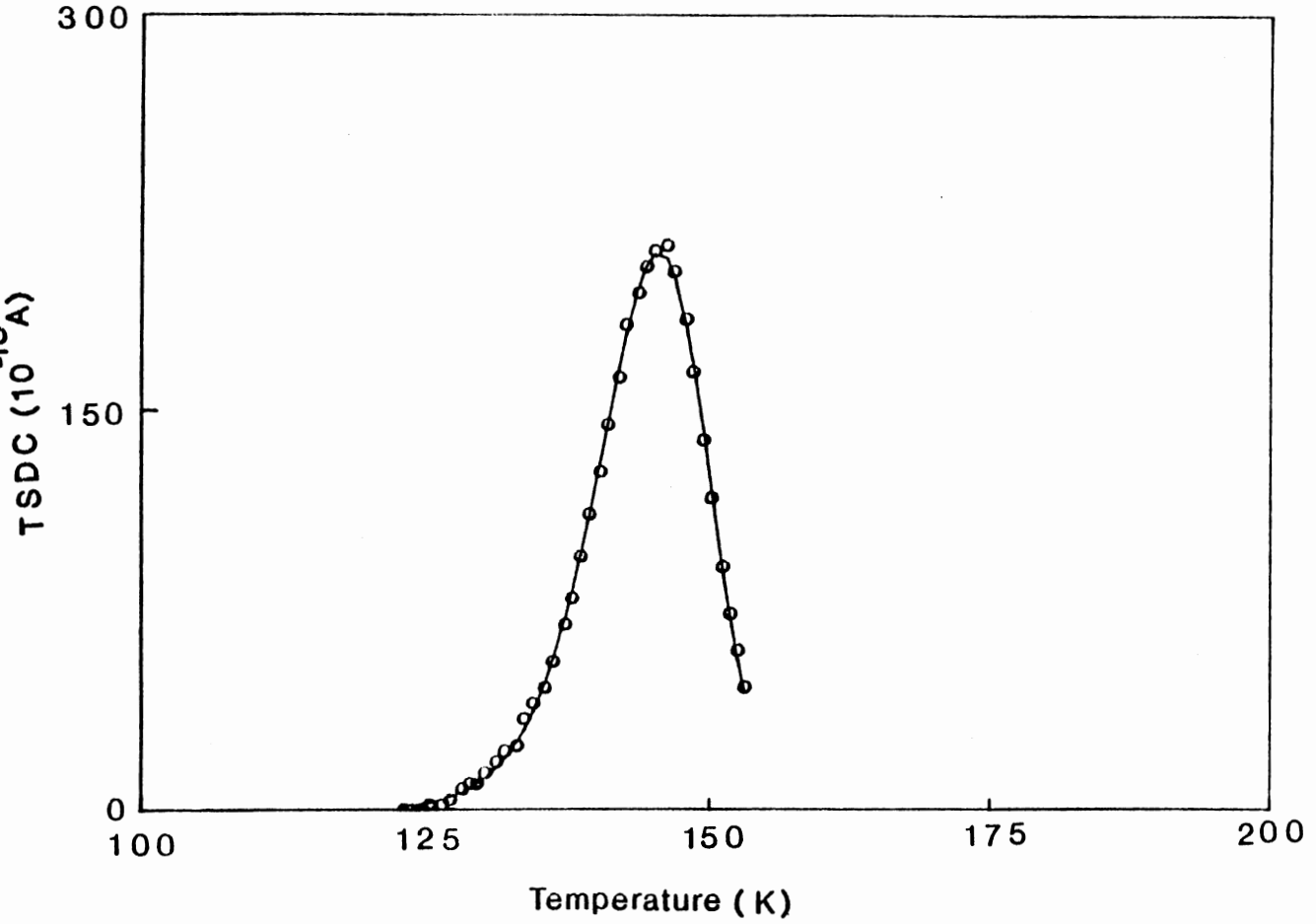

Figure 28. The TSDC spectrum from CaF_2:Ce (2.0%). Circles indicate experimental data, the solid line is the modified TSDC theoretical fit. The sum square as defined in the text is 223.

(equation 2.27) to the optical absorption band for the C_{4v} centers (303nm) shown in figure (5). The calculated values for N_d^t and N_d^o are given in tables 1 and 2.

Section A

$\underline{CaF_2}$:Ce

In figure (29) we plot N_d^t "apparent" dipole concentration versus N_d^o "actual" concentration. As can be seen there exists no one to one correspondence between N_d^t and N_d^o (dashed line). Instead as N_d^o is increased (with increasing Ce concentration), N_d^t, after an initial increase, actually decreases. We explain the effects as follows.

Assuming dipoles with a separation r, the rotational behavior of such dipoles is affected by the interaction between them for distances r less than R (i.e. for r<R they do no longer act as free dipoles). Now as the Ce concentration is increased the distances among these dipoles is decreased i.e. more and more dipoles now have separations r<R. Thus interaction among these dipoles results in a reduction of the net dipole moment (i.e. polarization) for the specimen. Consequently, this reduces the size of the TSDC peak from which the dipole concentration is calculated. Hence the dipole concentration calculated by the TSDC method represents an "apparent" dipole concentration not the "actual" dipole concentration. However, the 4f-5d transitions of the single 4f electron within Ce^{3+} ions in the C_{4v} dipoles are not affected by interactions among them. This is because the transitions are shielded by the outer shell electrons. Thus, the C_{4v} centers act as free dipoles from the point of view of optical absorption. Hence the calculated concentration will represent the "actual" concentration in these

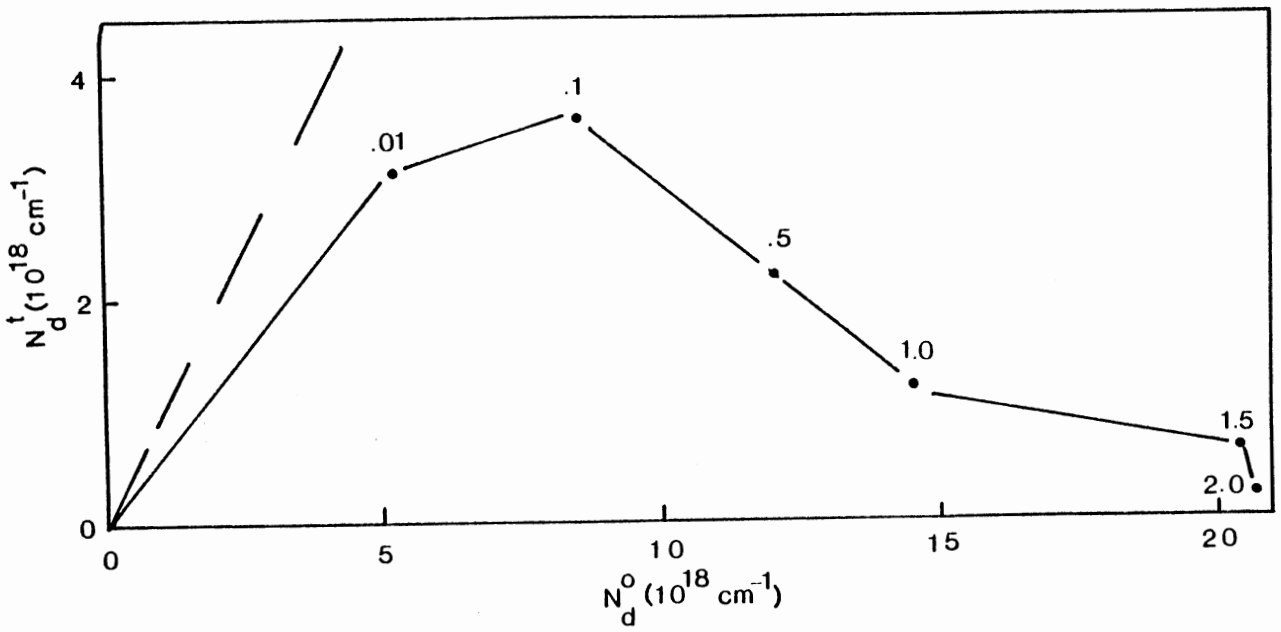

Figure 29. The concentration of C_{4v} dipoles as determined by TSDC as a function of the concentration of C_{4v} dipole concentration as defined by optical absorption. The dashed line represents the expected one to one correspondence between N_d^t and N_d^o. Each datum point as noted in the figure represents a different crystal of different Ce concentration (0.01, 0.1, 0.5 and 2.0%).

measurements. Based on this, as shown in figure (29), we should not obviously expect a one-to one correspondence between N_d^o and N_d^t.

Calculation of characteristic distance, R.

As we noted above the closeness of the dipoles (C_{4v} centres) to each other plays a crucial role in the dipole relaxation process. Thus, we found it informative, by using the following simple model (similar to the one given in reference 67), to estimate how close two dipoles have to be in order that the interactions between them affect the height of the TSDC peak.

Let us define the distance R between two dipoles to be the radius of a sphere such that the dipoles outside this sphere act as free dipoles, but inside the sphere they behave like a dipolar pair and do not contribute to the TSDC peak. If P(r) is the probability of not finding another dipole inside the radius r, then the probability of not finding another dipole inside a radius (r+dr) is:

$$P(r+dr) = P(r)P(dr)$$

$$= P(r)(1-4\pi r^2 dr N_d^o) \qquad (4.1)$$

where N_d^o is the concentration of free dipoles. After expansion of the equation (4.1) about the point r and integrating within the limits of a spherical volume of radius R, the probability of finding dipoles that contribute to the TSDC peak (i.e. they are not in the sphere of radius R) is given as:

$$P(R) = \exp-(4\pi R^3 N_d^o/3). \qquad (4.2)$$

Thus one can calculate the concentration of dipoles contributing to the TSDC peak from:

$$N_d^t = N_d^o \exp(-4\pi R^3 N_d^o/3). \qquad (4.3)$$

Rewriting equation (4.3) as

$$\ln(N_d^t/N_d^o) = -(4\pi/3)N_d^o R^3, \qquad (4.4)$$

and using the obtained experimental values for N_d^t and N_d^o from table 1, $\ln(N_d^t/N_d^o)$ can be plotted versus N_d^o. This is done in figure (30). The value for R is then obtained from the slope of the straight line in figure (30) and is found to be ~12.0 lattice sites. The values of R reported by other authors are 9 and 14 lattice sites.[67,74]

Effect of Ce concentration on E and p.

In figure (31) the values of E_B and E_I are plotted versus dipole concentration (N_d^o). The E_I value, except for the sample containing 2% Ce was found to remain constant as the dipole concentration increased; whereas E_B was found to decrease. The unexpected behavior of the E_B stems from using the Bucci-Fieschi equation from which E_B is calculated i.e. this equation does not include any correction term to account for the broadening of the TSDC peak. The modified Bucci-Fieschi equation however does account for this effect.

Figure (32) displays the width distribution (p) versus dipole concentration (N_d^o). As we see the width parameter increases as dipole concentration is increased. This observation, along with those of figure (31) are in agreement with the model presented by previous workers.[61-64] In this model it is proposed that due to dipole-dipole interactions, the activation energy E is not single-valued, but is distributed about a mean value E_I (E_I does not change, viz figure 31), and consequently the width of distribution p will increase with increasing dipole concentrations (viz. figure 32). Alternative possibilities for such behavior are changes in the dipole environment

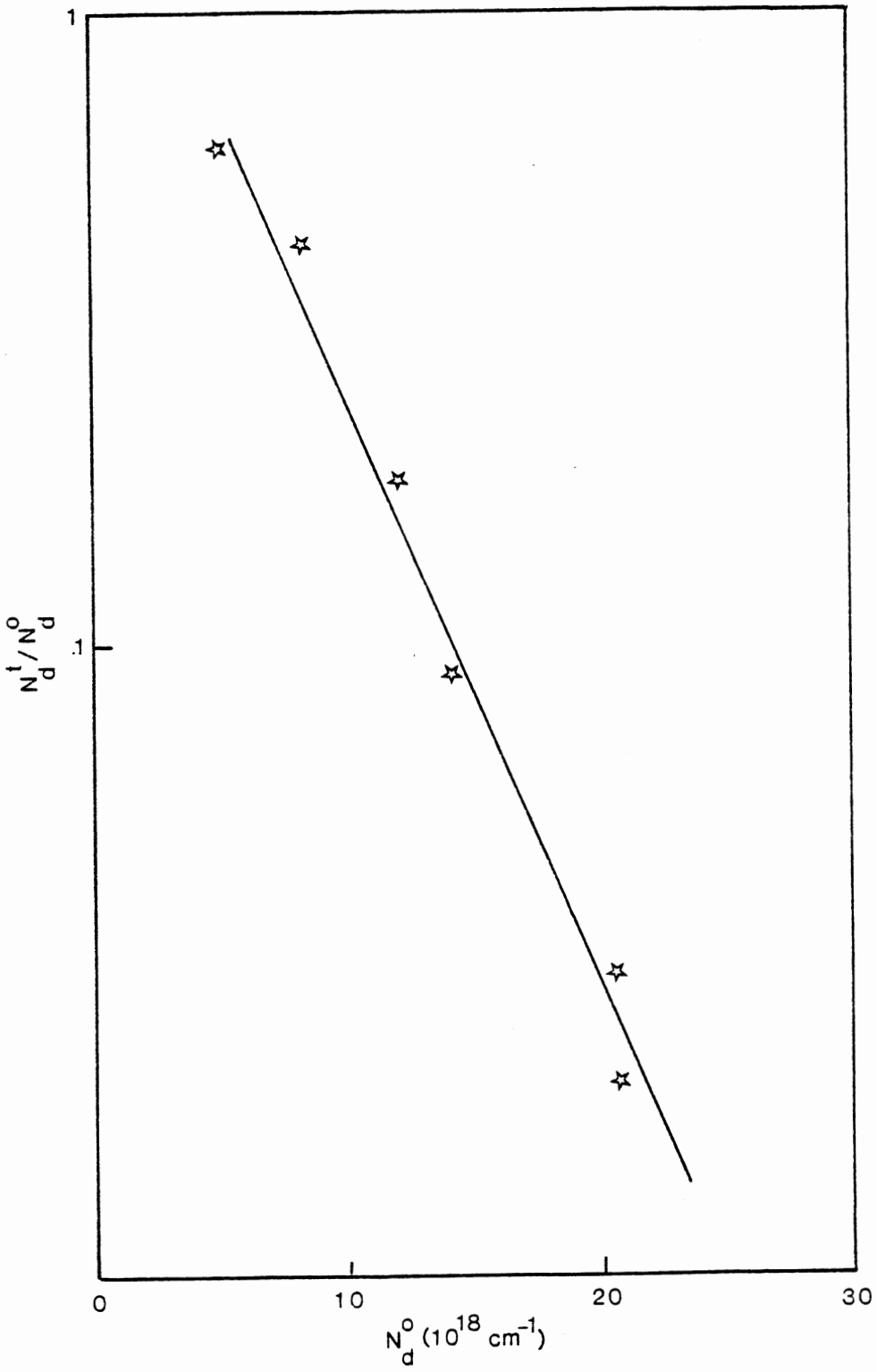

Figure 30. The logarithm of the ratio between N_d^t and N_d^o as a function of N_d^o. The value of R is calculated from the slope of the line.

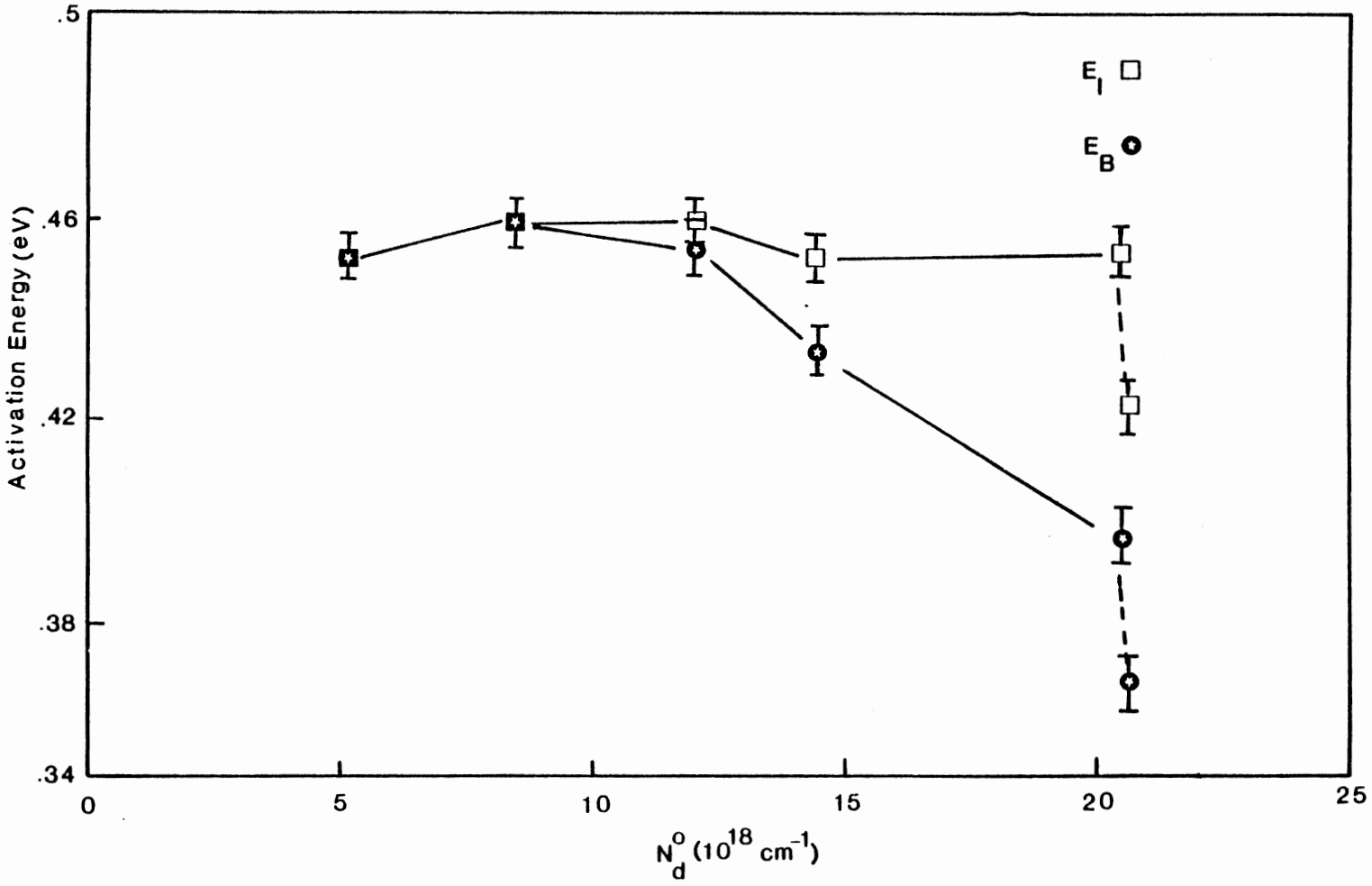

Figure 31. The variation in the activation energy (E_B, E_I) versus dipole concentration.

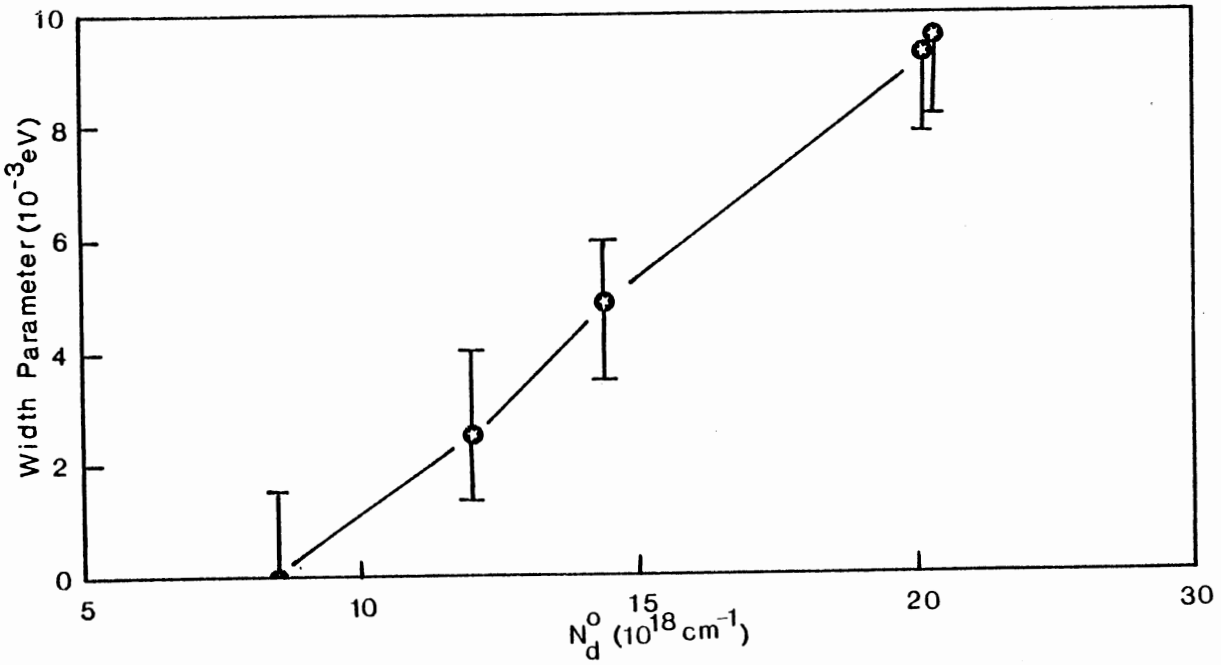

Figure 32. The variation in the width parameter p as a function of dipole concentration.

and clustering. However, since E_I value remains constant (figure 31), therefore the dipole environment does not change by much. Hence this cannot account for the above observations.

Order of clustering

It is well known that clusters are readily formed in rare-earth doped CaF_2.[68-72] Using audio-frequency capacitance and conductance measurements, it has been reported that in CaF_2 samples with low Ce concentrations there is a TSDC peak at ~400K which has the characteristic of a "gettered" 2:2:2 complex i.e. a usual 2:2:2 complex configuration plus an extra fluorine.[68] A 2:2:2 complex consists of 2 RE^{3+}, 2 interstitial fluorine along <001> and 2 displaced fluorine in lattice sites along <111> (figure 33).[72] At higher rare-earth concentration other types of clusters such as trimers are possible. It is unknown which is the dominant cluster in the CaF_2:Ce samples used by us. Therefore we wished, by the following calculation, to obtain the order of clustering in our samples.

All chemical reaction rates are proportional to the concentration of the reactants. The rate equations for reactions with such concentration dependence can be of the form:

$$\text{reaction rate} = k[C] \qquad \text{(1st. order)}$$

$$\text{reaction rate} = k[C]^2 \qquad \text{(2nd. order)}$$

$$\text{reaction rate} = k[C]^3 \qquad \text{(3rd. order)}$$

where C is the reactant concentration, k is the rate constant (see below). Reactions that proceed according to such simple rate equations are said to be reactions of the first, second, or third order as indicated. However not all reactions have such simple rate laws.[73]

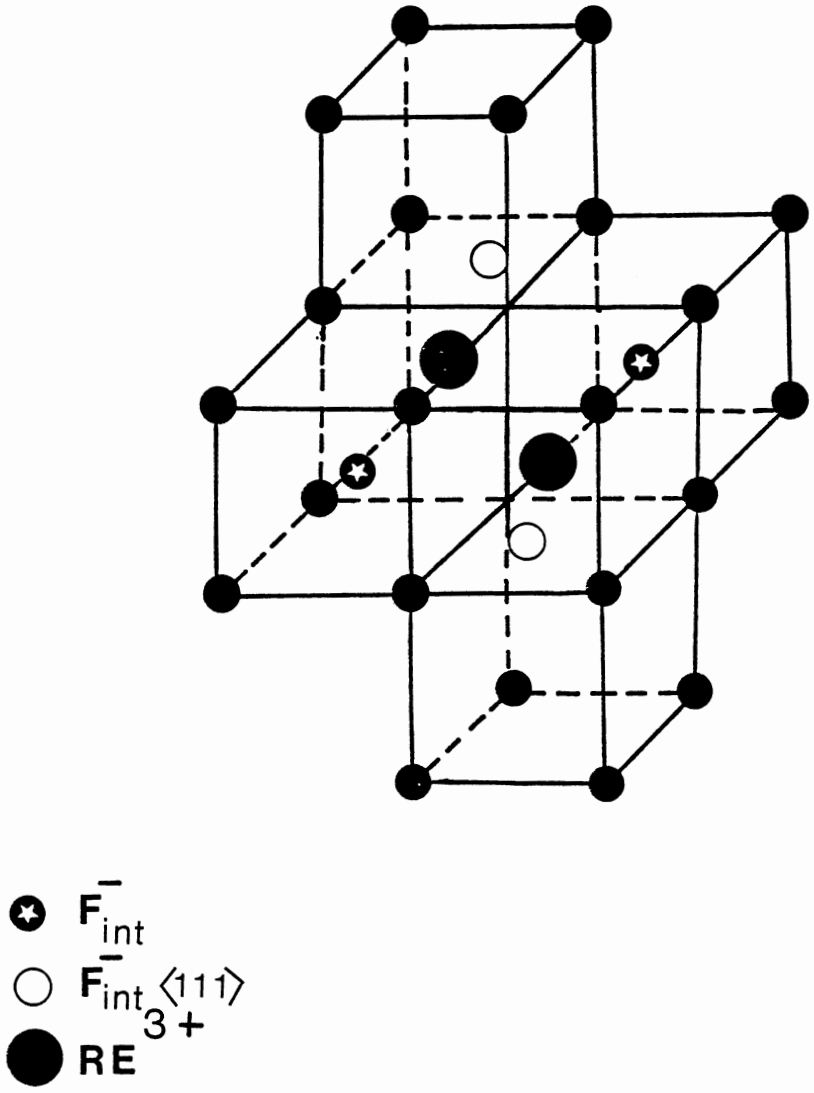

Figure 33. A 2:2:2 complex consists of 2 RE^{3+} ions, 2 interstitial fluorine ions along ⟨001⟩ and 2 displaced fluorine ions in lattice sites along ⟨111⟩.

We wish to apply these fundamental reaction kinetics to the following reaction between dipoles (D) and clusters (C) with respective concentrations N_d and N_c. The reaction considered is:

$$nD \leftrightarrow C_n. \tag{4.5}$$

In thermodynamic equilibrium, the law of mass action states:

$$kN_d = N_c \tag{4.6}$$

where k is given by

$$k = \exp(\Delta S/k)\exp(-\Delta H/kT) \tag{4.7}$$

where ΔS is the change in the entropy and ΔH is the change in the enthalpy for the reaction.

We assume only two possible reactions, i.e. second-order or third-order to yield dimers or trimers respectively, and let N_D and N_T denote the dimer and trimer concentrations respectively. The dimer and trimer reactions are written:

$$D + D \leftrightarrow C_2 \text{ (dimers)} \tag{4.8}$$

$$D + D + D \leftrightarrow C_3 \text{ (trimers).}$$

From the law of mass action we therefore have

$$N_D = kN_d^2 \tag{4.9}$$

$$N_T = kN_d^3 \tag{4.10}$$

The total Ce^{3+} concentration, C_o, for dimer and trimer reactions is given as

$$C_o = N_d + 2N_D \tag{4.11}$$

$$C_o = N_d + 3N_T. \tag{4.12}$$

Substituting (4.9) into (4.11), and (4.10) into (4.12) we have

$$C_o = N_d + 2k_1N_d^2 \tag{4.13a}$$

or

$$C_o = (1/2k_1)(1-X/X^2) \tag{4.13b}$$

$$C_o = N_d + 3k_2N_d^3 \qquad (4.14a)$$

or

$$C_o = [(1/3k_2)(1-X/X^3)]^{1/2} \qquad (4.14b)$$

In these equations $X = N_d/C_o$. By using the values for N_d obtained from the optical absorption measurements we can plot C_o against $(1-X/X^2)^{1/2}$ and against $(1-X/X^3)^{1/2}$. If the plot of C_o against $(1-X/X^2)$ gives a straight line, then dimer formation is indicated. Conversley, if the $(1-X/X^3)^{1/2}$ gives a straight line, then trimer formation is indicated.

By using the data for N_d^o and C_o in table 3 we found that the clustering reaction followed neither 2nd. nor 3rd. order (see figure 34). We believe this is because there are also higher-order clusters other than the simple 2nd. or 3rd.-order aggregates that we assumed in our calculation, i.e. not neglecting the higher-order cluster formation the equations (4.13b) and (4.14b) will not hold anymore.

Effect of ionizing radiation

We recall that Wagner and Mascarenhas[14] suggested that ionizing radiation reduces the size of the TSDC peak in CaF_2:Ce (i.e. a reduction in the C_{4v} dipoles concentrations), and furthermore, they concluded that for each four dipoles destroyed one photochromic center is formed. In order to monitor the effect of the ionizing radiation on the dipolar C_{4v} centers, we performed optical absorption and TSDC measurements on CaF_2 doped with 0.5% Ce before and after γ-irradiation. The dose chosen was 3.3kGy. We did not observe any reduction either in the size of the optical absorption peak at 303nm or in the size of the TSDC peak belonging to the dipolar C_{4v} centers. We, therefore, do not believe that the C_{4v} centers are the precursors to the PC centers as

TABLE III

Values of the Ce melt concentration, N_d^o (actual dipole concentration), the ratio (X) of C_o to N_d^o and the two functions of X (described in the text).

C_o (mole %)	N_d^o (mole %)	$X=\frac{N_d^o}{C_o}$	$(\frac{1-X}{X^3})^{\frac{1}{2}}$	$(\frac{1-X}{X^2})$
.01	.02	2.0	---	---
.1	.034	0.340	4.10	5.74
.5	.049	.098	31.0	94.0
1.0	.059	.059	68.6	27.0
1.5	.083	.055	76.0	312
2.0	.084	.042	109.8	544

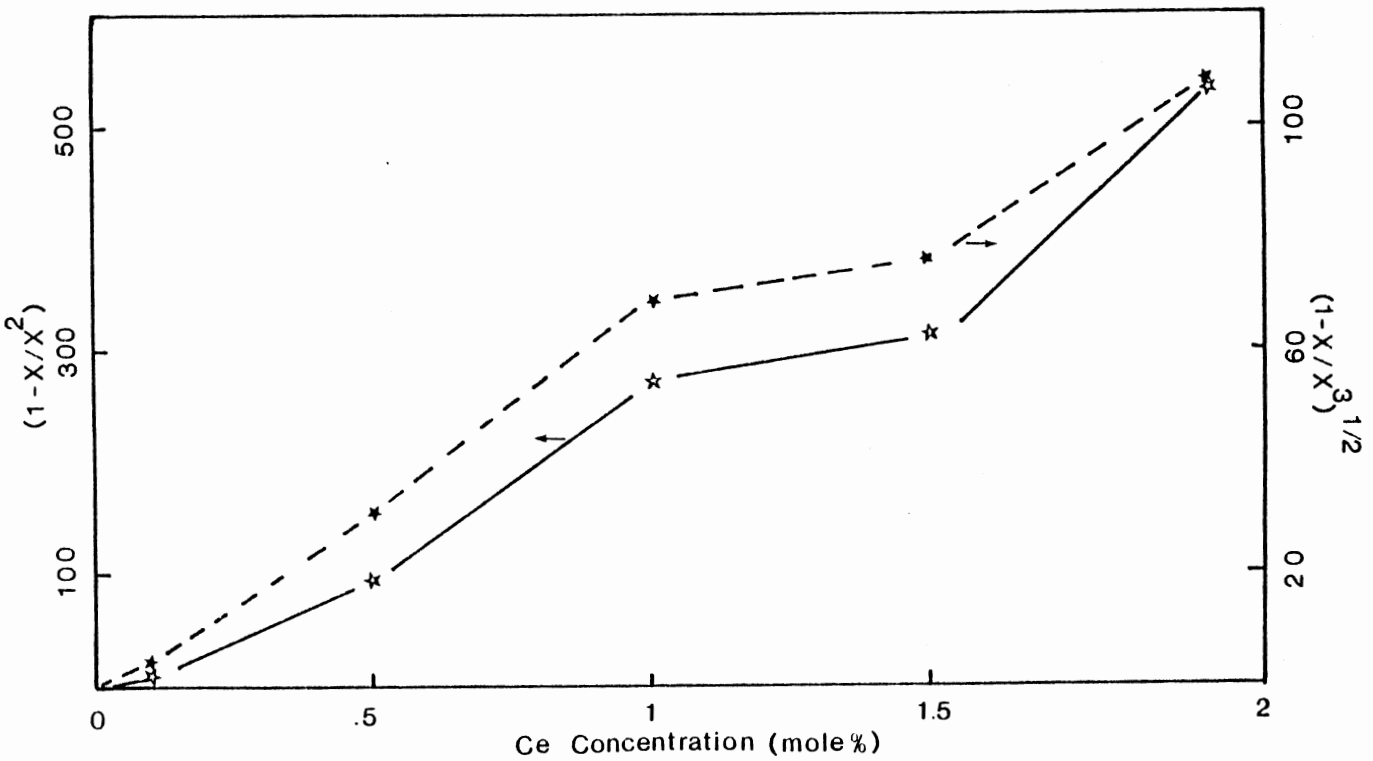

Figure 34. Plots of $(1-X/X^2)$ and $(1-X/X^3)^{1/2}$ versus C_o. (Table 3). Neither plot gives a straight line. The dashed lines are to guide the eyes only.

claimed by Wagner and Mascarenhas.[14] The possible Ce^{3+} site involved in forming PC centers is given in chapter 5.

Section B

$\underline{CaF_2}$:Ce,Mn

Figure (35) shows that as the Mn concentration is increased N_d^t decreases whereas N_d^o remains the same. Since the actual dipole concentration (N_d^o) does not change we cannot claim that the TSDC peak size is being reduced because of the C_{4v} dipoles getting close together. Instead we recall that the equation for the effective polarization (P_e) (equation 21) and note that, for constant T_{eff}, F_p and N_d (considering the actual dipole concentration), the dipole moment (μ) also affects the value of P_e. We believe, therefore, that as the Mn concentration is increased the dipole environment is altered, to the extent that the higher Mn concentration (2.0%) drastically changes the local crystal structure. Since the size of the TSDC peak is reduced as Mn concentration is increased we suggest that an increase in Mn concentration results in a lowering of the distance (d) between the Ce^{3+} and F^- ions in the $(Ce^{3+}\text{-}F^-)C_{4v}$ center, with a consequent reduction in the dipole moment ($\mu = ed$).

We also observed that the activation energy (both E_B and E_I) first started to increase and then decreased as the Mn concentration increased (figure 36). We can offer no detailed explanation for this behavior. In figure (37) we see that the width parameter (p) decreases as the Mn concentration is increased up to 0.5%. This might be as a result of the reduction in μ, as can be seen from the following equation

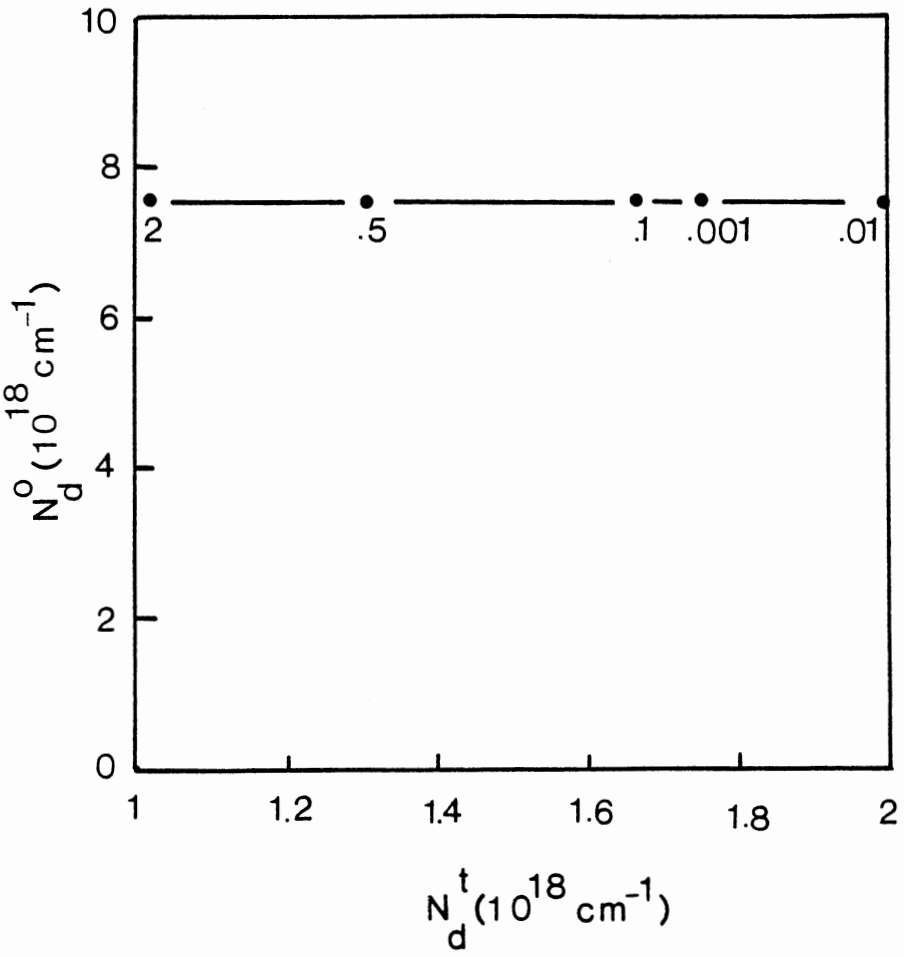

Figure 35. The concentration of C_{4v} dipoles as determined by optical absorption as a function of that determined by TSDC. The Ce content is fixed at 0.5%. The Mn content varies as indicated in the figure.

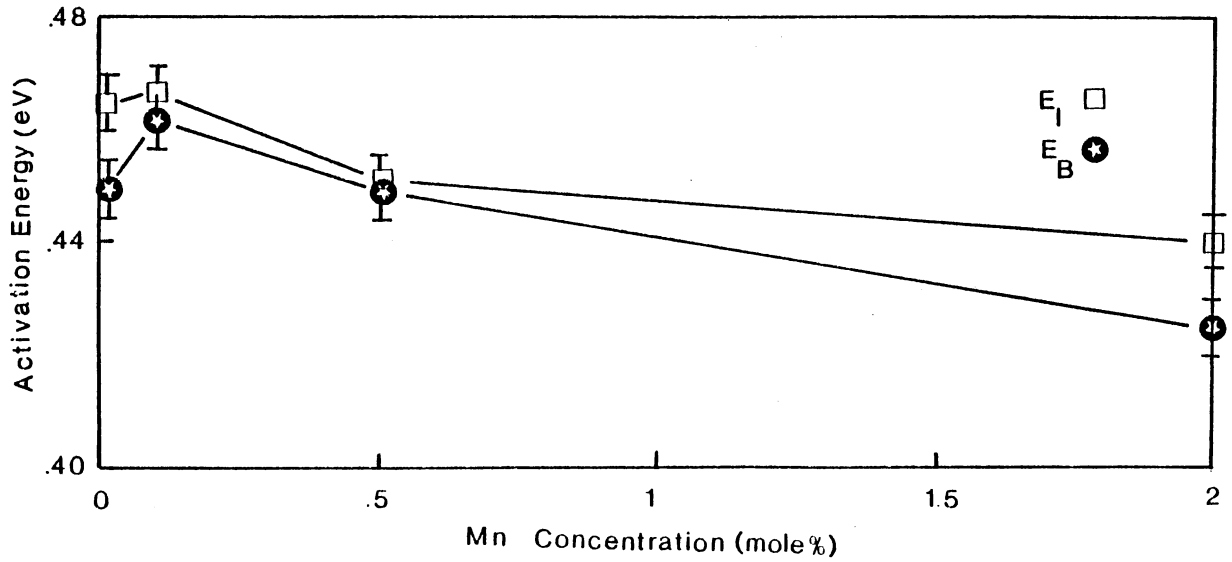

Figure 36. The variation in activation energy (E_B and E_I), as a function of the Mn concentration for samples with a fixed Ce concentration of 0.5%.

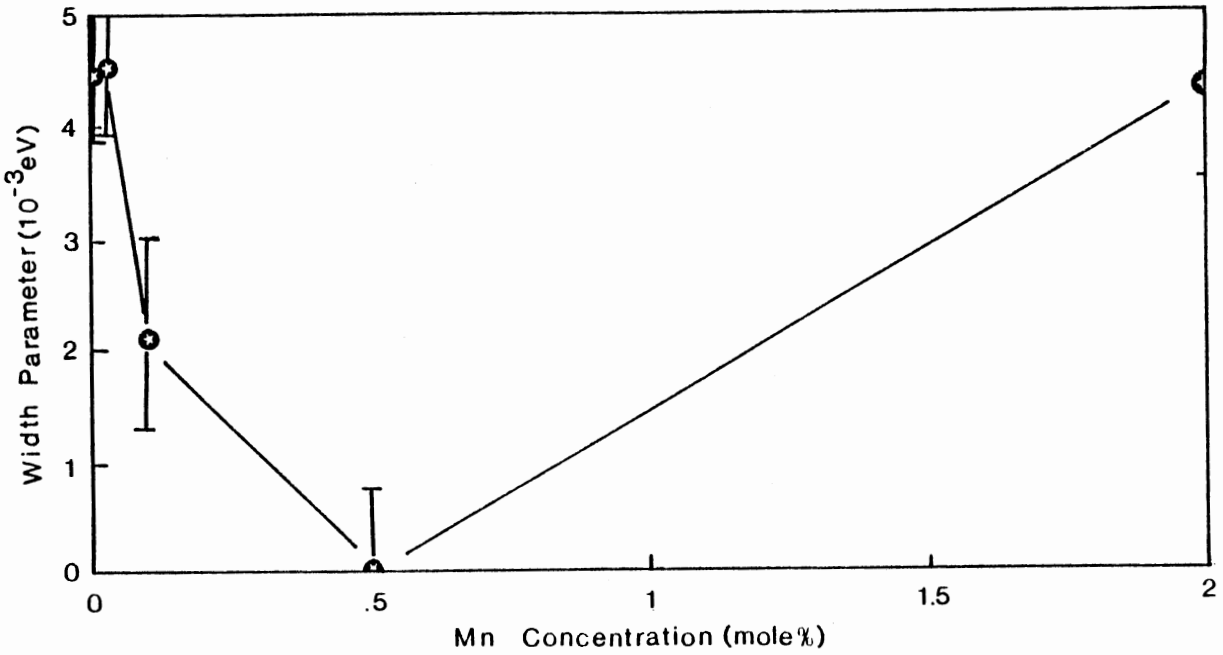

Figure 37. The variation in width parameter (p) as a function of the Mn concentration for samples with a fixed Ce concentration of 0.5%.

$$E_{int} = (1/4\pi\varepsilon\varepsilon_o)[(\vec{\mu}_1.\vec{\mu}_2)/r_{12}^3 - 3(\vec{\mu}_1.\vec{r}_{12})(\vec{\mu}_2.\vec{r}_{12})/r_{12}^5]. \quad (4.15)$$

Here E_{int} is the dipole-dipole interaction energy, $\vec{r}_{12}$ is the vector connecting the position of dipoles $\vec{\mu}_1$ and $\vec{\mu}_2$ and ε is 7.69. Thus, a reduced $\mu(\mu_1 = \mu_2 = \mu)$ results in a weaker interaction between the C_{4v} dipoles. This in turn will reduce the width parameter (p) in accordance with the data of the other workers on CaF_2:RE systems.[61-64] Beyond 0.5%Mn however, p increases once again. At these high dopant levels, although Mn substitutes for Ca, but there will be a transition of local crystal structure from CaF_2 to MnF_2 which is not isomorphous with CaF_2. Hence this might result in such behavior seen for concentrations beyond 0.5%Mn.

Section C

Summary and conclusions

The major observations of this study were:

(i) Ionizing radiation did not either reduce the size of the TSDC peak or the optical absorption peak at 303nm belonging to the dipolar C_{4v} centers.

(ii) The relaxation parameters E and p for dipole rotation changed as Mn concentration increased in CaF_2 with fixed Ce concentration.

(iii) Lack of one-to-one correspondence between N_d^t (concentration of dipoles using TSDC method) and N_d^o (concentration of dipoles using optical method).

Based on the above observations we conclude the following. (1) PC centers are not formed from dipolar C_{4v} centers during irradiation as claimed by Wagner and Mascarenhas[14](viz. observation i). (2) The presence of the Mn ions next to C_{4v} centers from which energy transfer

to these ions takes place can be detected by TSDC method (viz. observation ii). (3) The concentrations calculated by using TSDC method does not represent the actual dipole concentration (viz. observation iii).

CHAPTER V

CaF_2:Ce

In this chapter we report and discuss the results we have obtained, using optical absorption, photoluminescence and thermoluminescence, for CaF_2:Ce. And we also, based on these results, suggest the TL mechanism occuring in this material. We hoped that by understanding the TL mechanism in the samples intentionally-doped with Ce we would gain useful information into the behavior of Mn-doped CaF_2 which, inevitably, contains rare-earth impurities. As we will see later, rare-earth impurities have a strong influence on the TL production in these materials.

Section A

Optical absorption

The absorption spectrum of un-irradiated CaF_2:Ce reveals absorption bands due to 4f-5d transitions of the single 4f electron in Ce^{3+} ions in C_{4v} symmetry and clusters of these centers. The bands marked B, and E in figure (5) are attributed to the electronic transitions in Ce^{3+} in C_{4v} symmetry, whereas C and D are due to 4f-5d transitions within the unknown clusters of the C_{4v} centers.[17-19] We note in figure (38) that the bands C and D grow more rapidly with increasing Ce concentration than the C_{4v} bands, supporting the view that they are due to Ce aggregates.

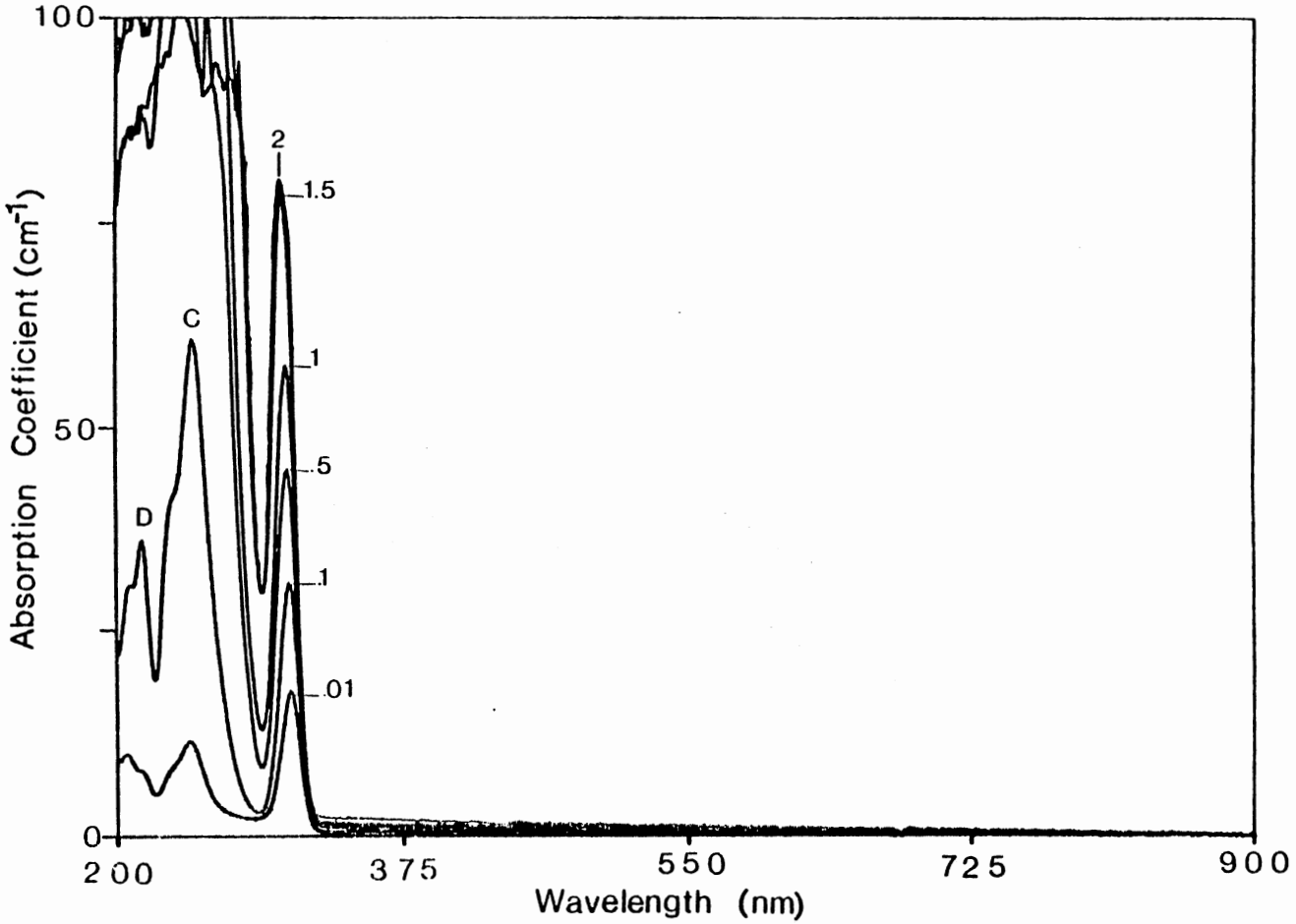

Figure 38. Optical absorption spectra for CaF_2 doped with Ce(of concentrations 0.01, 0.1, 1.0, 1.5 and 2.0%) representing the rapid growth of cluster bands marked C and D as a function of Ce concentration.

The optical absorption of a γ-irradiated sample (figure 39) reveals the growth of new, overlapping bands in the visible region (300-900nm); we also witness an overall enhancement of the bands in the UV region which indicates the growth of underlying bands. However, the absorption due to Ce^{3+} in C_{4v} symmetry and to the clusters of these centers are themselves apparently hardly affected. This agrees with our TSDC data (chapter 4 section A) which demonstrated no reduction in the height of the TSDC peak with irradiation.

Figure (40) shows the radiation induced bands in more detail. These have been identified by other workers to be due to Ce^{2+} in O_h symmetry and to PC centers (see chapter 3 section B). Absorption from PC^+ centers (see chapter 3 section B) is also observed. Thus we have labeled the Ce^{2+} (O_h) bands according to the identification by Alig et al[20], and the bands due to PC centers and PC^+ centers as identified by Staebler and Schnatterly.[75] The underlying absorption bands that we are observing in figure (39) (to which there is also a contribution by the PC and PC^+ centers) might contain absorption due to unidentified nonparamagnetic hole centers that are stable at room temperature (see chapter 3 section B).[37]

Figure (41) displays the effect of pulse annealing on the optical absorption of the γ-irradiated sample. The bands due to the Ce^{2+} (O_h) centers were observed to decrease at temperatures up to 150°C, and we also observed a slight increase in the PC absorption bands near 700nm. Figure (42) (obtained after heating to 150°C) clearly reveals the PC bands. These bands finally disappear between 250°C and 400°C and the crystal is apparently returned to its unirradiated state.

These observations can be understood from the photochromic

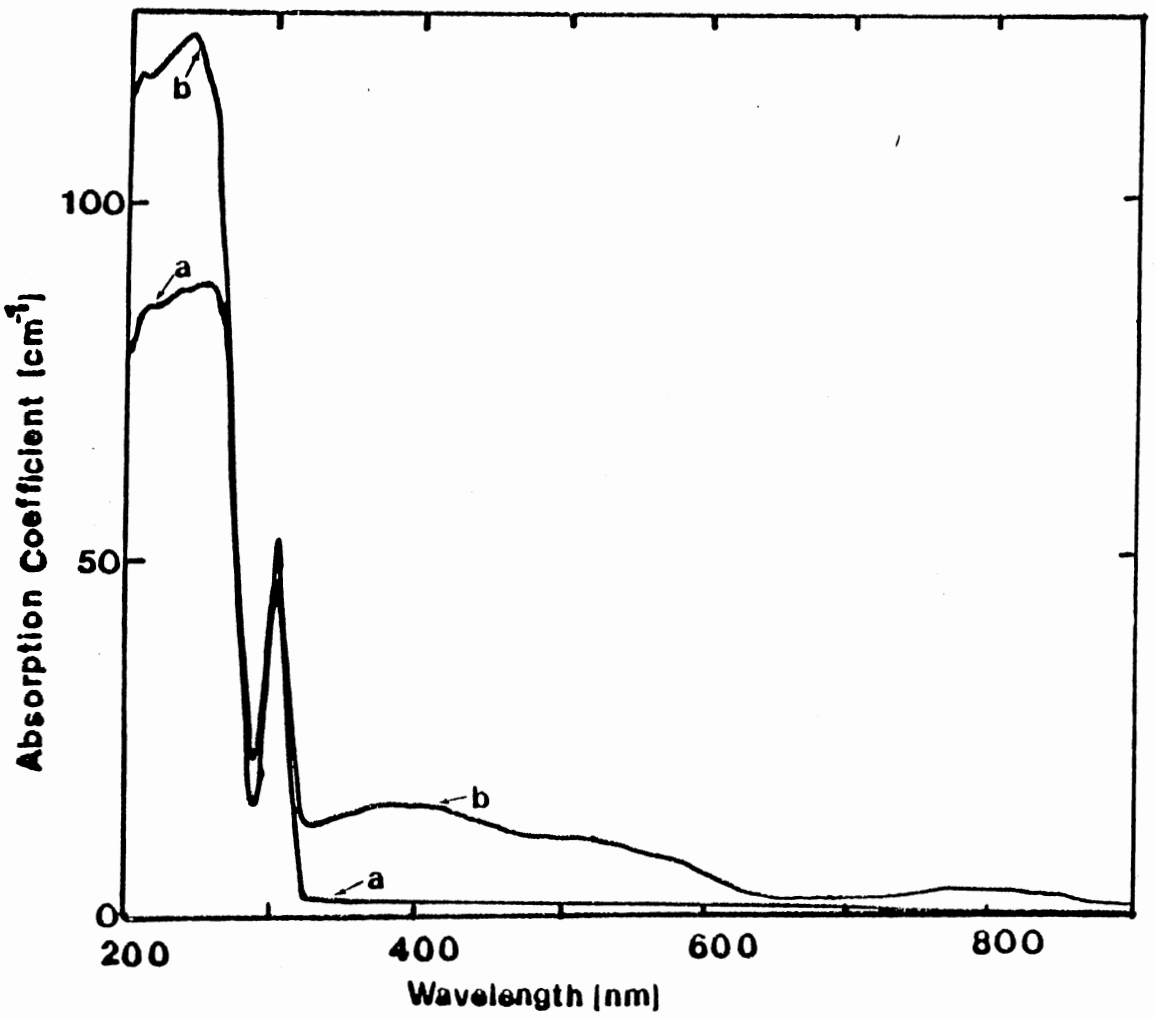

Figure 39. (a) Optical absorption of unirradiated CaF_2:Ce (0.5%). (b) Optical absorption of CaF_2:Ce (0.5%) γ-irradiated at room temperature (4.4kGy).

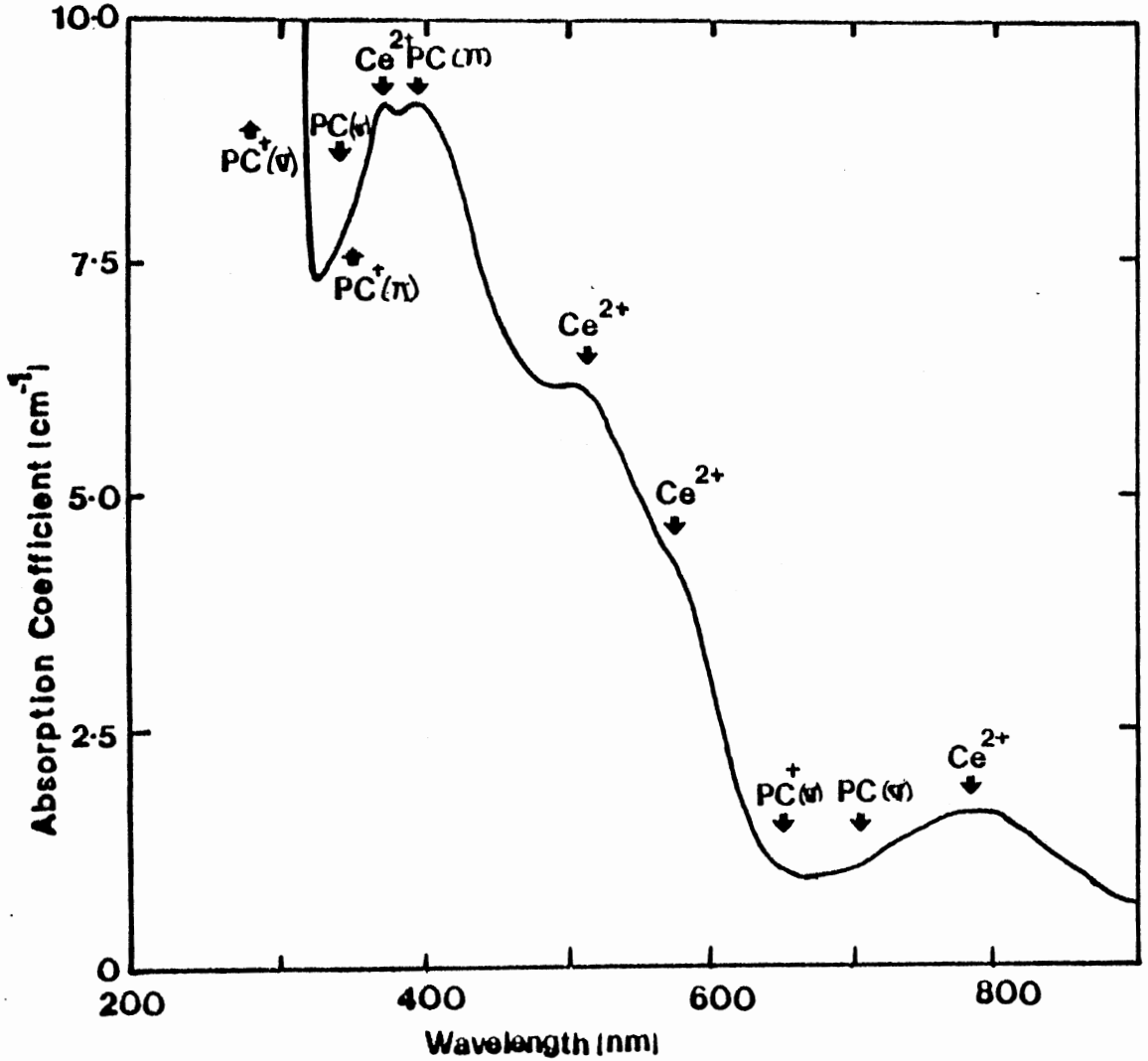

Figure 40. Optical absorption of CaF_2:Ce (0.5%) γ-irradiated at room temperature (4.4kGy) showing the position of the Ce^{2+} (O_h), PC and PC^+ bands.

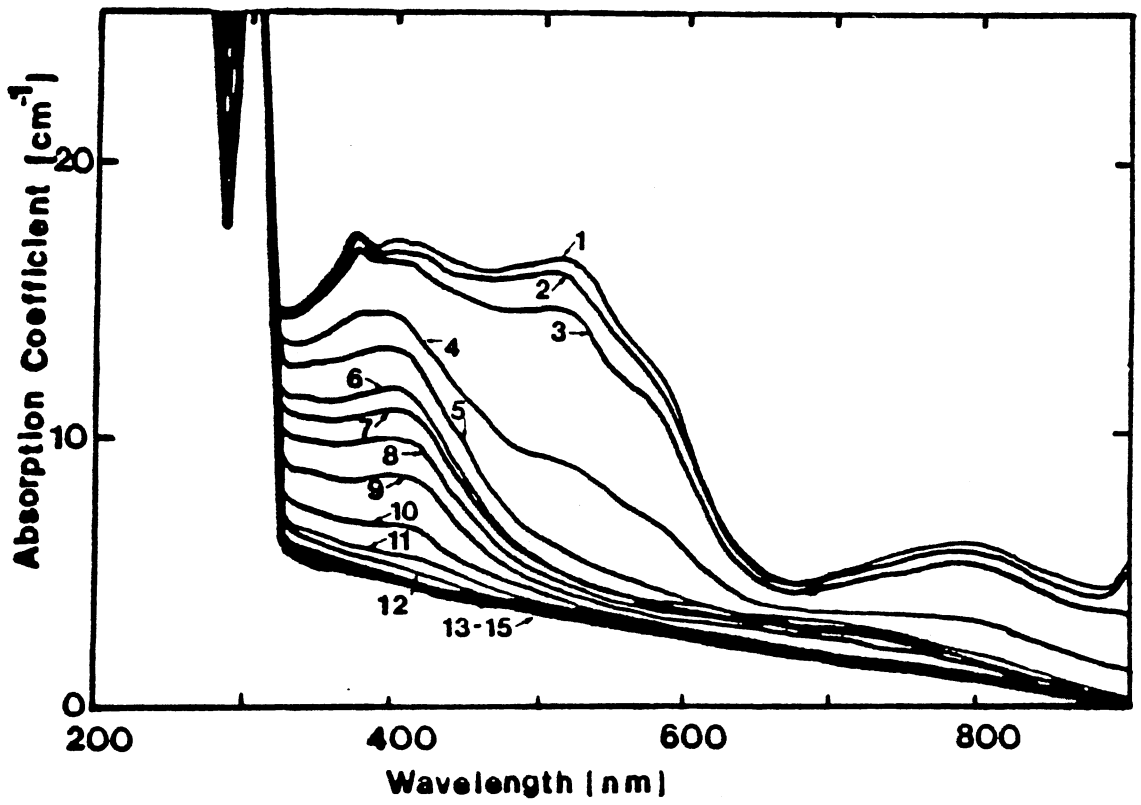

Figure 41. The effect of pulse annealing on the absorption spectrum of γ-irradiated CaF_2:Ce (0.05%) (4.4kGy). Curve #1 is that obtained immediately after irradiation. The other curves are obtained after heating the samples to the temperature indicated, thus: (2) 50°C; (3) 75°C; (4) 100°C; (5) 125°C; (6) 150°C; (7) 200°C; (8) 250°C; (9) 275°C; (10) 300°C; (11) 325°C; (12) 350°C; (13) 400°C; (14)450°C; (15)500°C. All absorption curves are obtained at room temperature.

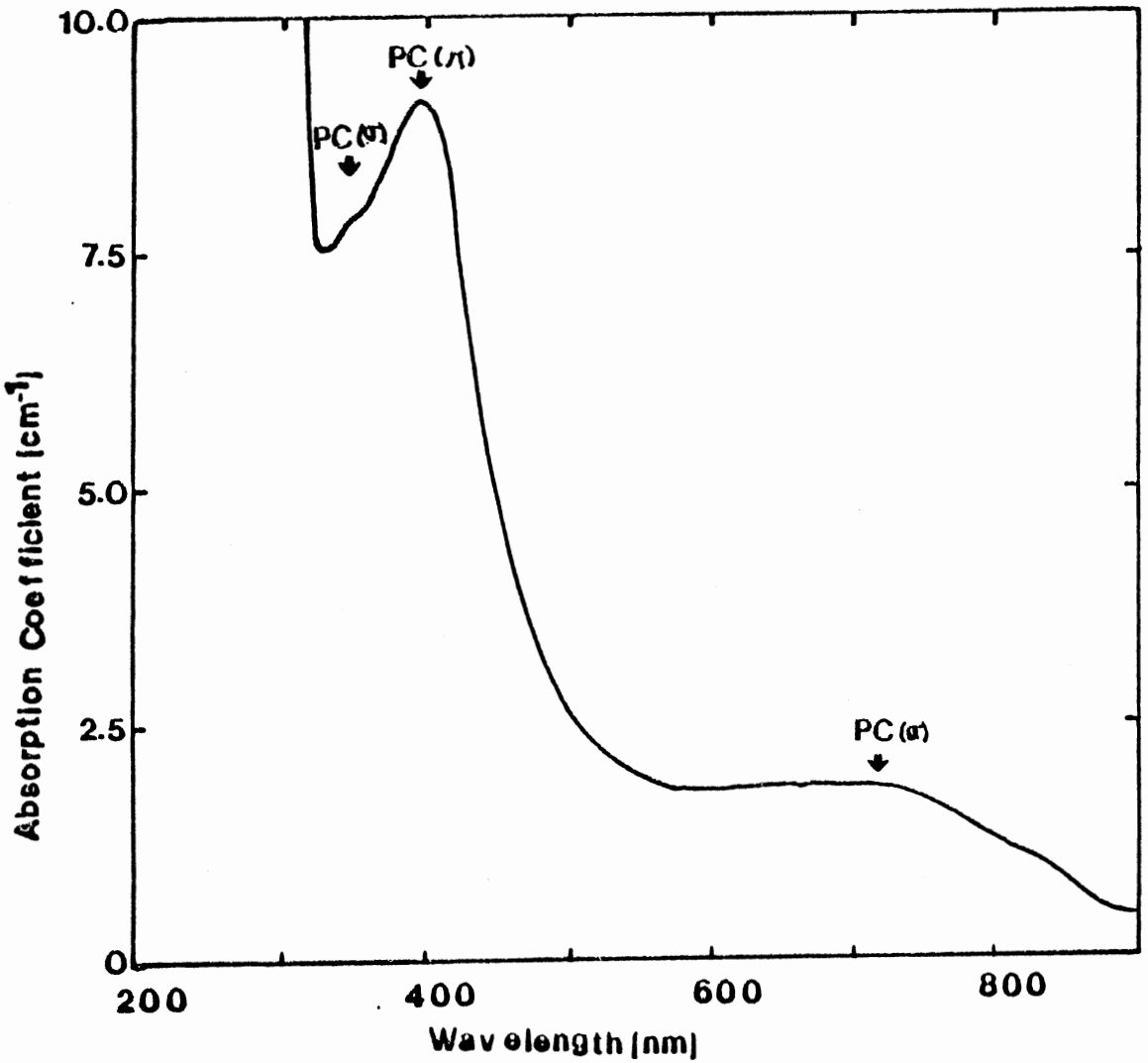

Figure 42. Optical absorption of γ-irradiated (4.4kGy) CaF_2:Ce (0.05%) at room temperature, after 150°C thermal anneal.

reaction as described by Staebler and Schnatterly,[75] namely

$$PC^{+} + Ce^{2+} \rightarrow PC + Ce^{3+} \qquad (5.1)$$

Here, an electron is released from Ce^{2+} and recombines with a PC^{+} center to form a PC center. However, we should note that not all the electrons released from the Ce^{2+} sites recombine with PC^{+} centers in this way. Some may be captured by the trapped-hole centers (which, as we noted above, remain unidentified at present).

Reaction (5.1) can also be induced by bleaching into the Ce^{2+} absorption bands (figure 43). Here we observe that 500nm bleaching produces a similar effect to 150°C heating, but not as strongly.

388nm illumination of a previously-heated sample (to 150°C) induces the reverse reaction to take place namely:

$$Ce^{3+} + PC \xrightarrow{h\nu} Ce^{2+} + PC^{+}. \qquad (5.2)$$

The effect of this is illustrated in figure (44) where we observe that the crystal does not return to the original irradiated state. This is because during the reaction (5.1) some electrons were lost by recombination with the trapped-hole centers. Reactions (5.1) and (5.2) make up the photochromic process which is discussed in some detail by several authors.[20,75]

Section B

Photoluminescence

We have investigated the excitation and emission spectra of CaF_2 doped with Ce. Figure (8) shows the emission spectrum under UV excitation of CaF_2:Ce (0.01%). As shown the emission is a doublet (320 and 340nm), and it is attributed to the deexcitation from lower energy levels of 5d to the $^2F_{5/2}$ and $^2F_{7/2}$ ground state energy levels of Ce^{3+}

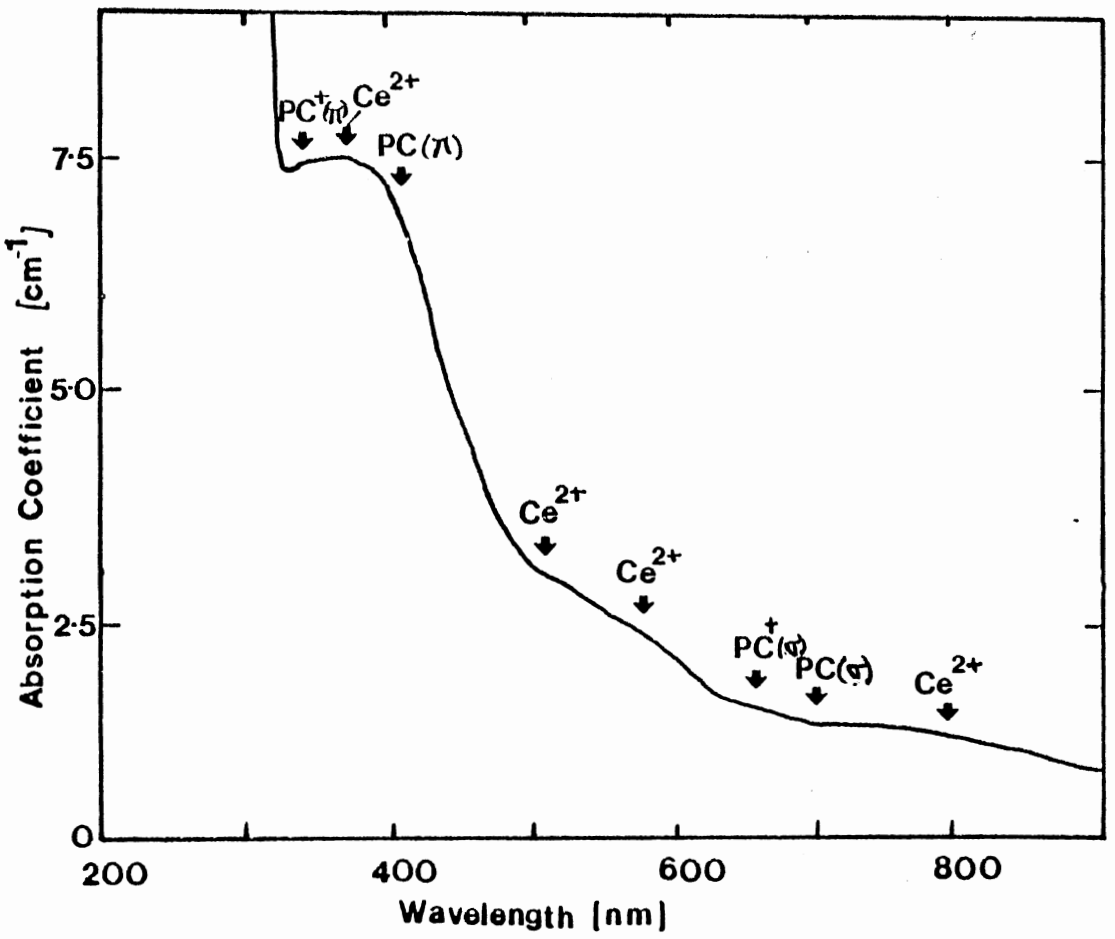

Figure 43. Optical absorption of γ-irradiated (4.4kGy) CaF_2:Ce (0.05%) at room temperature, after 500nm bleaching (~1 hour at room temperature).

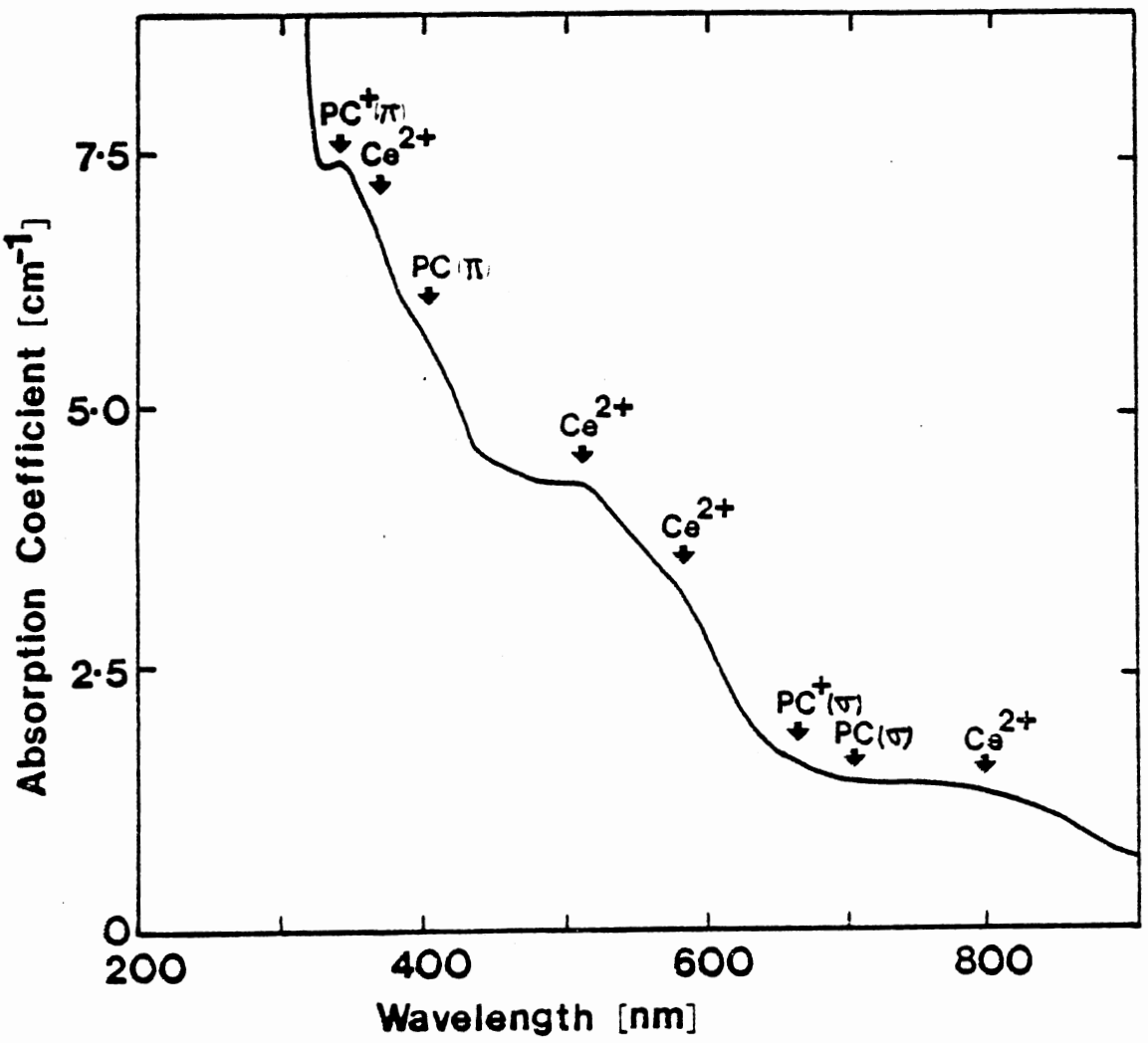

Figure 44. Optical absorption of γ-irradiated (4.4kGy) CaF_2:Ce (0.05%) at room temperature, after 150°C thermal anneal followed by bleaching with 388nm light.

which are split by the spin-orbit interaction and C_{4v} crystal field. As can be expected, the excitation spectrum, shown in figure (45), has the same characteristic as the C_{4v} absorption band. The 250nm excitation band may be due to the clusters. Although there is not an absorption band peaking at ~250nm, this wavelength falls into the region of the broad absorption band of the clusters.

500nm light illumination of a γ-irradiated CaF_2:Ce (0.5%) also results in the same Ce^{3+} doublet and in a 290nm luminescence feature (figure 46). We believe that during 500nm (absorption band of Ce^{2+}) irradiation electrons liberated from cubic Ce^{2+} ions recombine with stable hole centers producing (V_k+e) type recombination luminescence at 290nm.[37] Since this emission overlaps with the absorption bands of the Ce^{3+} ions in C_{4v} symmetry and the clusters of these centers, radiative energy transfer from the electron-hole recombination to Ce^{3+} may take place by reabsorption and the Ce^{3+} doublet luminescence is the result. It is to be noted that the emission shown in figure (46) is only observed following 500nm illumination of a freshly irradiated sample. Although exposure to 388nm light of a γ-irradiated sample, which has been previously heated to 150°C, causes recovery of the thermally-annealed absorption bands, subsequent 500nm light illumination does not produce luminescence. This observation can also be explained using the photochromic reactions discussed above. We observed that heating an irradiated sample to 150°C caused some electrons to recombine with trapped-hole centers, thus removing the trapped-hole recombination sites. Although we may then induce reaction (5.2) by 388nm light bleaching, subsequent illumination with 500nm light does not produce luminescence because the trapped-hole centers

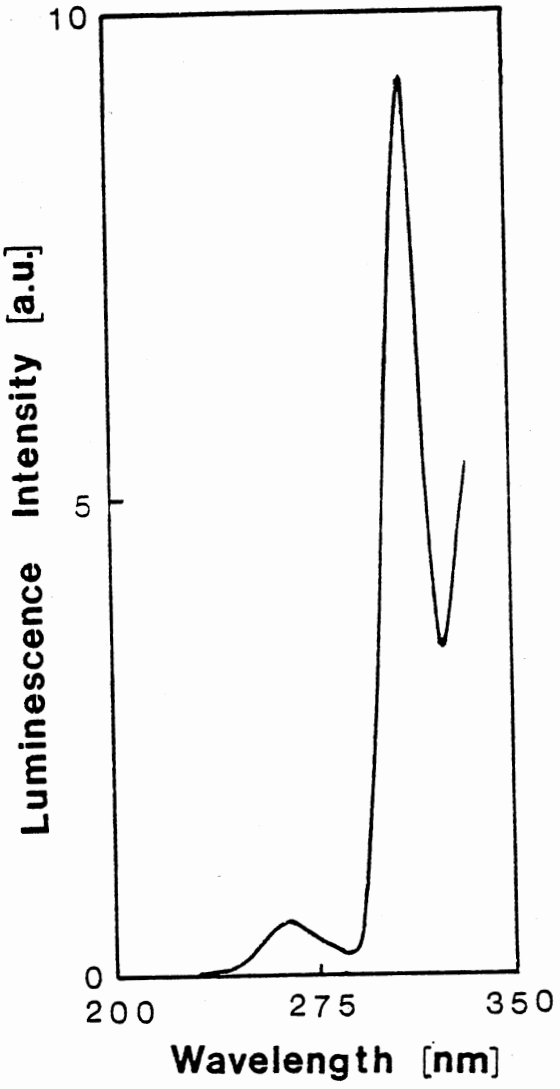

Figure 45. Excitation spectrum of CaF_2:Ce (0.01%) for the doublet Ce (320 and 340nm) emission at room temperature (the spectrum is uncorrected for the emission response of the excitation source). The monochromator for emission was set to 348nm (the tail of the doublet emission) for performing the experiment.

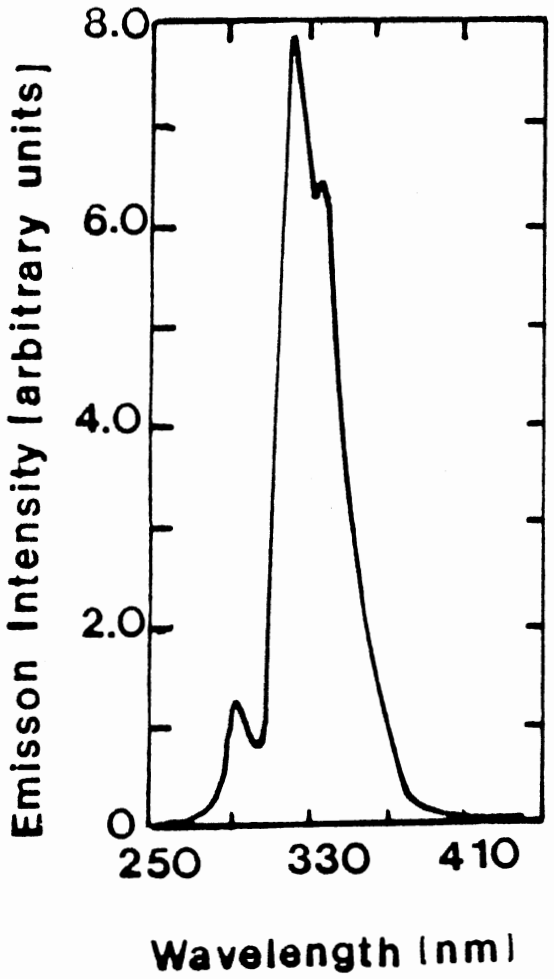

Figure 46. Emission spectrum of room temperature γ-irradiated (3.3kGy) CaK_2:Ce (0.5%). The excitation wavelength was 500nm.

are no longer available in appreciable numbers. Thus 500nm light only induces luminescence on a freshly irradiated sample. We further conclude from these observations that electron capture by PC^+ centers is a non-radiative process.

Section C

Thermoluminescence

The TL from γ-irradiated CaF_2:Ce at room temperature shows two, major, composite peaks at ~130 and 350°C (figure 47a). Spectral decomposition of the TL glow curves throughout the temperature range reveals Ce^{3+} emission and (V_k+e) type recombination luminescence. The observed spectra are identical to the spectra shown in figure (46).

The 130°C peak appears in the same temperature range over which the Ce^{2+} and PC^+ bands disappear and the TL in the higher temperature range coincides with the annealing of the PC bands. The TL glow curve of a 150°C thermally-bleached sample, shown in figure (47b), exhibits a drastic reduction in the 130°C peak. Figure (47c) displays the TL glow curve of a 150°C thermally-bleached sample, but exposed to 388nm light. As it is observed, the 130°C peak is not reproduced; it only appears during heating a sample immediately after γ-irradiation. We also note that the TL in the higher temperature region is reduced by the 388nm bleaching. This is consistent with the contention that this TL is related to the PC centers.

Section D

Summary and conclusions

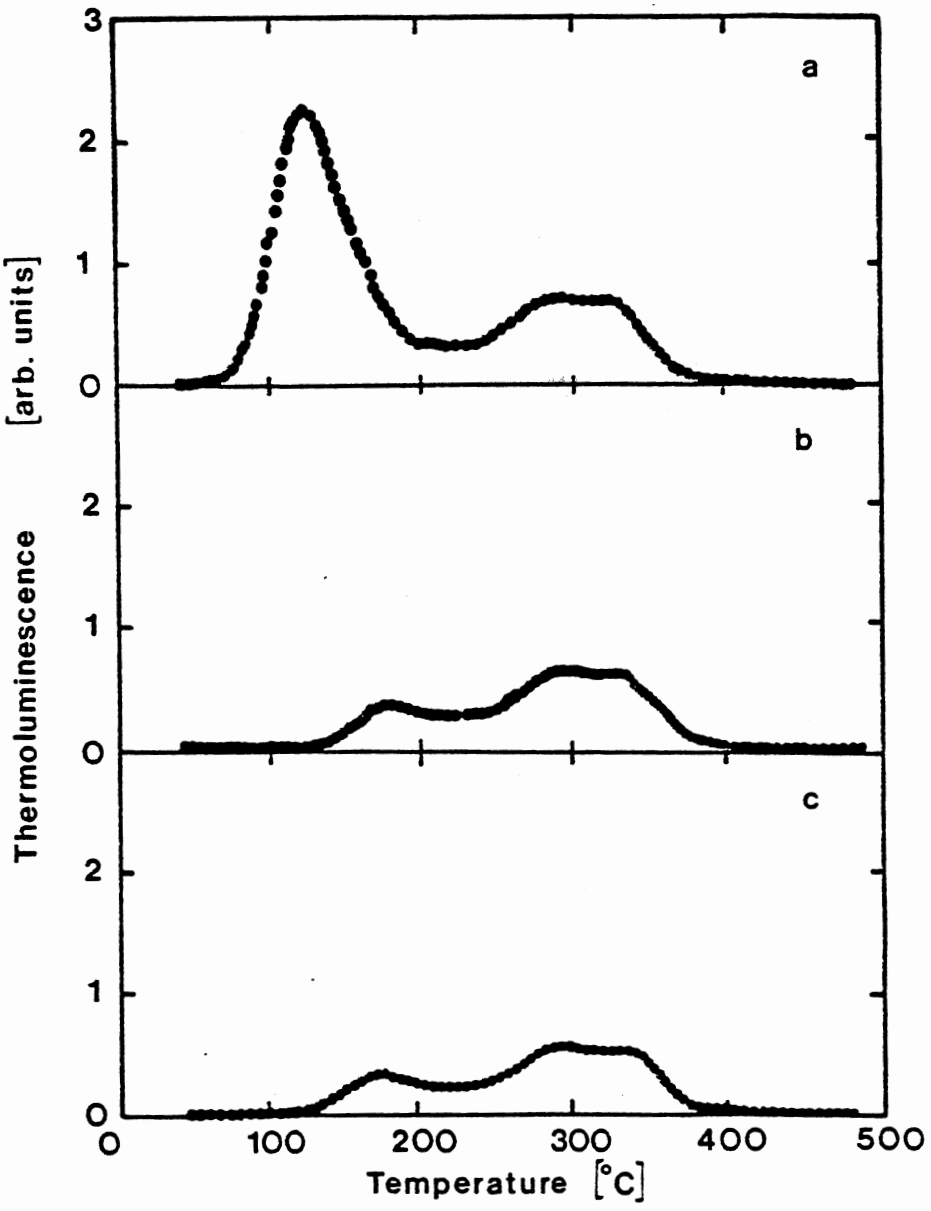

Figure 47. TL glow curves from CaF_2:Ce (0.5%). (a) after γ-irradiation (~0.2 kGy). (b) after γ-irradiation (~0.2kGy) but thermally annealed to 150°C. (c) after γ-irradiation (0.2kGy) but thermally annealed to 150°C followed by 388nm light bleaching for 1/2 hour at room temperature.

The major observations of this work are:

(i) Ce^{3+} in O_h symmetry is reduced to Ce^{2+} after ionizing radiation (figure 40). This confirms the presence of trapped-hole centers in the crystal, which are stable above room temperature.(37)

(ii) The appearance of the PC bands after 150°C thermal bleaching (figure 42) and the simultaneous fading of the Ce^{2+} and PC^{+} absorption bands. This can also be induced by 500nm bleaching.

(iii) The disappearance of the PC bands at higher temperature (~350°C) (figure 41). The PC bands are also reduced by 388nm bleaching (figure 44).

(iv) The correspondence between the TL glow curve (figure 47) and the step annealing of the optical absorption spectra of figure (41).

(v) The agreement between the TL spectra and photoluminescence spectra.

(vi) No reduction in the optical absorption of the C_{4v} and cluster bands due to ionizing radiation, which agrees with the TSDC data which demonstrated no reduction in the height of the TSDC peak with irradiation.

In the light of these observations we propose the following model for the TL production above room temperature in CaF_2 doped with Ce. During ionizing radiation electrons and holes are created and electrons are captured by Ce^{3+} ions in O_h symmetry, thus reducing them to Ce^{2+}. The fact that it is those Ce^{3+} ions in O_h symmetry which are reduced to Ce^{2+} is supported by EPR measurements on CaF_2:Tm by Hayes and Twidel.(76) These authors suggest that only those Tm^{3+} ions remote from the charge compensating defects (i.e. the F^- interstitials) trap electrons, because of the repulsive coulombic effect of the negative charge compensator. The holes are trapped in other lattice sites, the

identity of which is unknown at present. However, investigations of trapped-hole centers in CaF_2:Tm by Beaumont and co-workers[37] and additional work on different types of hole centers by Hall and co-workers,[35-36] clearly demonstrate the existance of stable hole centers at room temperature. Heating to 150°C results in the release of electrons from the Ce^{2+} ions. We have demonstrated that the capture of electrons by PC^+ centers is non-radiative. We therefore suggest that the TL emission is the result of electron recombination with V_k centers. This process will yield luminescence at ~290nm which overlaps with the absorption bands due to Ce^{3+} in C_{4v} symmetry sites and clusters of these sites. In this way some of the energy from (V_k+e) type recombination will be absorbed giving Ce^{3+} in an excited state. Relaxation of these ions will produce the Ce^{3+} doublet. Thus we expect that the thermally stimulated electron released from Ce^{2+} centers will produce thermoluminescence characteristic of (V_k+e) type recombination (290nm emission) and Ce^{3+} relaxation (320nmand 340nm emission). This process may be represented as follows:

$$\text{crystal} + \gamma\text{-ray} \rightarrow Pc^+ + PC + Ce^{2+}(O_h) + V_k \qquad (5.3)$$

$$Ce^{2+} + \text{heat}(150^oC) \rightarrow Ce^{3+} + e \qquad (5.4)$$

$$V_k + PC^+ + 2e \rightarrow PC + 290\text{nm light(TL)} \qquad (5.5)$$

$$Ce^{3+} + 290\text{nm light} \rightarrow Ce^{3+*} \qquad (5.6)$$

$$Ce^{3+*} \rightarrow Ce^{3+} + 320\text{nm and } 340\text{nm light(TL)}. \qquad (5.7)$$

The observation that heating the sample above 400°C induces the thermal recovery to the virgin state of the crystal supports the view that the PC centers recombine with different thermally stable F^o interstitial centers to regain the perfect lattice at higher temperatures. Similar processes involving vacancy/interstitial

recombination have been demonstrated to yield thermoluminescence in alkali halide crystals.[13,77] Thus, the TL observed at ~350°C in the present samples may be the result of similar mechanisms taking place at the PC centers. F-H recombination in CaF_2 is known to result in 280nm emission.[78] Thus, the 290nm emission observed in this work may be viewed as resulting from the recombination between interstitials and the vacancies present within the PC centers. Once 290nm emission is produced, it may be partialy reabsorbed by the Ce^{3+} ions to produce the Ce^{3+} doublet luminescence as before. The details and subtelties of these mechanisms are unavailable to us at present and must await more detailed studies.

Finally, concerning observation (iv) we propose the following. Since neither the TSDC peak (see chapter 4, section A) nor the optical absorption band due to the C_{4v} dipole centers are affected by irradiation, the claim by Wagner and Mascarenhas[14] that PC centers are formed from Ce^{3+} in C_{4v} sites during irradiation is rejected. Instead, it is known that Ce^{3+} ions, which substitute for Ca^{2+} in the CaF_2 lattice, are also located in O_h sites. Hence, since from our observations we concluded that PC centers are not formed from C_{4v} dipoles, a plausible alternative is that Ce^{3+} ions in O_h sites are the precursors to the PC centers. The trapping of an F-center by a Ce^{2+} ion in a nn position (along <111>) would produce a PC center directly.

CHAPTER VI

CaF_2:Ce,Mn

The primary reason for investigating CaF_2:Ce,Mn was the result of the claim by Sunta[8] that TL emission from Mn^{2+} in CaF_2:Mn was the consequence of energy transfer from rare-earth ions (e.g. Ce^{3+}) to the Mn^{2+} ions. During this study, from the results of our measurements, we gained valuable information concerning the affects of Ce ions on the TL production in CaF_2:Mn. This information opens a new window into the understanding of the TL mechanism in CaF_2:Mn as will be discussed in chapter 7.

Section A

Optical absorption

Optical absorption of unirradiated CaF_2:Ce,Mn (0.01%, 0.5%) is shown in figure (48). This absorption spectrum is very similar to the absorption spectrum of the Ce-only doped CaF_2 shown in figure (39a). The observed bands in the UV region, as mentioned in chapter 2, are assigned to Ce^{3+} (C_{4v}) centers and clusters of these centers.

Figure (49) displays the absorption spectrum of CaF_2:Ce,Mn (0.5%, 0.5%) following 2.56kGy γ-irradiation at room temperature. From a comparison between this spectrum and that of CaF_2:Ce (0.5%) (figure 39b), the similarity in the radiation induced absorption bands can easily be seen. For comparison purposes we show in figure (50) the

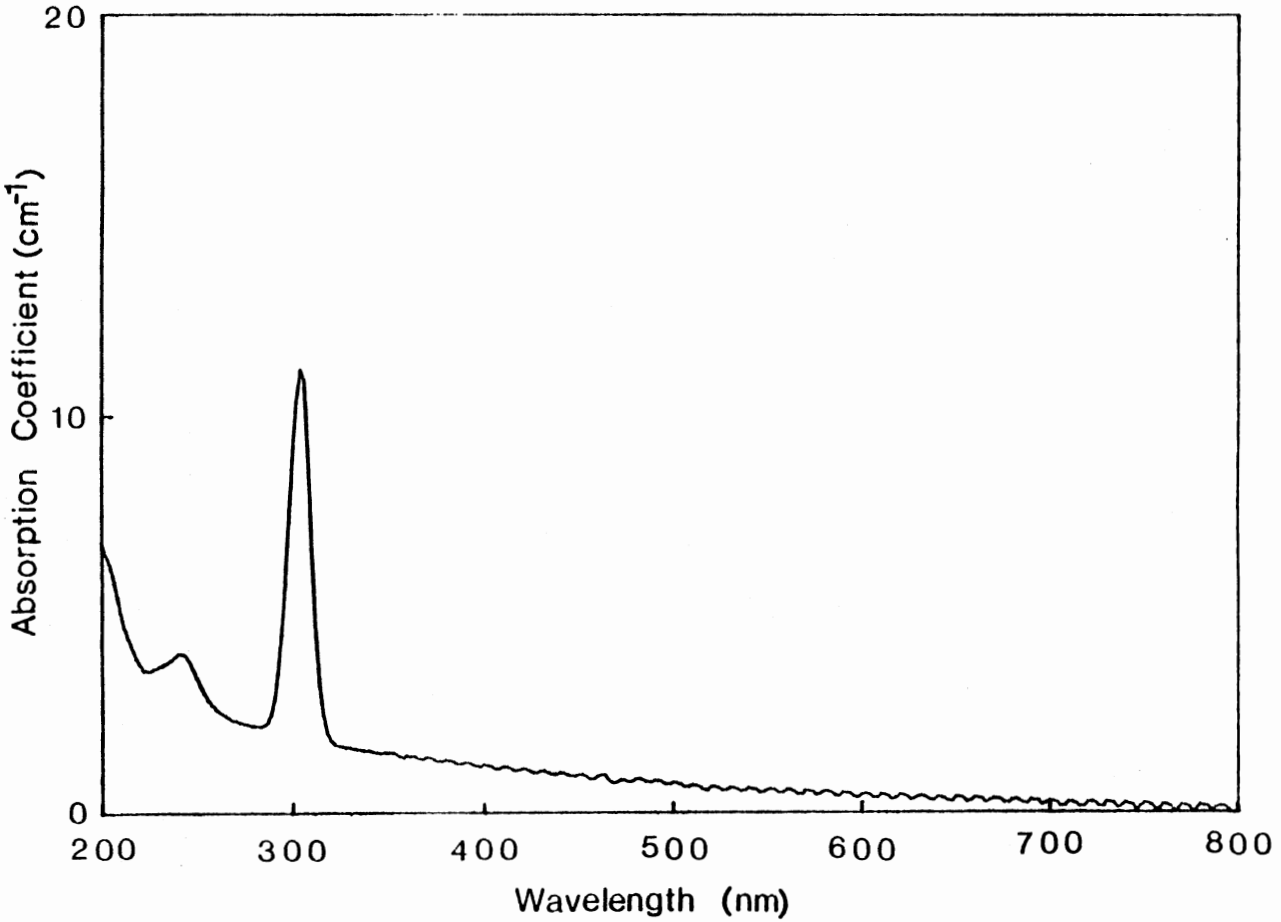

Figure 48. Optical absorption from an unirradiated sample of CaF_2:Ce, Mn (0.01%, 0.5%) at room temperature.

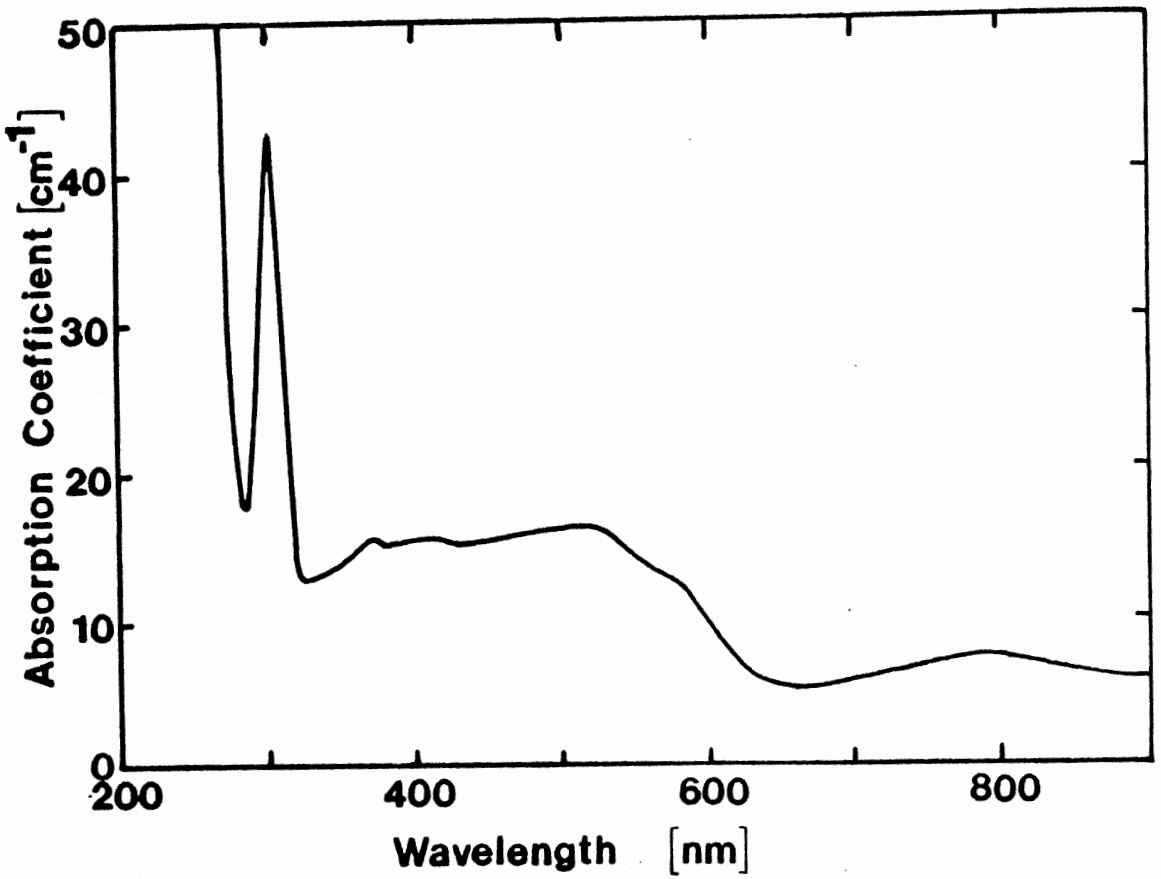

Figure 49. Optical absorption from a sample of CaF_2:Ce, Mn (0.5%, 0.5%) following irradiation at room temperature with 2.56kGy ^{60}Co gamma rays.

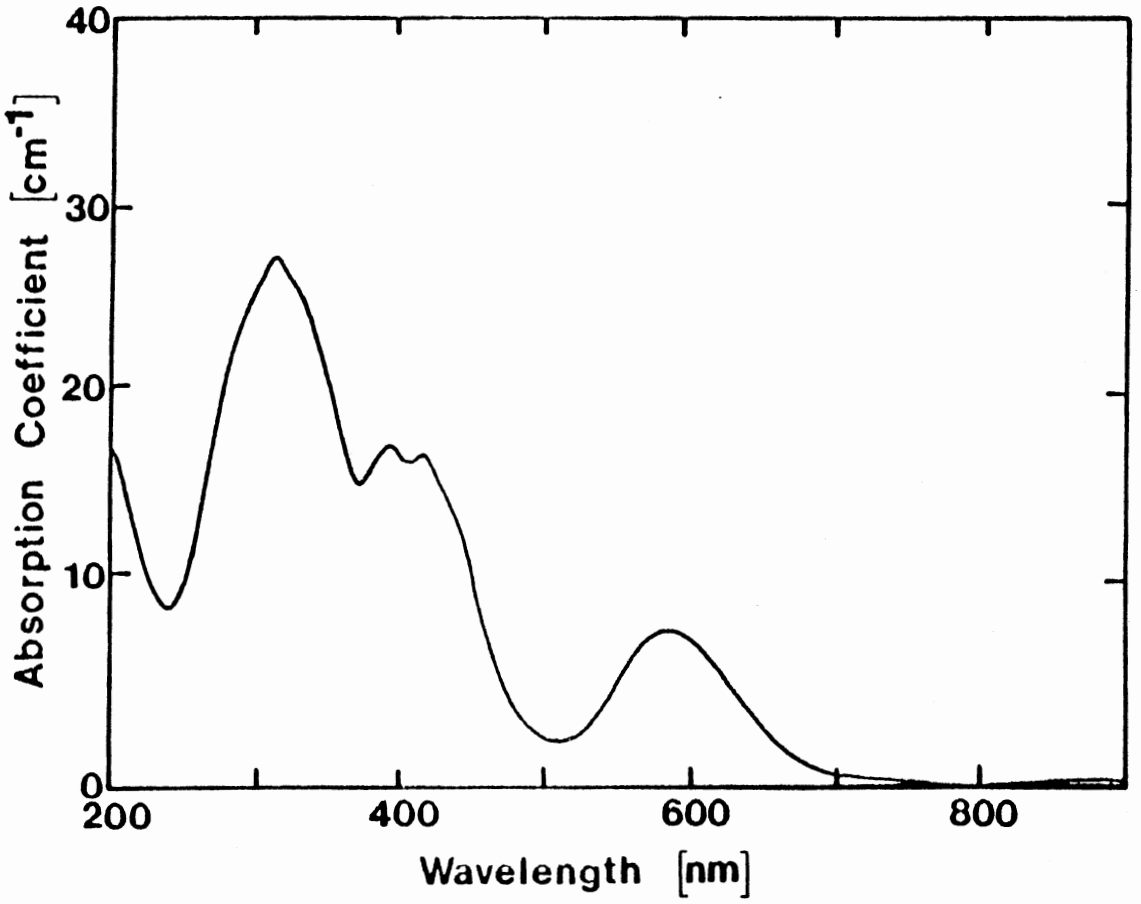

Figure 50. Optical absorption from a sample of CaF_2:Mn (0.5%) following irradiation at room temperature with 2.56kGy of ^{60}Co gamma rays.

optical absorption of CaF_2:Mn (0.5%) which reveals the absorption bands due to presently unidentified Mn/radiation induced defects. Although the Ce and Mn contents are the same in this material the Mn-related bands have been suppressed in figure (49).

To study this effect more we investigated samples of CaF_2 containing fixed Mn (0.5%) with variable Ce concentrations of 0, 0.01, 0.1, 0.5, and 2.0%. The results are shown in figure (51) where we display the optical absorption for each sample following irradiation. We note that, according to figure (51c) even for a 0.01% Ce concentration, i.e. a Ce content of 50 times less than that of Mn, the Ce-related absorption bands dominate the spectrum. At Ce concentrations of 0.1% and higher the appearance is given that Mn is not present in these materials at all (figure 51d-f). However from photoluminescence measurements, we have confirmed the presence of Mn in these materials.

Figure (52) displays the effect of pulse annealing on the optical absorption of a CaF_2:Mn,Ce (0.5%, 0.5%) sample γ-irradiated at room temperature. This spectrum is very similar to that of CaF_2:Ce (figure 41) and is seen to contain bands due to $Ce^{2+}(O_h)$, PC and PC^+ centers. The absorption bands due to $Ce^{2+}(O_h)$ centers were observed to decrease over the temperature range from room temperature up to 150°C. We also observed a slight increase in the PC absorption bands near 700nm over the same temperature interval. These latter bands disappear between 250°C and 400°C. The main reaction which governs these observations is the photochromic reaction (5.1) discussed in chapter 5.

Section B

Photoluminescence

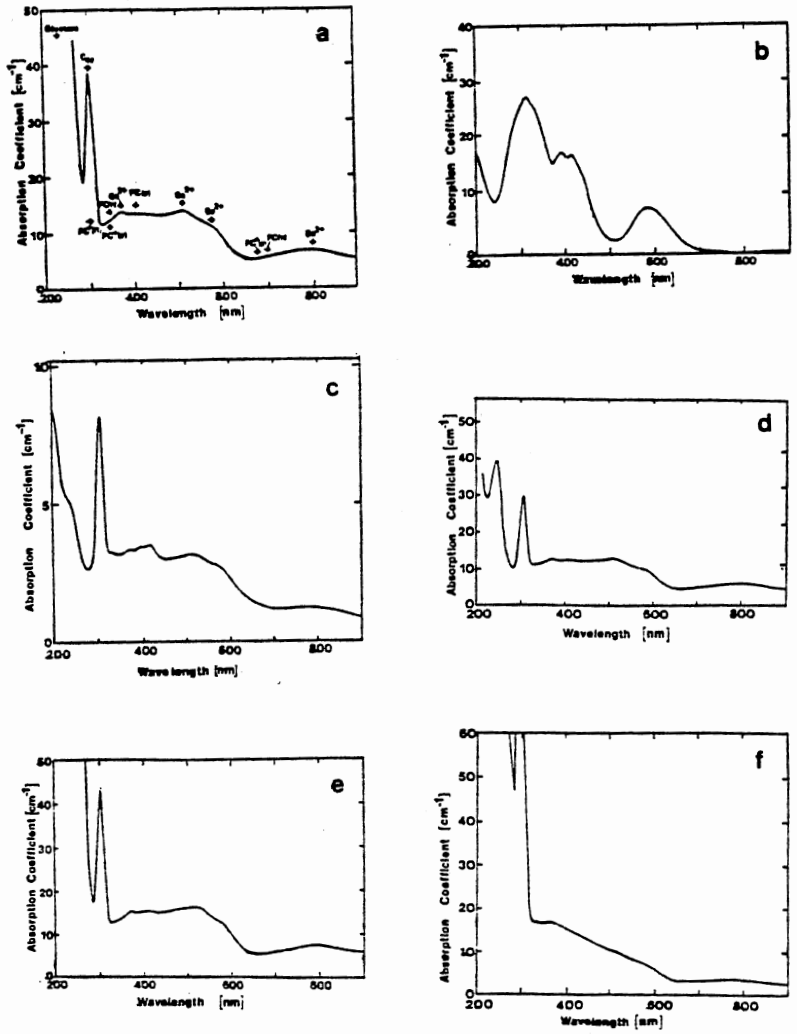

Figure 51. Optical absorption of CaF_2 samples doped with (a) Ce (0.5%); (b) Mn (0.5%0; (c) Mn,Ce (0.5%, 0.01%); (d) Mn,Ce (0.5%, 0.01%); (e) Mn,Ce (0.5%, 0.5%); (f) Mn,Ce (0.5%, 2.0%) following 2.57kGy of ^{60}Co gamma rays at room temperature.

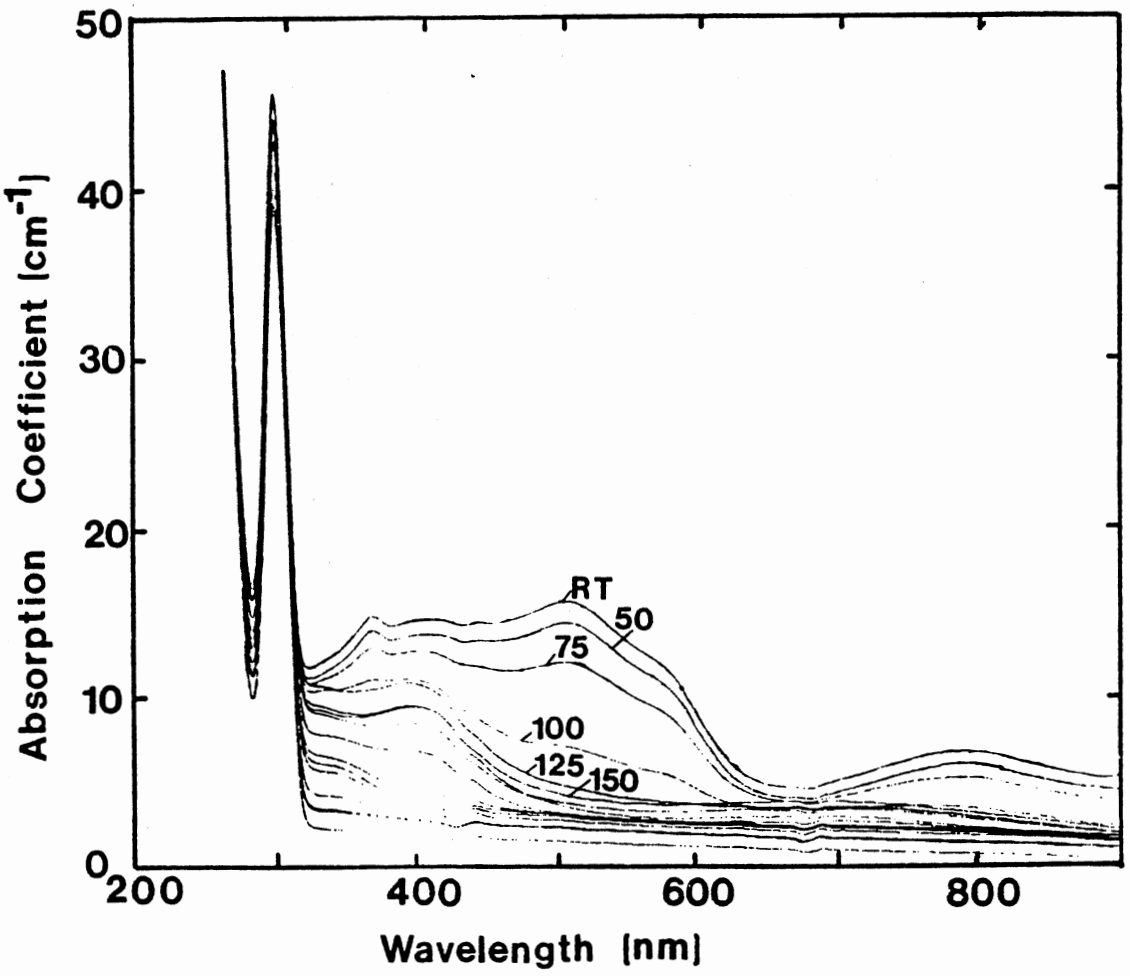

Figure 52. The effect of pulse annealing on the absorption spectrum of γ-irradiated CaF_2:Ce,Mn (0.5%, 0.5%). The curve marked R.T. is taken immediately after irradiation. The other curves are obtained after heating the sample to the temperature indicated (50, 75, 100, 125, 150, to 500°C in 50°C steps). All absorption curves are obtained at room temperature.

The emission spectrum following excitation at ~285nm (a region of the absorption band of the Ce^{3+} (C_{4v}) centers) for CaF_2:Ce,Mn (0.01%, 0.5%) is shown in figure (53). This spectrum displays the same doublet emission feature (320 and 340nm) as that of CaF_2:Ce (0.01%). As reported earlier, this emission belongs to Ce^{3+} ions (see chapter 2 section B). Excitation at 310nm, in addition to the Ce^{3+} doublet emission, also produces a spectrum characteristic of emission from Mn^{2+} (figure (54)). This emission which peaks at ~510nm, is attributed to the relaxation of electrons from the excited $^4G(^4T_{1g})$ level to the ground state $^6S(^6A_{1g})$ within Mn^{2+} ions. We also witness a weak emission at ~430nm. This emission is possibly from traces of impurities contained in this material. The position of the emission from the Mn^{2+} (510nm) is reported by other authors[19] to peak at ~520nm. We should mention that the data reported by us are uncorrected for the response of the detection system. This may in part explain some of the discrepancy. Nevertheless we, at this point do not know the exact nature of the wavelength difference.

Excitation at 395nm (i.e. one of the Mn^{2+} absorption bands) produces emission from Mn^{2+} which peaks at ~490nm (figure 55). The lack of correspondence between this emission (490nm) and that produced by excitation at 310nm (i.e. 510nm emission) is discussed by McKeever et al.[19] They conclude that since the Ce^{3+} ions which substitute for Ca^{2+} ions have a larger ionic size, thus their association with Mn^{2+} to which energy transfer from Ce^{3+} ions takes place results in an increased ligand field around the Mn^{2+} ions. This, therefore, causes a larger Dq splitting of the Mn ^4G energy levels, which results in a longer-wavelength emission. They further suggest that the association

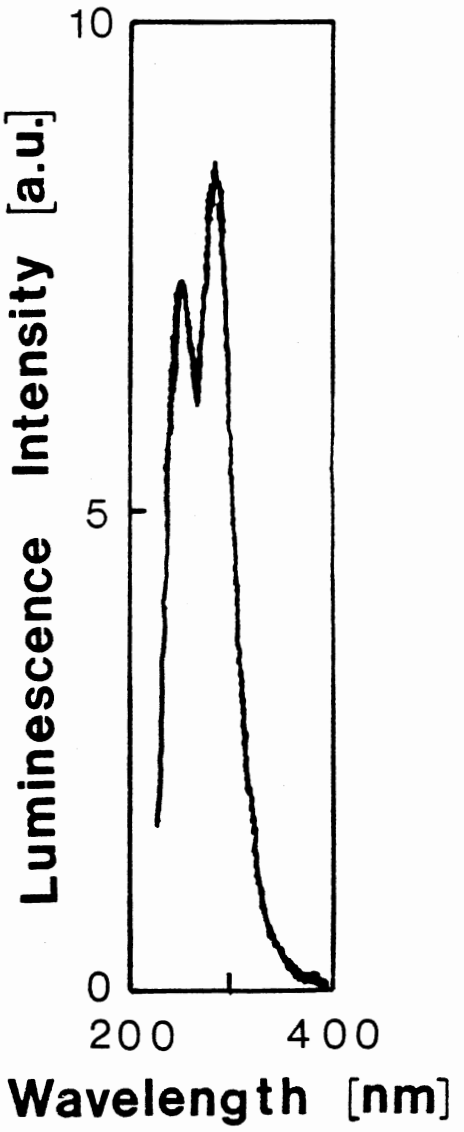

Figure 53. Emission spectrum revealing doublet emission from Ce^{3+} for CaF_2:Ce,Mn (0.01%, 0.5%). Excitation is at ~285nm.

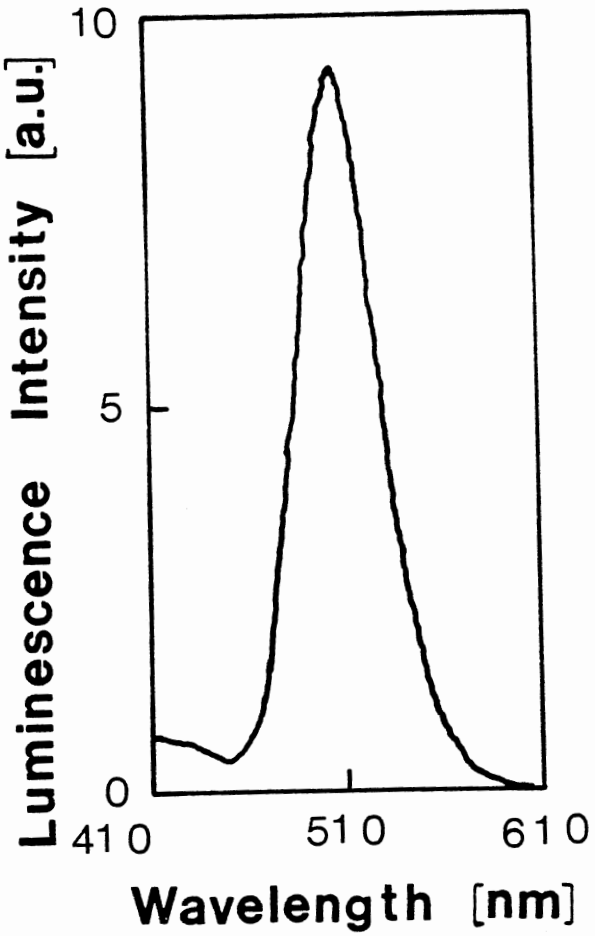

Figure 54. Emission spectrum, showing emission from Mn^{2+} ions, in CaF_2:Ce,Mn (0.01%, 0.5%) as a result of excitation at ~310nm.

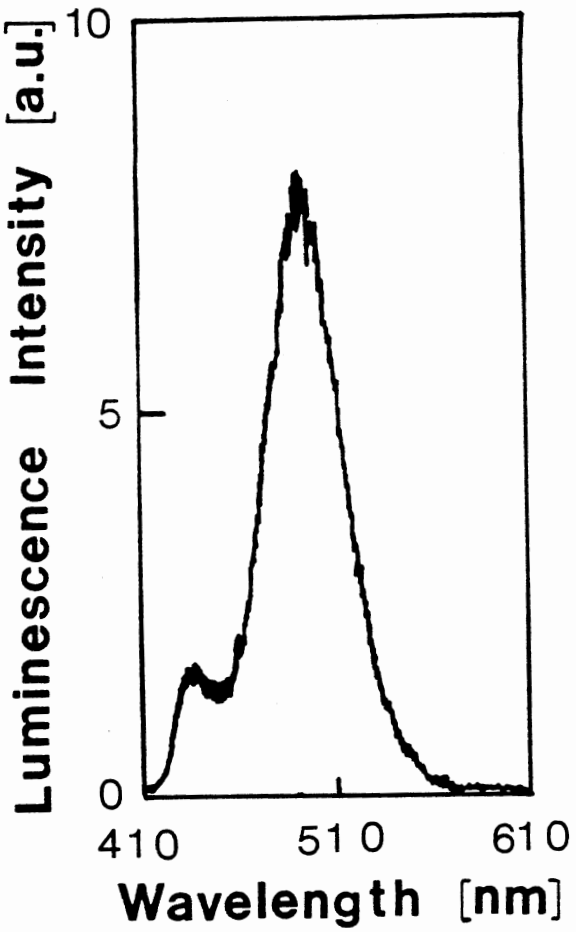

Figure 55. Emission spectrum displaying emission from Mn^{2+} ions in CaF_2:Ce,Mn (0.01%, 0.5%) as a result of excitation at 395nm.

of Ce^{3+} ions also changes the symmetry of the Mn^{2+}. This in turn via a decrease in the forbiddance reduces the lifetime from 55ms for the 490nm emission to 38ms for 520nm emission.

Figure (56) displays the excitation spectrum for the 510nm emission. As indicated in this figure, the excitation bands are characteristic of both Ce and Mn absorption. However, it can easily be seen that the dominant excitation band for the 510nm emission from Mn belongs to Ce^{3+} (C_{4v}) absorption (see figure 48).

Section C

Thermoluminescence

For the purpose of investigating the suggested energy transfer from Ce to Mn during TL in CaF_2:Mn, we performed TL measurements above room temperature on CaF_2:Mn (0.5%) with variable Ce concentration (0.01, 0.1, 0.5 and 2.0%).

The TL glow curves are shown in figure (57). As seen they display similar features to the TL from CaF_2:Ce (figure 47a). The spectral decomposition of the TL glow curves has revealed the presence of 495nm emission.[80] We have also, by using Corion-narrow-bandpass interference filters (334 and 490nm) in order to discriminate between emission from Mn^{2+} and emission from Ce^{3+} ions, confirmed the above observation. The presence of this 495nm emission, as a component of TL light and also the appearance of a weak TL emission at temperatures greater than 400°C are the main and obvious differences between the TL emission from this material and that of CaF_2:Ce (chapter 5, section C).

As in CaF_2:Ce, the 130°C glow peak appears in the same temperature range over which the Ce^{2+} and PC^{+} bands disappear and the

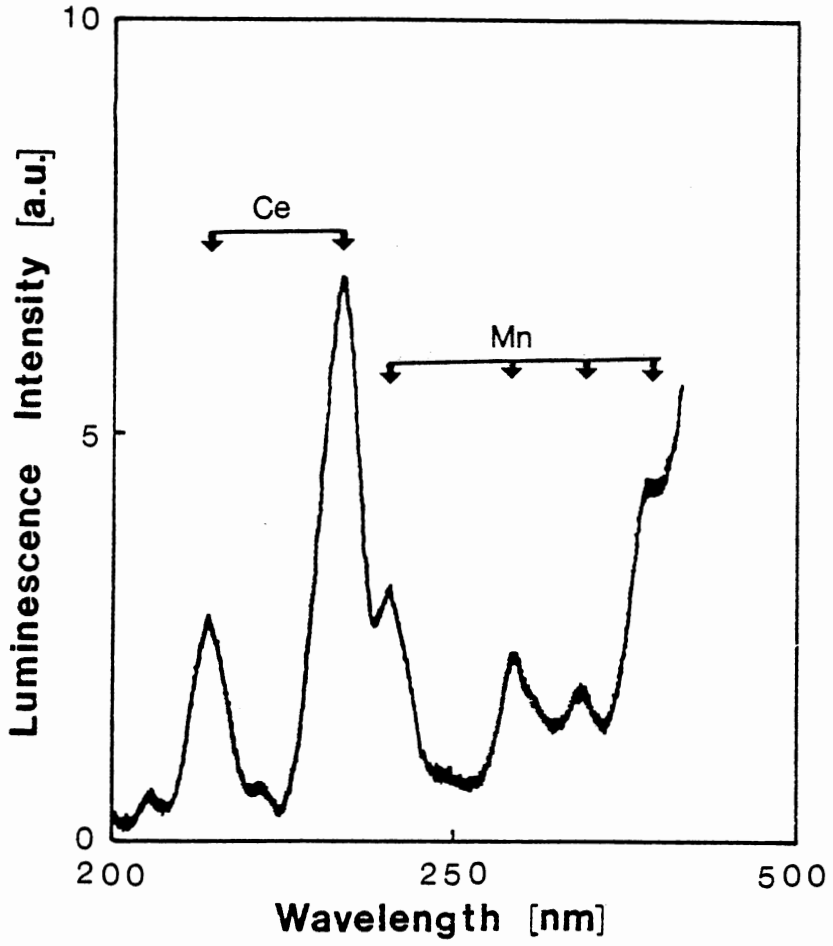

Figure 56. Excitation spectrum for emission at 510nm from Mn^{2+} in CaF_2:Ce,Mn (0.01%, 0.5%).

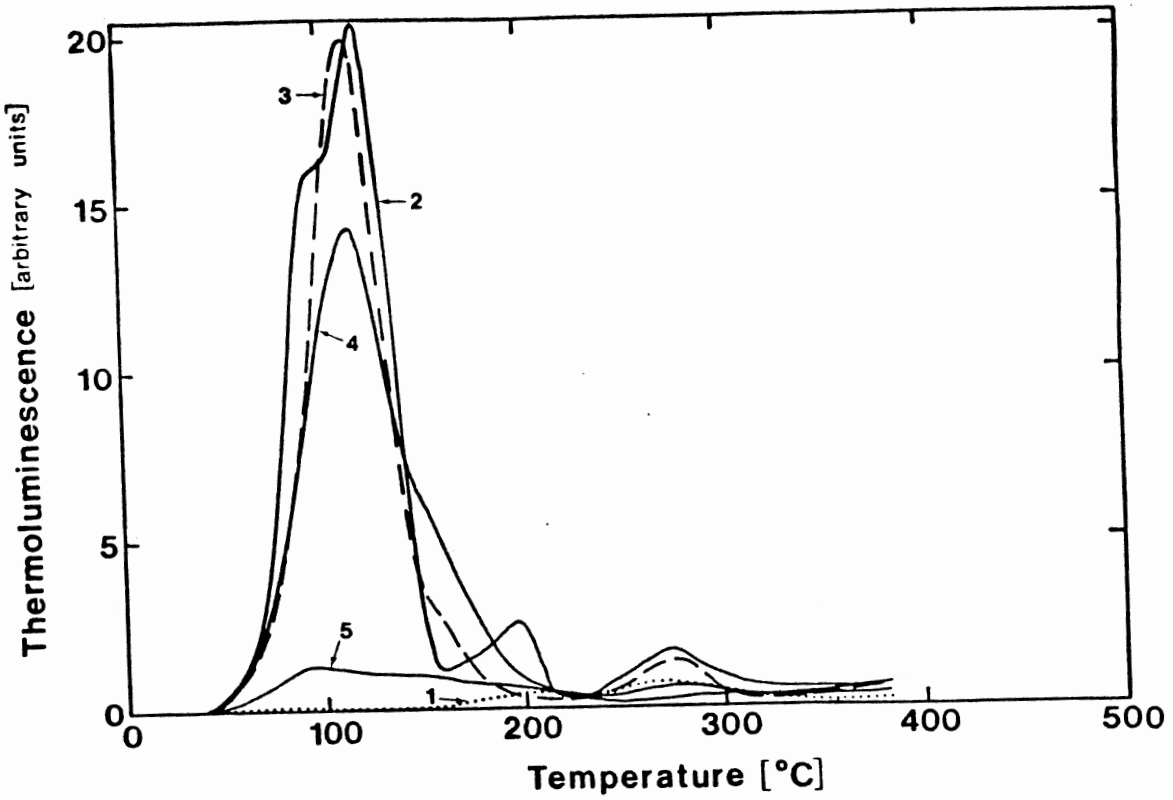

Figure 57. TL glow curves from CaF_2:Ce,Mn for (1) 0% Ce; (2) 0,01%; (3) 0.1%; (4) 0.5%; (5) 2.0%. Mn content is 0.5%. Irradiation is performed at R.T. with 2.56kGy of ^{60}Co gamma rays.

TL in ~350^{o}C coincides with the annealing of the PC bands. In figure (58) we compare the TL from CaF_2:Ce,Mn with CaF_2:Ce and CaF_2:Mn. As can be observed the TL glow curve from CaF_2:Ce,Mn apparently shows the same features as CaF_2:Ce rather than CaF_2:Mn. Thus we note that in the TL from CaF_2:Ce,Mn, the presence of Ce dictates the main features of the glow curves. This is similar to the conclusions we have already reached regarding optical absorption.

By using the Corion-narrow-bandpass interference filters (490 and 334nm) to isolate the emission from Mn and Ce and monitoring the glow peak height at 130^{o}C we observed the following. The TL emission from Mn^{2+} diminished as the Ce content was raised (figure 59). Also the increase in the Ce content resulted in an enhancement of the Ce emission (figure 60).

In order to understand the mechanism(s) by which TL emission from Mn in this material is produced we performed TL measurements on CaF_2:Ce(0.5%) with variable Mn concentration (0.001, 0.01, 0.1, 0.5 and 2.0%). We noticed that increasing the Mn concentration results in an increase in Mn emission from these ions (figure 61). We also witnessed a decrease in the Ce emission with increasing Mn concentration (figure 62). Once again these measurements were taken using 320 and 490nm interference filters to isolate the Mn and Ce emission components.

Section D

Discussion and conclusions

The primary observations of this study are:

(i) The severe reduction of the Mn-related optical absorption bands when Ce is present.

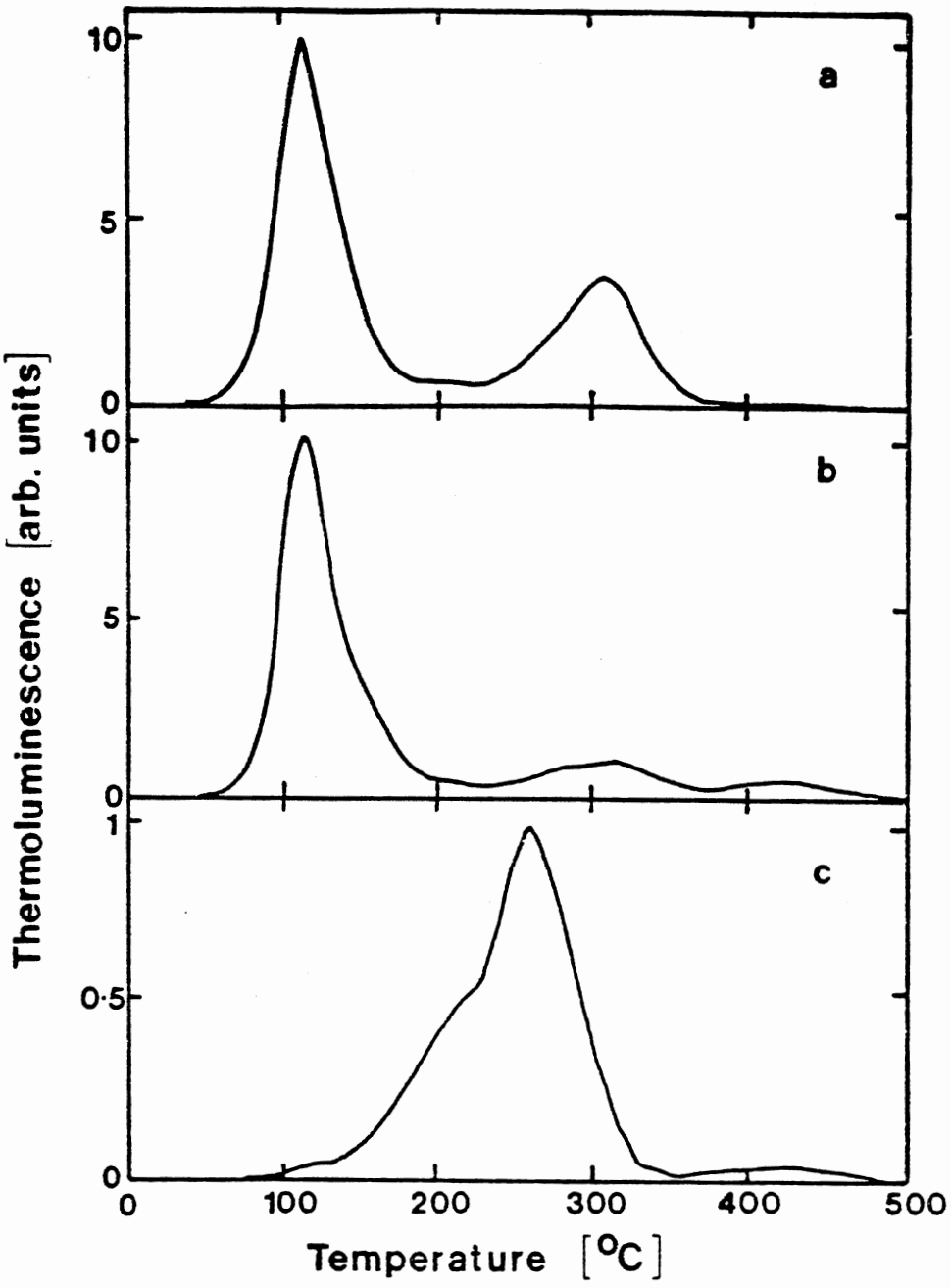

Figure 58. TL glow curves following 2.56kGy of gamma dose at room temperature. (a) CaF_2:Ce (0.5%); (b) CaF_2:Mn,Ce (0.5%, 0.5%); (c) CaF_2:Mn (0.5%).

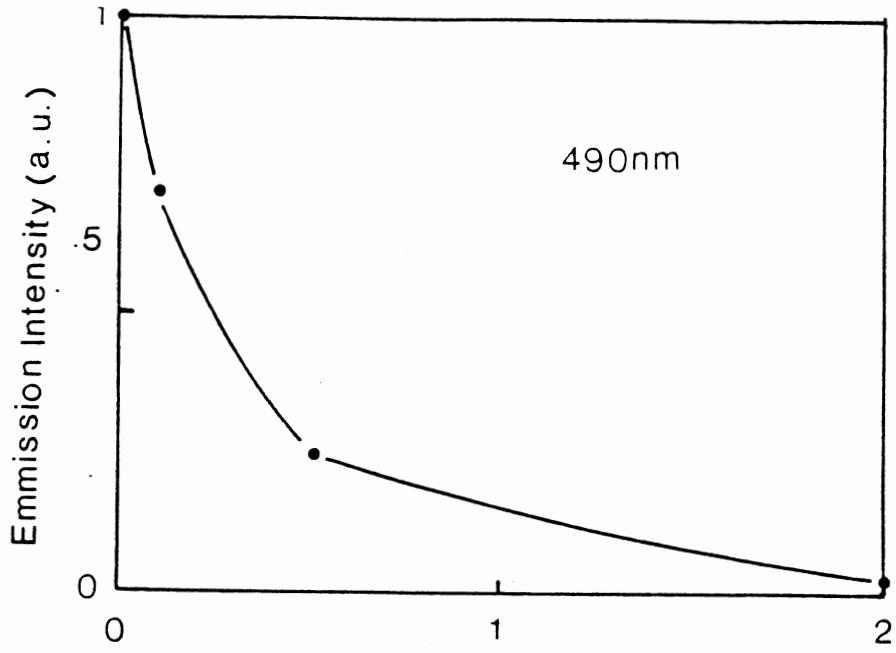

Figure 59. Variation in the intensity of emission from Mn^{2+} ions during TL as a function of Ce content.

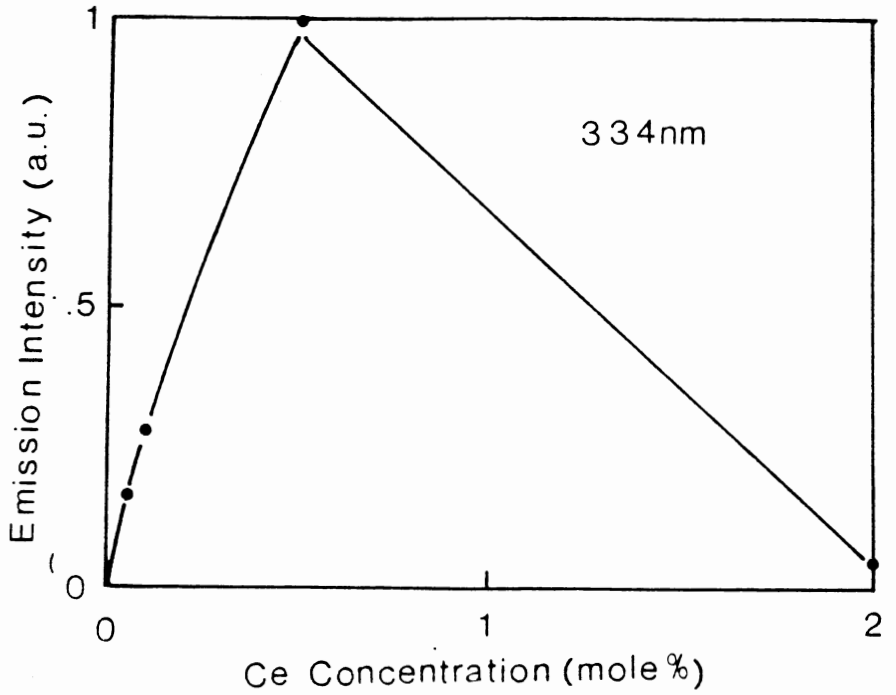

Figure 60. Variation in the intensity of emission from Ce^{3+} ions during TL as a function of Ce concentration.

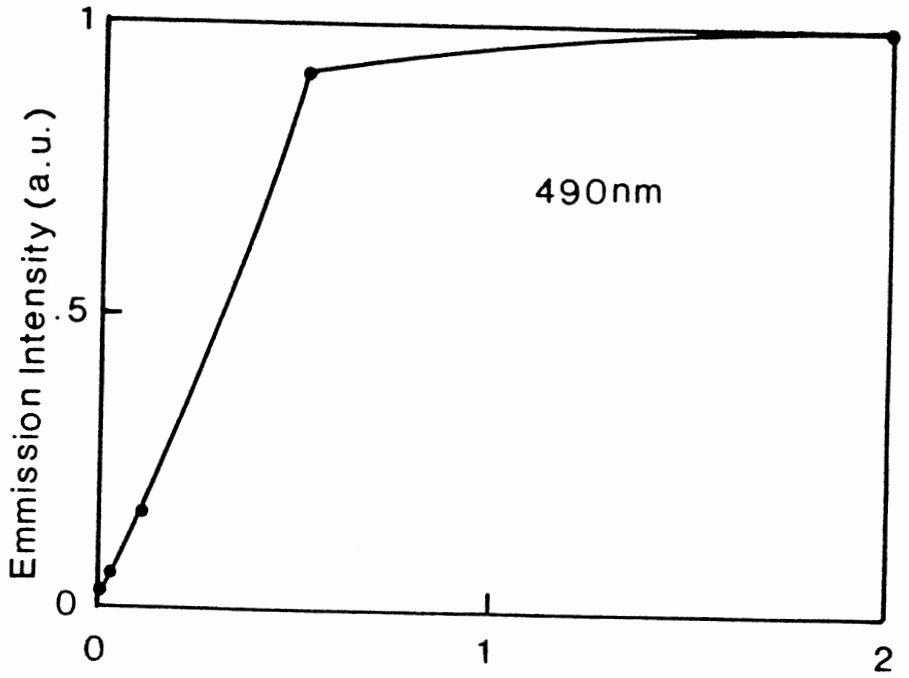

Figure 61. Variation in the intensity of emission from Mn^{2+} ions during TL as a function of Mn content.

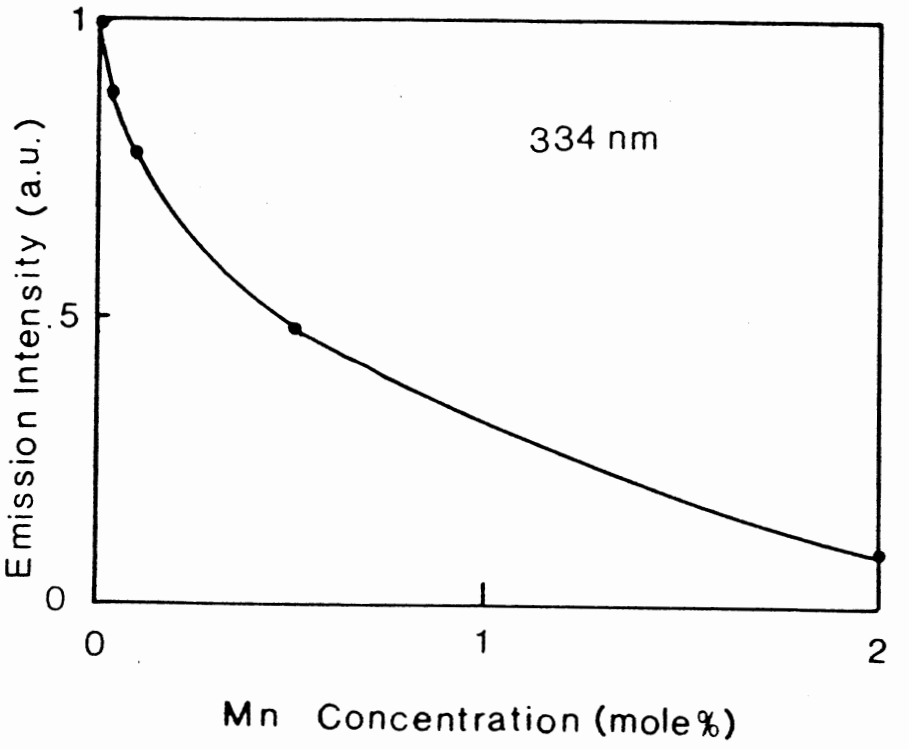

Figure 62. Variation in the intensity of emission from Ce^{3+} ions during TL as a function of Mn concentration.

(ii) The similarity of the TL and optical absorption curves between CaF_2:Ce and CaF_2:Ce,Mn.

(iii) The presence of emission from Mn^{2+} as a component of the TL emission in CaF_2:Ce,Mn, and the appearance of a weak TL emission at temperatures higher than 400^{o}C in these samples.

(iv) Identical features in the effects of pulse annealing on the optical absorption of γ-irradiated CaF_2:Ce and CaF_2:Ce,Mn.

(v) The existence of a strong excitation band due to Ce^{3+} (C_{4v}) absorption and an excitation band due to the clusters of these centers for emission from Mn^{2+}. This observation agrees with that of McKeever et al.(57)

(vi) A reduction in the TL emission from Mn, and a gain in the TL emission from Ce as a result of an increase in the Ce concentration.

(vii) An increase in the TL emission from Mn, and a decrease in the TL emission from Ce, as a consequence of adding more Mn.

Based upon the above observations we conclude the following:

(A) Ce has a strong influence on the optical absorption and TL from CaF_2:Ce,Mn, i.e. it acts as a very strong competitor to Mn in forming impurity/radiation induced defects during ionizing radiation (viz. observation (i) and (ii)). This effect is so strong that Ce dictates the observed features of the TL and optical absorption spectra from this material.

(B) Energy transfer from Ce^{3+} (C_{4v}) to Mn^{2+} takes place with high efficiency to produce emission from Mn^{2+} during photoluminescence (viz. observation (v)). Energy transfer from clusters to Mn^{2+} also produces emission from Mn^{2+}.

(C) We believe the model for TL production at above room temperature in

this material (except for observation (iii)) is akin to that in CaF_2:Ce (viz. observations (ii) and (iv)). i.e. the mechanism producing the ~130°C glow peak as discussed in chapter 5, is governed by the reaction (5.3-5.7), and the TL observed at ~350°C is probably the result of F-H type recombination.

Concerning the emission from Mn^{2+} as a component of TL emission in this material, we, from our observations and the work of other authors, suggest the following possible mechanisms.

1. Re-absorption model. In this model it is assumed that some of the 290nm light produced during V_k+e recombination which occurs during heating to 150°C (see chapter 5, section D) is absorbed by Mn/radiation induced defects. These defects have strong absorption bands in this spectral region (figure 50). This thus leaves the Mn^{2+} ion in an excited state. Relaxation to the ground state yields 490nm emission. Some observations relevant to this model are as follows:

X-ray-induced luminescence data by McKeever et al[19] show the production of 290nm emission during X-ray irradiation in CaF_2:Ce,Mn (figure 63). The excitation spectrum from irradiated CaF_2:Mn (figure 64) obtained by McKeever and Halliburton[79] reveals that absorption at 290nm produces emission from Mn^{2+}. By adding Mn/radiation induced defect absorptions bands increase thus increasing emission from Mn^{2+} during TL (observation (vii)). Observation (vi) shows that as Ce is increased the number of Mn/radiation induced defects decreases This thus results in the observed reduction of the emission from Mn^{2+}.

2. Energy transfer model. This model assumes that reabsorption of 290nm light produced by V_k+e recombination during heating to 150°C leaves Ce^{3+} (C_{4v}) in an excited state. Then the non-radiative energy transfer

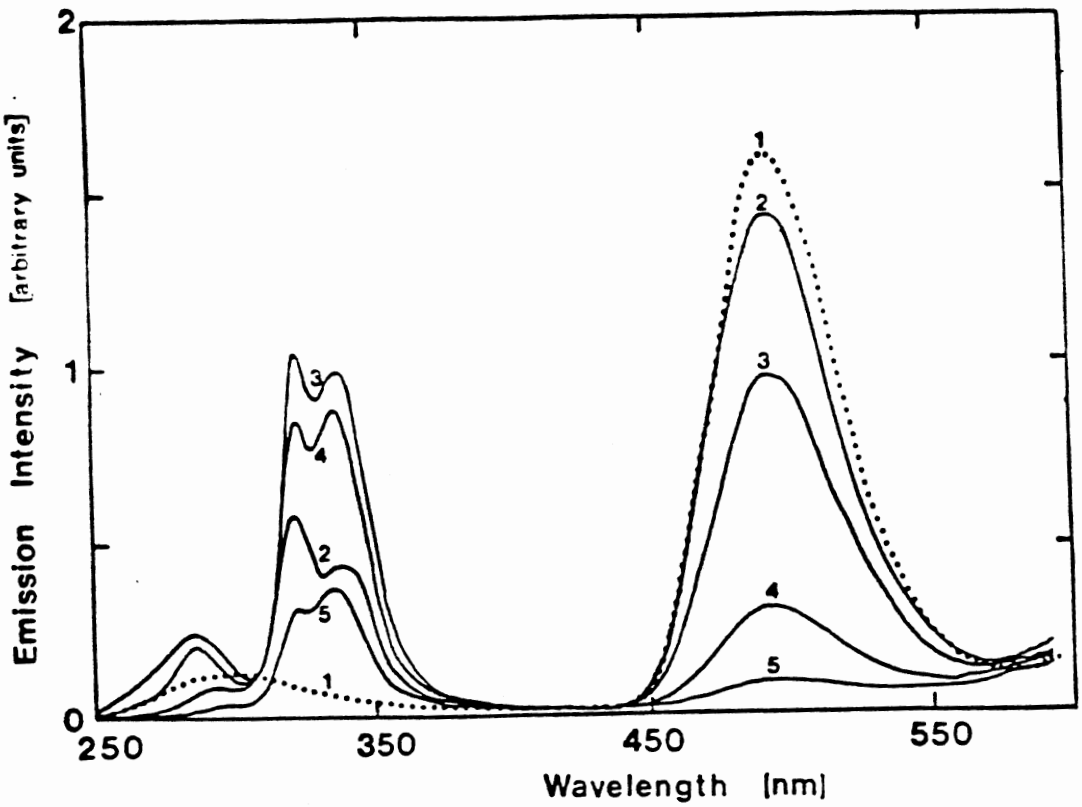

Figure 63. X-ray-induced emission spectra for CaF_2:Mn,Ce 1. (0.5%, 0%), 2. (0.5%, 0.01%), 3. (0.5%, 0.1%), 4. (0.5%, 0.5%), 5. (0.5%, 2.0%). (After McKeever et al[79]).

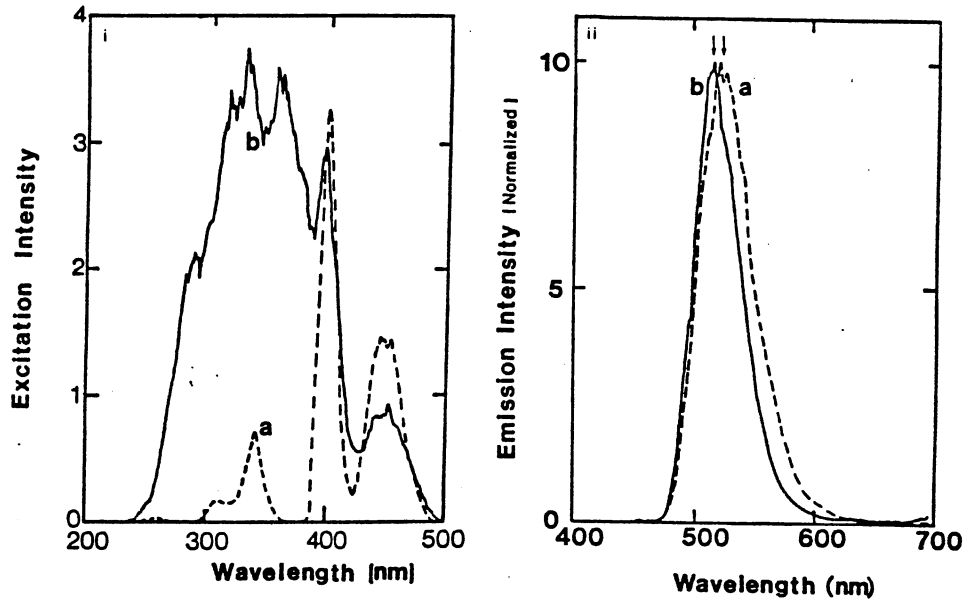

Figure 64. Excitation (i) spectrum before (a) and after (b) irradiation for CaF_2:Mn (3.0%). (ii) corresponding emission spectra. All data taken at room temperature. (After McKeever et al[79]).

from some of these excited Ce^{3+} ions to Mn^{2+} causes emission from Mn^{2+} ions. Observation (v) provides evidence for energy transfer from Ce^{3+} (C_{4v}) centers and clusters of these centers to the Mn^{2+} ions. However observation (vi), which is similar to data from X-ray-induced luminescence reported by McKeever et al,[19] shows that adding Ce decreases emission from Mn^{2+} rather than increasing it. In contrast, photoluminescence measurements by the above authors show an entirely different behavior. This difference is summarized in figure (65). The diminishing emission from Mn^{2+} may possibly be a consequence of Ce-to-Ce energy transfer when Ce is added, but this does not explain why the photoluminescence is so different from the TL and X-ray luminescence data.

Lastly, the TL emission from Mn^{2+} at ~350°C and above 400°C can be envisioned as a result of F-H pair recombination and will be discussed in chapter 7. However, we note briefly here that this mechanism will also produce 290nm emission. Absorption of this emission by Mn^{2+} (which possess a weak absorption band at 290nm)[15] may then result in 490nm emission.

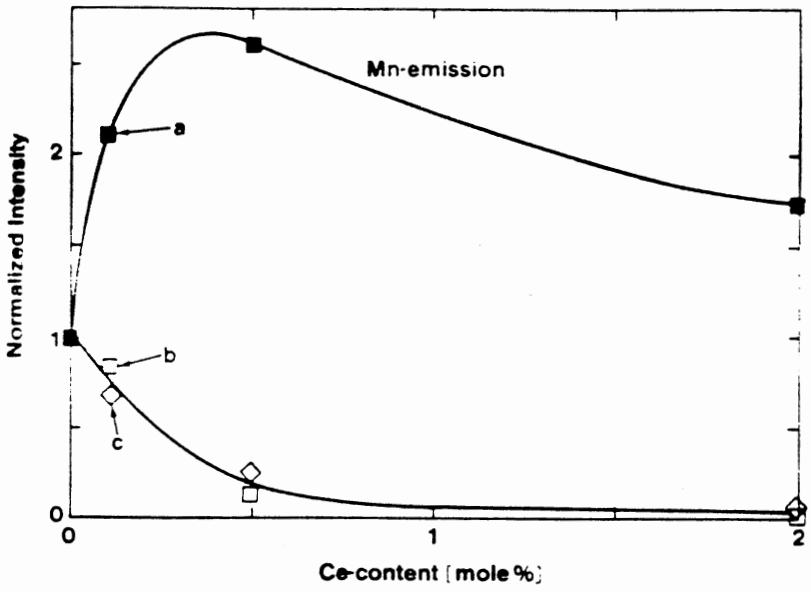

Figure 65. Variation in the intensity of the emission from Mn^{2+} as a function of Ce content: (a) photoluminescence-measured at 500nm and excited at 315nm; (b) TL-intensity at 100°C measured at 490nm; (c) X-ray-induced luminescence measured at 495nm. (After McKeever et al[57]).

Chapter VII

CaF_2:Mn

Owing to its attractive TL properties, such as high radiation sensitivity and large linear dose range, CaF_2:Mn has been used as a popular TLD material. Surprisingly, however, this material has an initially high fading rate (signal loss caused by heat, light or anomalous effects.) Although its properties regarding its TLD performance have received much attention by researchers, the exact TL production mechanism in this material is still uncertain. A knowledge of the TL mechanism (i.e. the identification of the defects involved in the TL process) may play an important role in understanding the cause of the undesired factors. For example, what role does the presence of trace impurities play in the production of TL? The results of neutron activation analysis (performed at the Chemistry Department of the University of Maryland) on the representative samples of CaF_2:Mn used by us is given in table (IV). This table represents the presence of trace elements in these materials. This table also reveals that for low Mn concentration the actual Mn content in the crystal is the same as the melt Mn-contents whereas for higher dopant levels the actual Mn-contents in the crystal are approximately half of the melt concentration.

These and other factors are addressed in this chapter. The chapter is divided into two sections (A and B). In section (a) we present TL and optical absorption data concerning the effects of

TABLE IV

Neutron activation analysis of a representative set of CaF_2 samples

Element	Samples			
	Optovac (0.1% Mn)	Optovac (1.0% Mn)	Optovac (3% Mn)	Harshaw TLD-400
Mn	0.109%	0.701%	1.430%	1.570%
	± 0.013%	± 0.010%	± 0.010%	0.010%
B	1.200	0.600	0.600	1.300
	± 0.300	± 0.200	± 0.200	± 0.700
Na	96.000	91.000	90.000	86.000
	± 5.000	± 5.000	± 5.000	± 5.000
K	-	-	-	5.000
	-	-	-	± 3.000
Sc	0.013	0.017	0.020	0.011
	± 0.004	± 0.003	± 0.004	± 0.004
Cr	-	0.900 ppb	1.300 ppb	26.000 ppb
	-	± 0.400 ppb	± 0.400 ppb	± 3.000 ppb
Fe	80.000	60.000	60.000	120.000
	± 30.000	± 30.000	± 30.000	± 30.000
Co	0.230	-	-	0.160
	± 0.080	-	-	± 0.080
Zn	8.900	5.000	-	10.600
	± 2.600	± 2.400	-	± 3.4000
As	-	-	0.050	0.019
	-	-	± 0.025	± 0.008
Br	1.060	-	-	0.230
	± 0.090	-	-	± 0.020
Sr	240.000	240.000	140.000	280.000
	± 20.000	± 10.000	± 20.000	± 20.000
Mo	-	-	-	0.230

TABLE IV (continued)

	Optovac (0.1% Mn)	Optovac (1.0% Mn)	Optovac (3% Mn)	Marshaw TLP-400
	-	-	-	± 0.110
Cd	0.600	0.400	1.000	0.200
	± 0.300	± 0.200	± 0.300	± 0.100
Sb	0.118	0.020	0.400	0.008
	± 0.011	± 0.070	± 0.030	± 0.004
Ba	55.000	250.000	420.000	71.000
	± 13.000	± 20.000	± 30.000	± 16.000
La	15.400	18.500	14.500	0.021
	± 0.800	± 0.900	± 0.700	± 0.010
Ce	0.750	0.100	0.540	-
	± 0.220	± 0.030	± 0.260	-
Sm	148.000 ppb	108.000 ppb	105.000 ppb	3.000 ppb
	± 9.000 ppb	± 6.000 ppb	± 8.000 ppb	± 0.800 ppb
Yb	0.180	0.130	0.180	-
	± 0.060	± 0.040	± 0.060	-
Lu	15.000 ppb	9.000 ppb	8.000 ppb	-
	± 3.000 ppb	± 3.000 ppb	± 3.000 ppb	-
Hf	0.110	-	-	0.110
	± 0.030	-	-	± 0.030
W	0.028	-	-	0.025
	± 0.014	-	-	± 0.005
Au	3.200 ppb	1.400 ppb	4.000 ppb	1.300 ppb
	± 0.300 ppb	± 0.200 ppb	± 0.300 ppb	± 0.200 ppb
Th	0.080	-	0.160	-
	± 0.030	-	± 0.050	-
U	0.058	0.200	0.108	0.044
	± 0.009	± 0.030	± 0.015	0.005

background rare-earth impurities on the optical absorption and TL. Section (B) contains TL and optical absorption from high Mn-content crystals. In this latter section a mechanism for TL production in these materials is presented.

Section A

Optical absorption

For the sake of further discussion, concerning the role of trace impurities on the optical absorption bands from CaF_2Mn, we first investigated the optical absorption from "pure" CaF_2 samples. Figure (66) shows optical absorption from "pure" CaF_2 after γ-irradiation (383Gy) at room temperature. Profiles (a) and (b) are, respectively obtained from samples purchased from Optovac and Harshaw. Both curves exhibit similar features except that the Optovac sample shows more absorption. The observed profiles reveal Smakula's "four band" structure. As seen, the major peaks are observed at ~325, 385 and 600nm. The fourth peak, which is located at ~200nm, is not seen in this figure. A careful qualitative comparison between this spectrum with those obtained for CaF_2 intentionally doped with a variety of rare-earth ions by other authors[4] suggests that the spectrum observed by us is due to the PC centers, possibly formed from a trace of Y or Tb which must be present in this material. Some PC^+ centers may also be present.

It should be noted that RE^{3+} ions are converted to RE^{2+} ions during ionizing radiation.[81] These RE^{2+} ions do not give rise to absorption in the visible region (except La^{2+}, Ce^{2+} and Tb^{2+}).[20] However, there might be a small contribution to the spectrum in figure

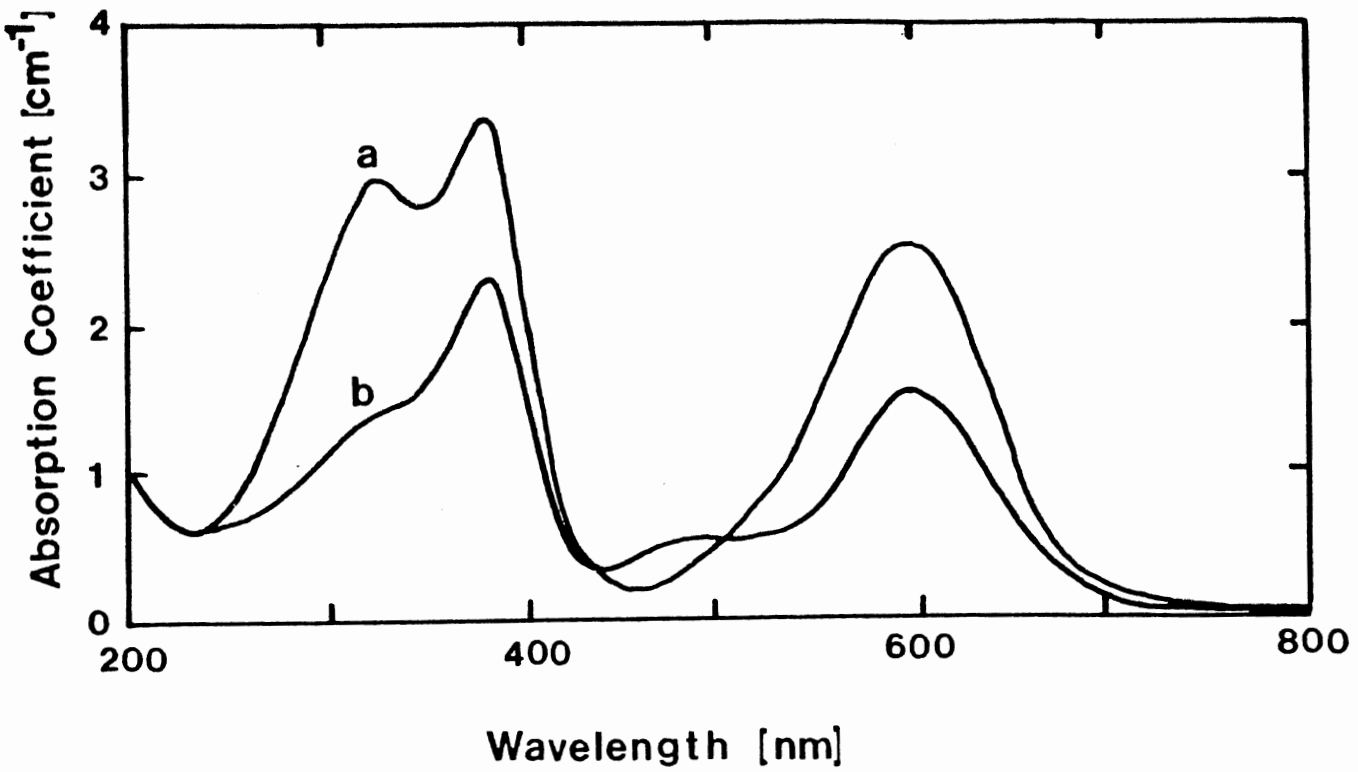

Figure 66. Optical absorption from "pure" CaF_2 samples, after 383Gy γ-irradiation at room temperature, from (a) Optova and (b) Harshaw.

(66) from some divalent ions.

Figure (67) exhibits the effect of thermal annealing on the observed "four band" spectrum in figure (66). As seen all the absorption peaks anneal together and decay between room temperature and 200°C.

Optical absorption from a CaF_2:Mn (0.5%) sample γ-irradiated (2.57kGy) at room temperature was already displayed in figure (50). As can be seen, the spectrum contains the "four band" structure and new "Mn-related" absorption bands. Thermal annealing of this spectrum reveals that the "four band" component decreases over the room temperature to 200°C whereas the Mn-related absorption bands increase over this region. This is seen particularly in figure (68) where we see that the absorption bands at ~440nm and ~560nm (Mn-related) increase while those at ~385nm and ~600nm (due to PC centers) decrease. We note that after 200°C anneal the spectrum shows a different feature (curve 5). This new absorption feature which is Mn-related shows a major annealing step over the region from 200°C to 300°C. The remaining components of this new absorption feature start to anneal at ~400°C.

Figure (69) exhibits the absorption curve for the 3.0% Mn-doped material. This absorption spectrum has the same features as that of 0.5% Mn-doped material after 200°C anneal (figure 68, curve 5). Thus, at 3%Mn the Mn-related bands totally dominate the spectrum. Hence, we observe that as Mn is added to the material the Mn-related absorption bands dominate <u>and</u> the absorption due to the trace impurities is suppressed. This observation is also clearly seen in optical absorption data obtained from CaF_2 doped with variable Mn concentration by McKeever[82] (figure 70). We interpret this observation based on the

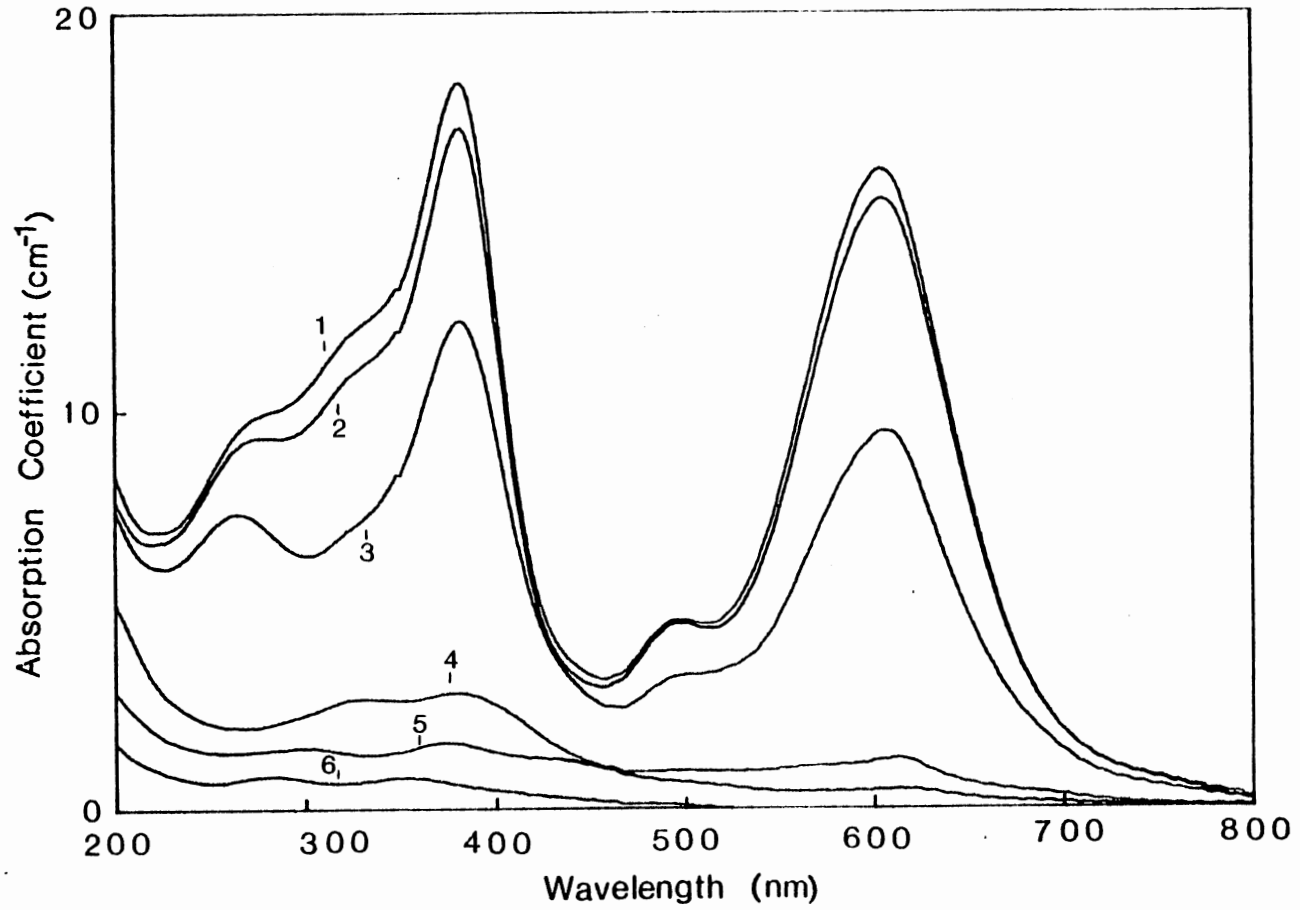

Figure 67. Optical absorption from a "pure" CaF_2 sample after 383Gy γ-irradiation and annealing at the following temperatures: (1) room temperature (2) 50°C (3) 100°C (4) 150°C (5) 200°C (6) 300°C.

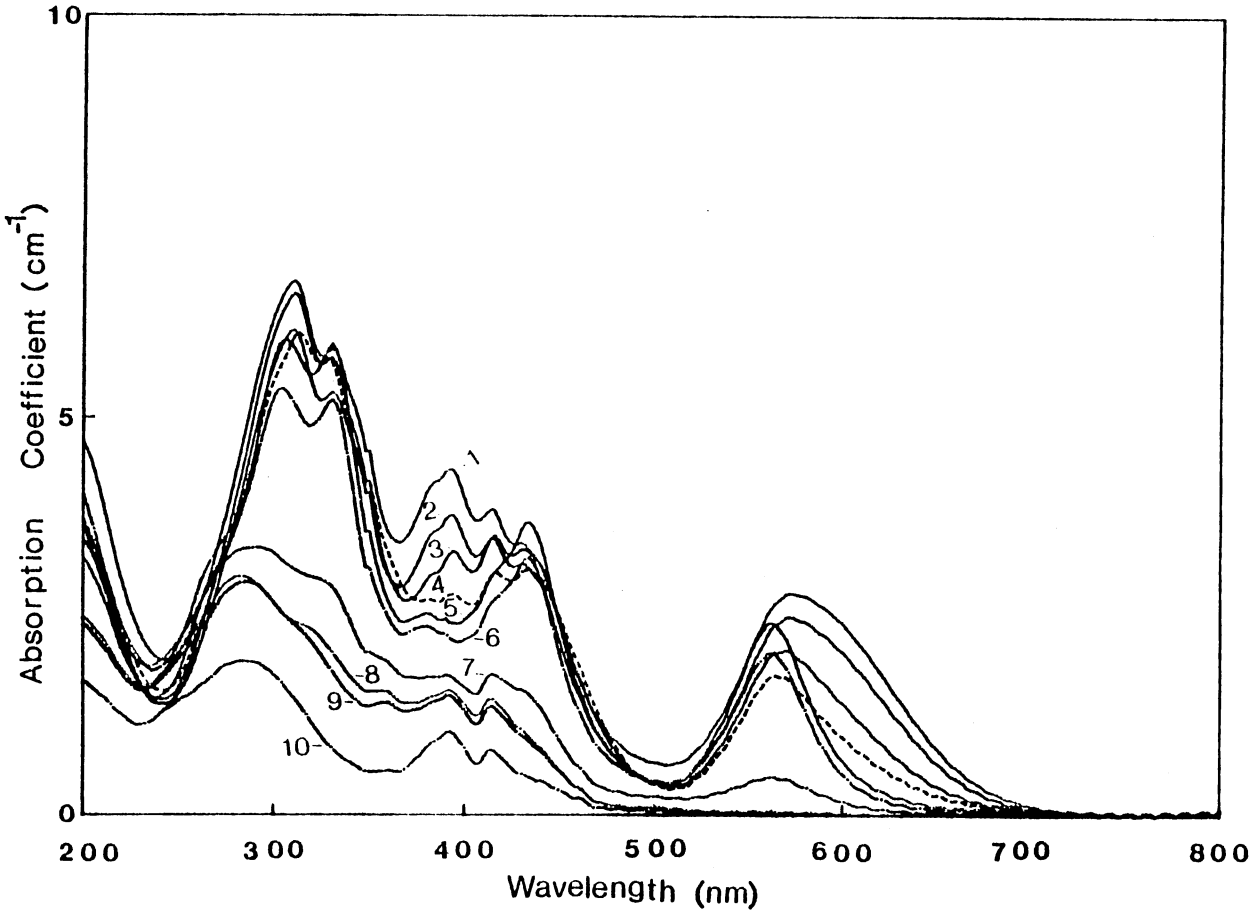

Figure 68. Optical absorption from CaF_2:Mn (0.5%) following a gamma dose of 383Gy at room temperature. The annealing temperatures are: 1-room temperature; 2-to-11 -50°C- to -450°C in steps of 50°C.

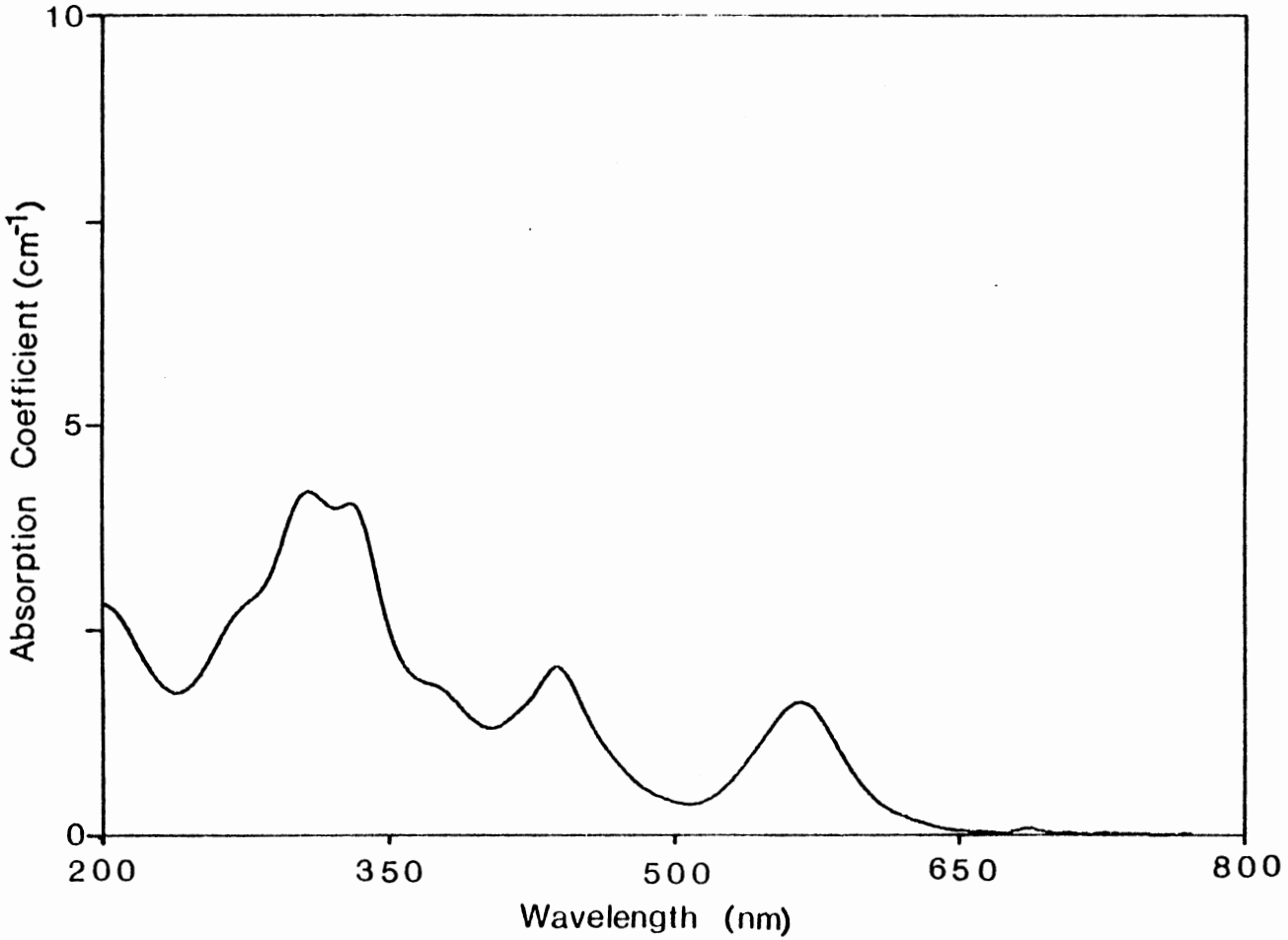

Figure 69. Optical absorption from CaF_2:Mn (3%) following a γ dose of 383Gy at room temperature.

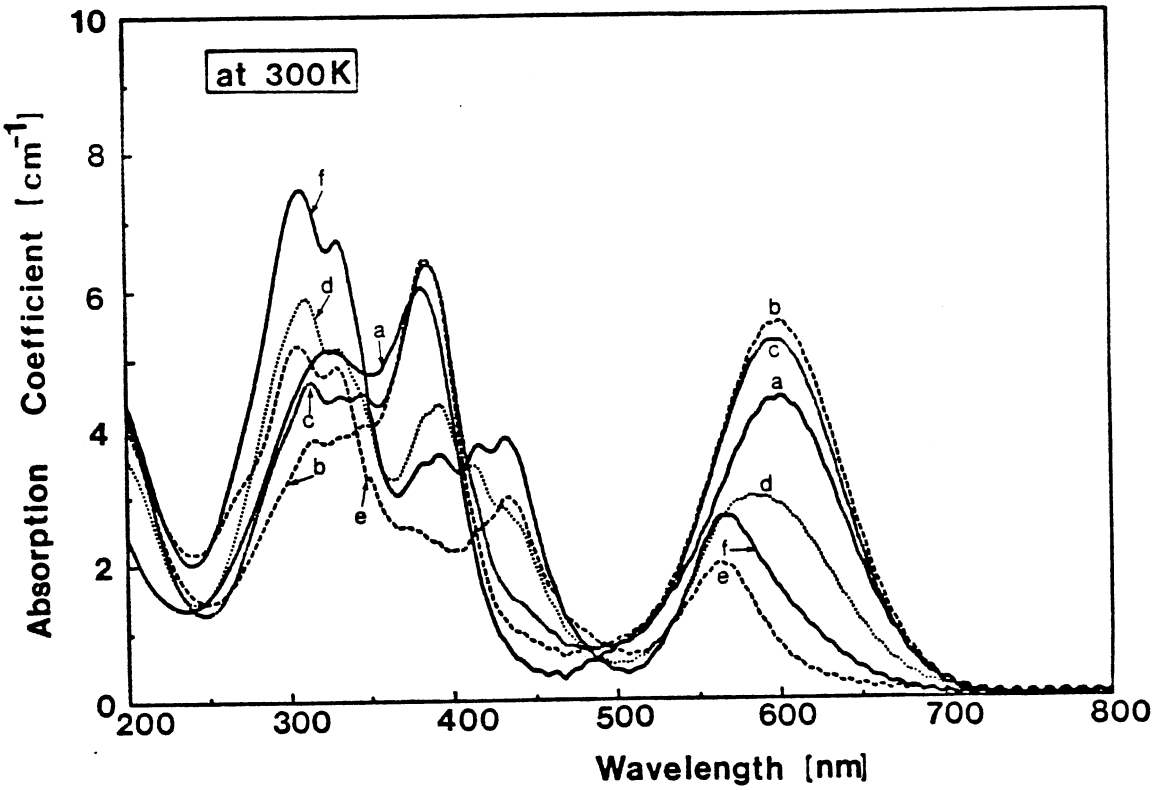

Figure 70. Optical absorption for a series of γ-irradiated (137Gy at room temperature) samples of CaF_2:Mn for various doping levels. (a) "pure"; (b) 0.01% Mn; (c) 0.1% Mn; (d) 0.5% Mn; (e) 1.0% Mn; (f) 3.0% Mn.

nature of competition between Mn and trace of RE ions for forming impurity-radiation induced defect(s). This interpretation is entirely consistent to what we saw in chapter 6, for intentionally Ce-doped CaF_2:Mn. In chapter 6 we observed that Ce had a very strong influence on the optical absorption and TL from CaF_2:Mn.

Thermoluminescence

TL from "pure" CaF_2 following 1.5Gy of γ-irradiation at room temperature reveals three weak TL emissions (figure 71). The two glow peaks at 80 and 190°C are associated with the major annealing of the "four band" structure absorption bands from these samples over the room temperature-to-200°C region. The annealing of the very weak remainder of the absorption bands corresponds to the appearance of the third TL peak at ~300°C.

Figure (72) exhibits TL glow peaks for 0.01% Mn-doped CaF_2. In this figure we are witnessing two major glow peaks one at ~190°C and the other at 260°C. The TL from CaF_2 doped with Mn of concentrations 0.1% and 0.5% (figure 73 and 74) show a similar picture to that of CaF_2:Mn (0.01%) but it should be noted that as the Mn concentration is increased the higher-temperature peak grows larger with respect to the lower-temperature peak. For CaF_2Mn (1%) the higher-temperature peak showed a composite structure and it was also shifted to a higher temperature, whereas the lower-temperature peak started to diminish (figure 75). At 3.0% Mn-doped CaF_2 we only observe one intense, single composite peak at ~280°C (figure 76).

In order to see the effects of Mn concentration on the TL glow curves observed above, we show in figure (77) the relative heights of

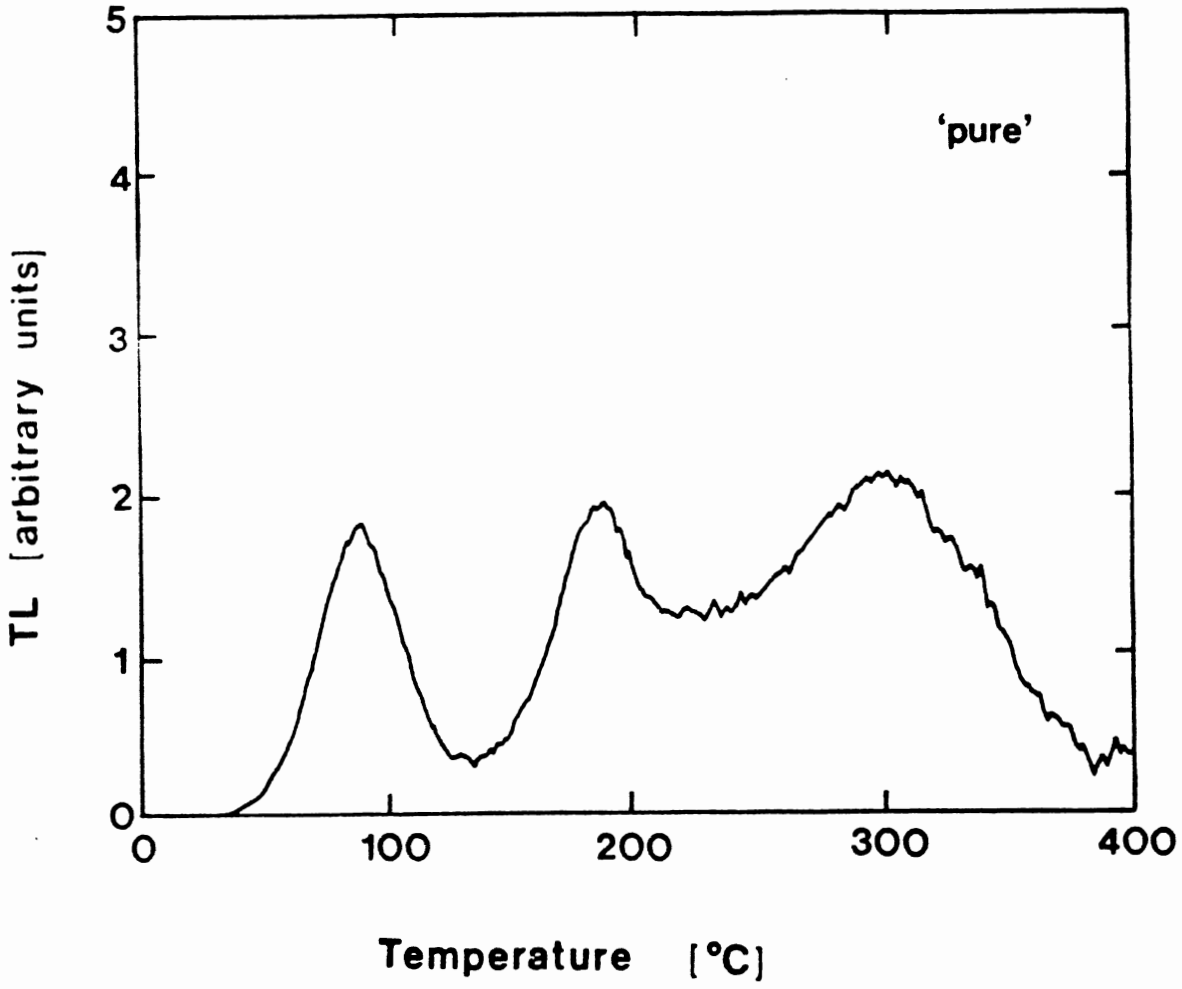

Figure 71. TL from "pure" CaF_2 following 1.5Gy γ-irradiation at room temperature.

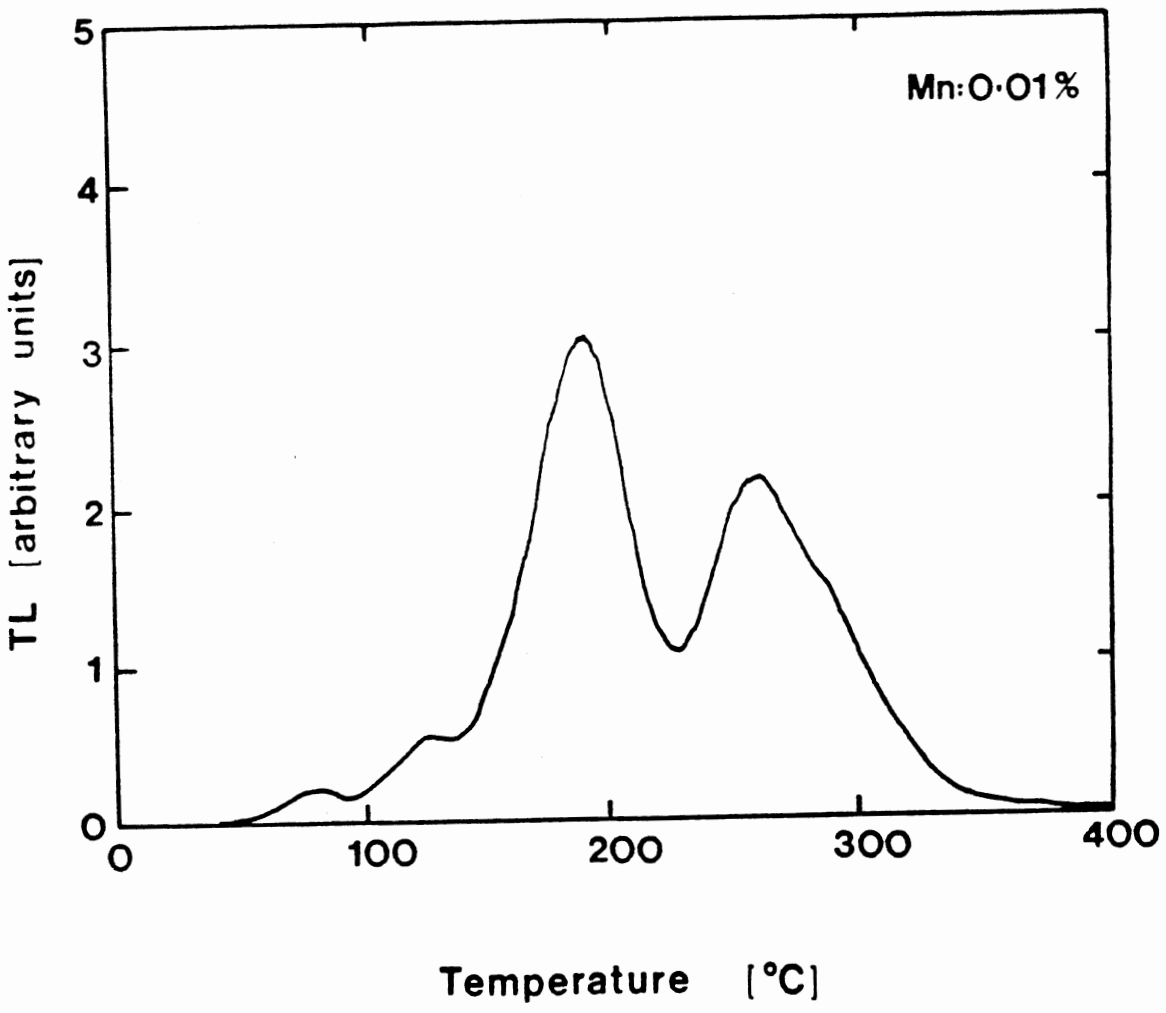

Figure 72. TL from CaF_2:Mn (0.01%) following 1.5Gy γ-irradiation at room temperature.

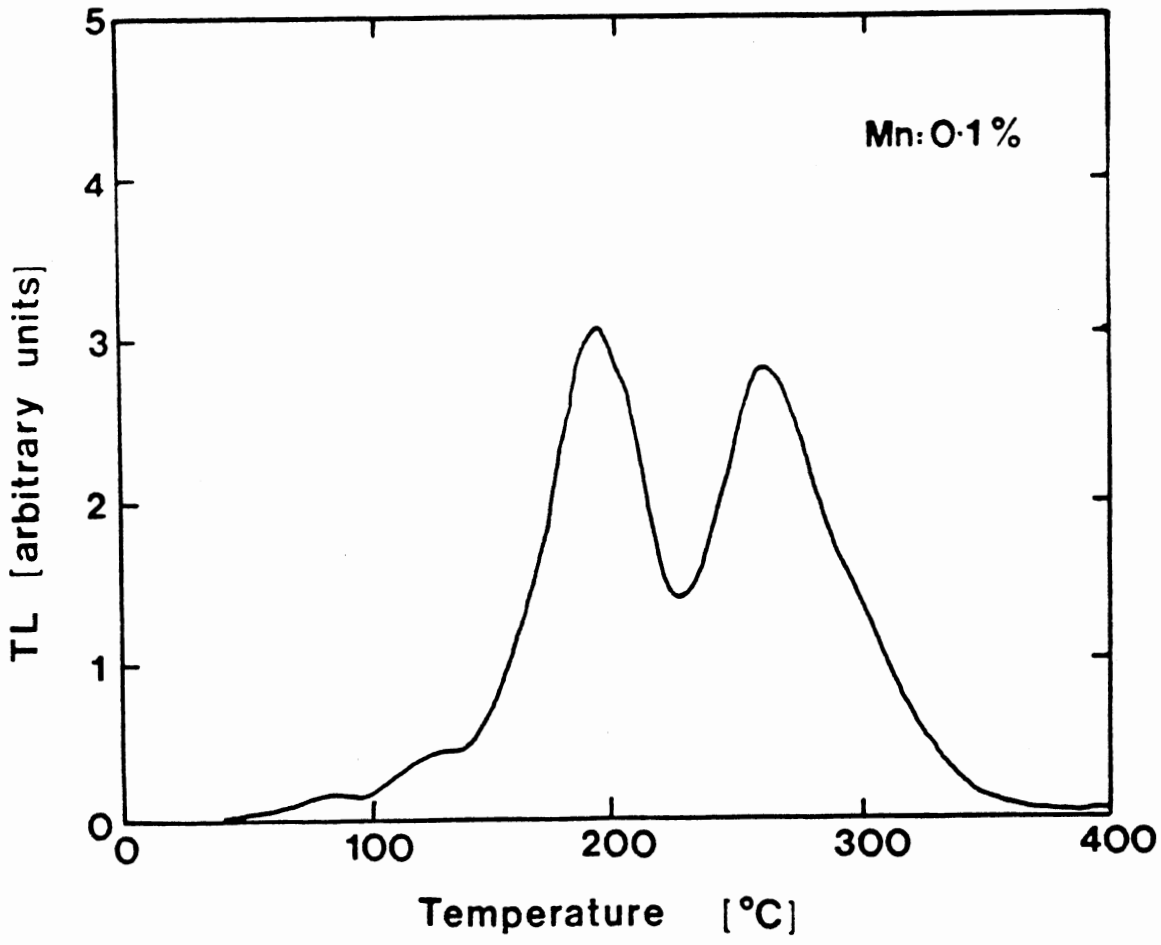

Figure 73. TL form CaF_2:Mn (0.1%) following 1.5Gy γ-irradiation at room temperature.

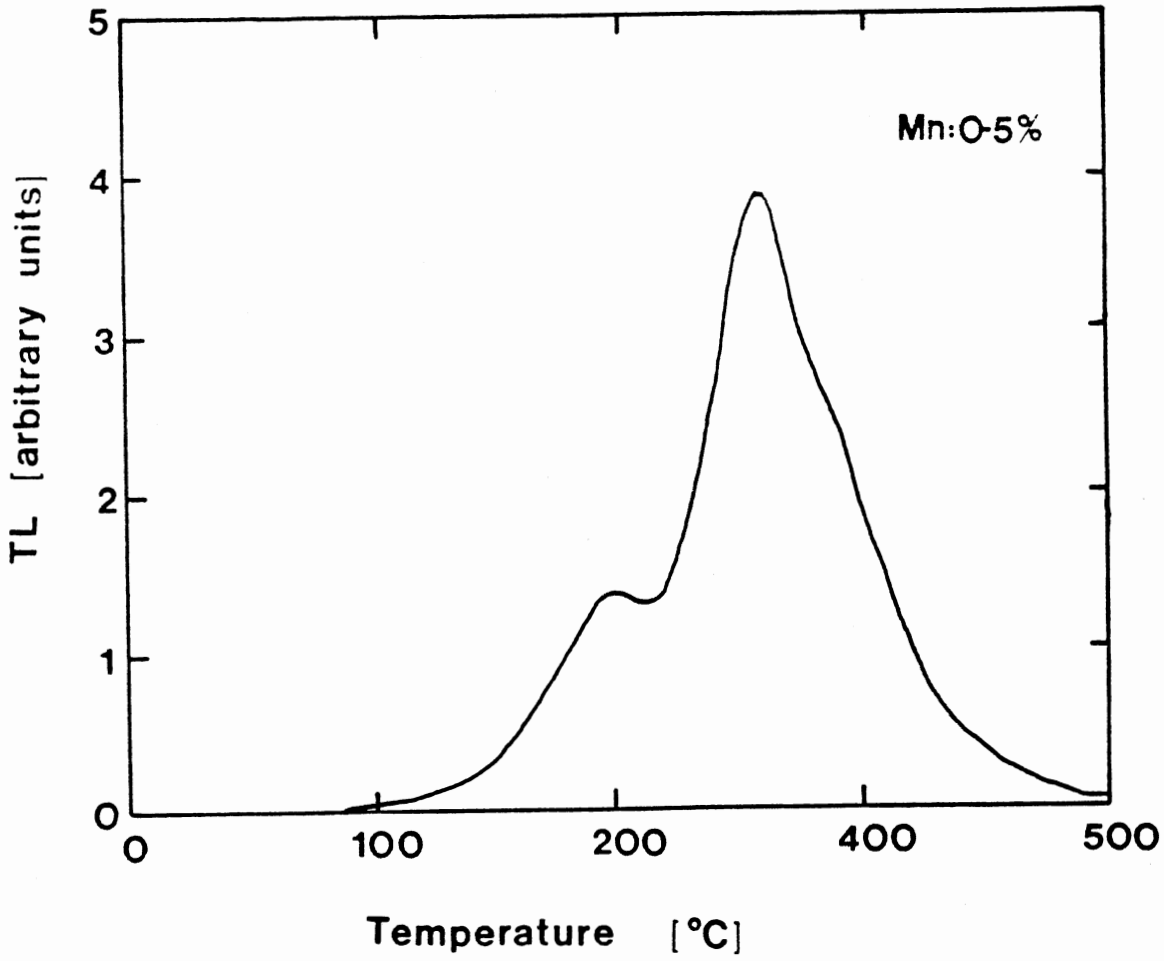

Figure 74. TL from CaF_2:Mn (0.5%) following 1.5Gy γ-irradiation at room temperature.

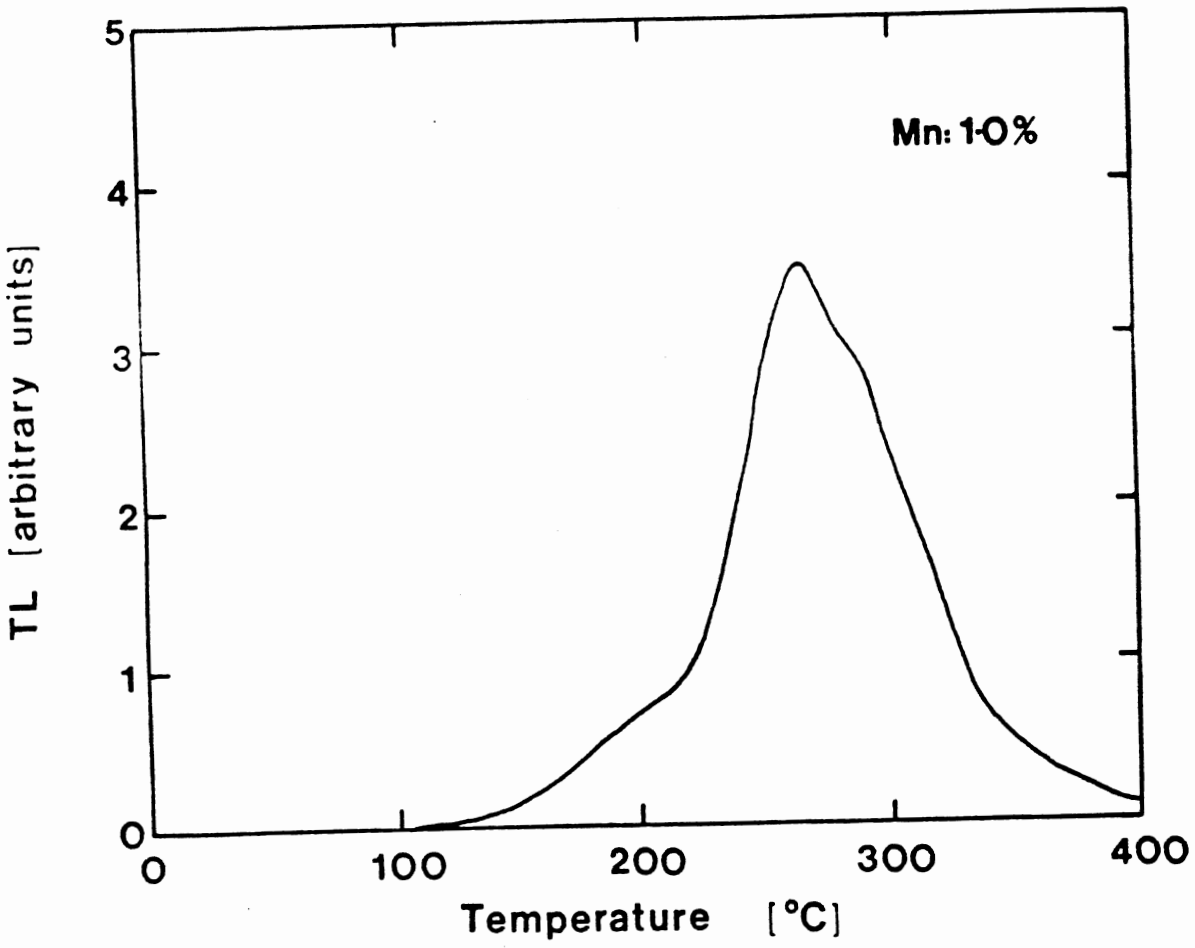

Figure 75. TL from CaF_2:Mn (1%) following 1.5Gy γ-irradiation at room temperature.

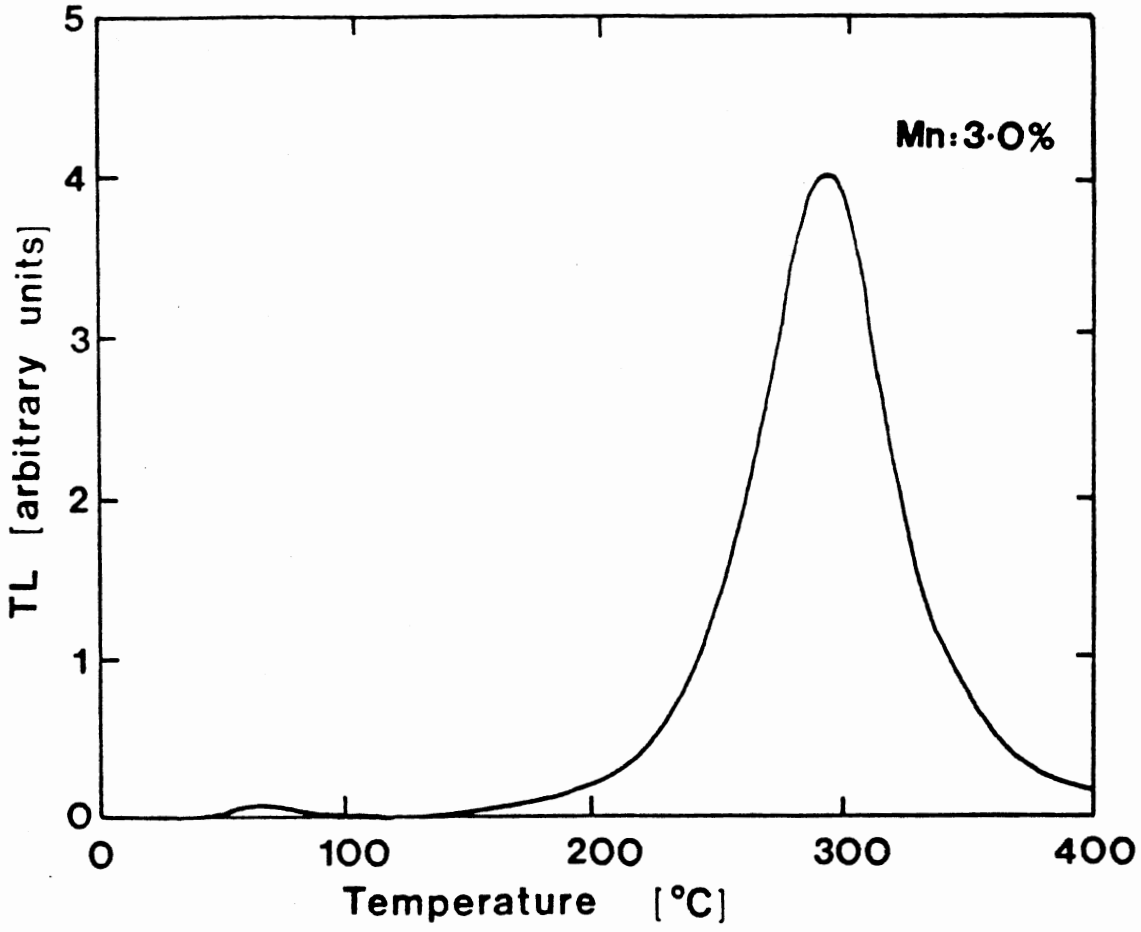

Figure 76. TL from CaF_2:Mn (3%) following 1.5Gy γ-irradiation at room temperature.

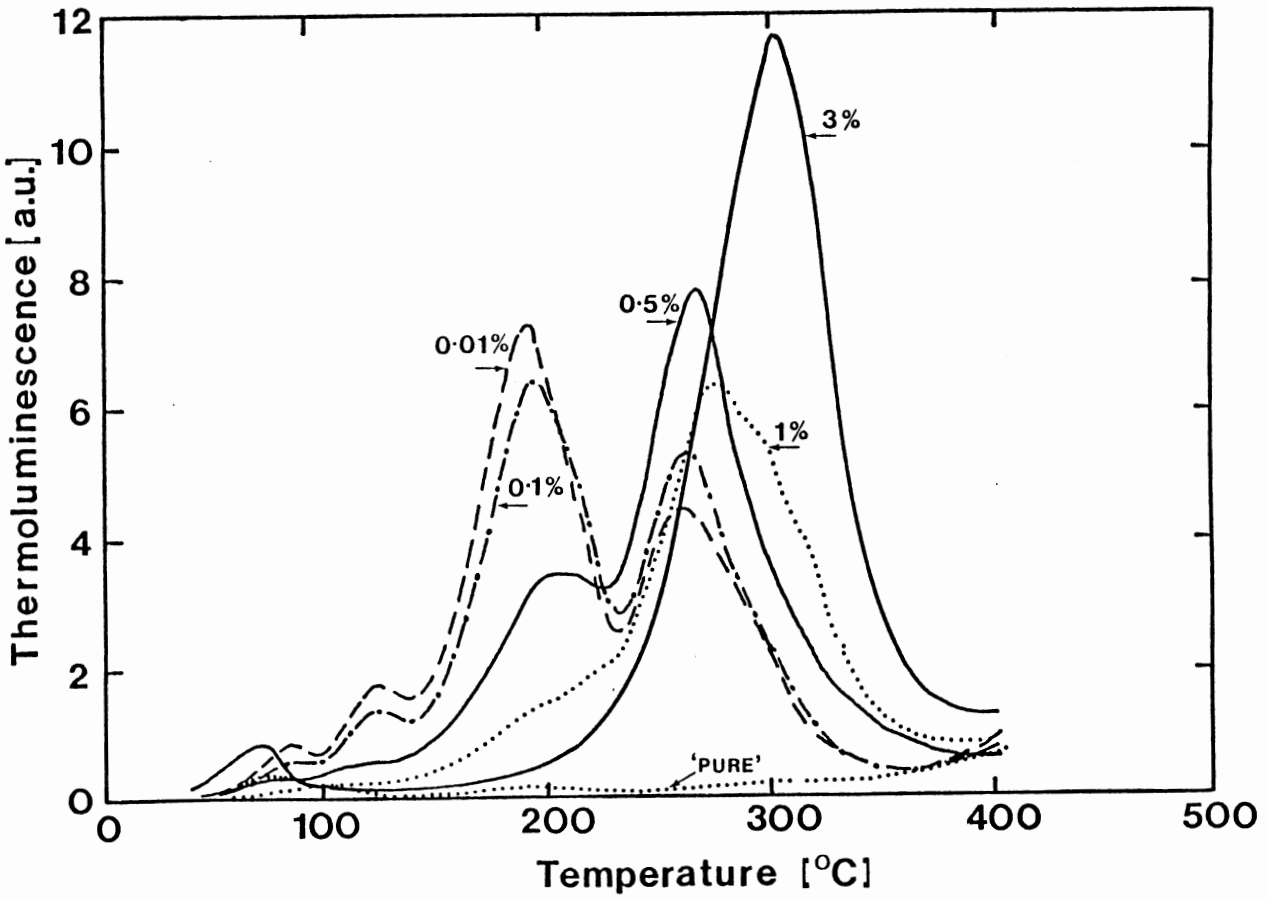

Figure 77. Comparison of the normalized TL curves of figures 71-76.

the various TL peaks. We see the consistancy between this observation and the optical absorption data which, we recall, showed that increasing the Mn content suppressed the absorption bands due to the trace rare-earth impurities (i.e. PC and PC^+ centers). Thus the lower-temperature TL peak is associated with the annealing of these centers. On the other hand, the higher-temperature peak is associated with the annealing of the Mn-related absorption bands.[82] As will be discussed in section B we believe these bands to be due to (Mn^{2+}-F) complexes.

Lastly, in figure (78) we demonstrate the effect of the trace impurities on the TL from CaF_2:Mn (3%) belonging to two different batches but from the same manufacturer. As seen, they exhibit different features, i.e. one of them shows more structure in the lower temperature region. We believe that this is due to the unwanted presence of rare-earth impurities in the starting material used in the crystal growth process. These samples were grown by Optovac and they used natural Mexican Fluorite as a starting material.

Thus, the above results show that trace rare-earth impurities affect both the size and stability of the various optical absorption bands and, therefore, the TL.

Section B

Optical absorption

As we noted in figure (69) the spectrum for higher concentration (3%) was totally dominated by Mn-related bands.

The origin of these Mn-related absorption bands will now be discussed. There are several possibilities, each of which will be discussed separately. We will start with a consideration of Mn^+ and

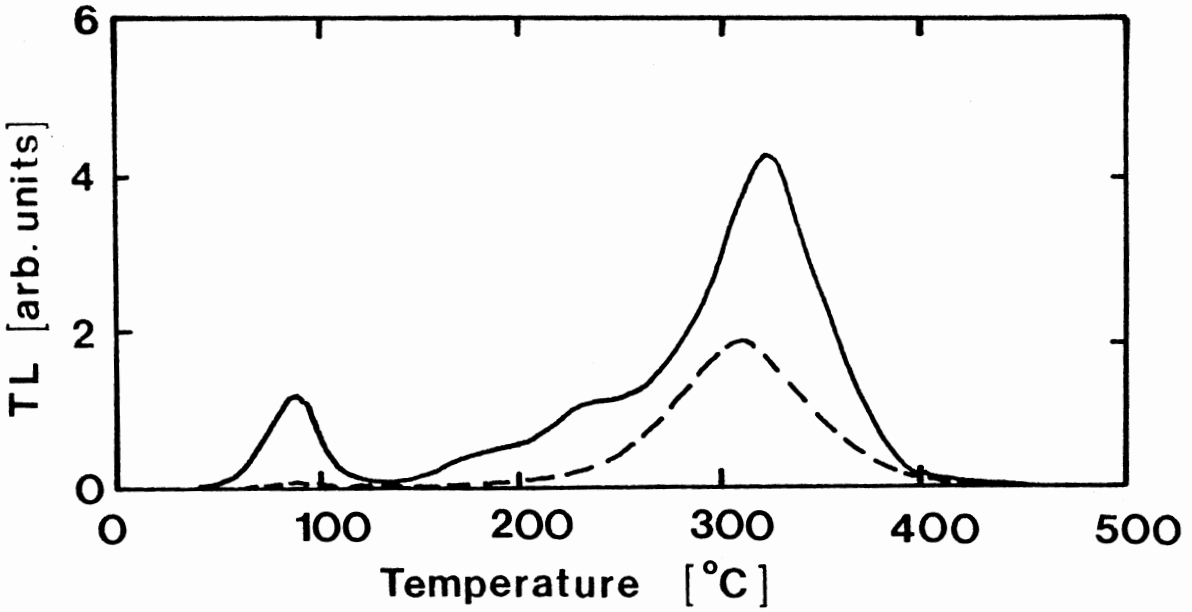

Figure 78. Comparison of the TL from CaF_2:Mn (3%), produced from two different batches, but from the same manufacturer. (Optovac Inc.).

Mn^{3+}.

From EPR measurements,[79] it was observed that Mn^{+} (Mn^{2+} capturing an electron) was <u>not</u> formed during ionizing irradiation at room temperature. Since Mn^{3+} (Mn^{2+} capturing a hole) and Mn^{+} both have an even number of electrons in the 3d shell, their EPR spectra reveal very similar features. No evidence of Mn^{3+} was seen in the EPR data either. Thus, it is not unreasonable to claim that Mn^{3+} ions are also not formed during ionizing irradiation at room temperature. Therefore one does not expect contributions from either Mn^{2+} or Mn^{3+} to the Mn-related absorption bands.

It has been reported[83-86] that in systems such as MgF_2, $RbMgF_3$ and $KMgF_3$ doped with Mn^{2+}, a radiation-induced defect (e.g. an <u>F</u> center) with a diffuse wave function can enhance the oscillator strength of a nearby Mn^{2+} ion by a factor $\sim 10^5$. This achieved via an exchange interaction and, in turn, results in the observation of the otherwise-forbidden internal transitions within these ions. Figure (79) shows the schematic diagram for the exchange interaction between the ground and first excited states of an isolated Mn^{2+} ion and an <u>F</u> center. McKeever et al,[15] by assuming that the observed spectrum (figure 70) is from such internal Mn^{2+} transitions, has estimated an oscillator strength increase of the order of 10^3 (i.e. a strength of 10^{-4}). They also from thermal and optical bleaching studies observed the following: Annealing of the main peaks (including 564nm band) over the same temperature interval, which may indicate that they are all due to the same defect. Thus annealing results in 495nm TL emission and it is assigned to a transition from the lowest excited state of Mn^{2+} to its ground state. Hence the ~564nm absorption band cannot be from Mn^{2+}

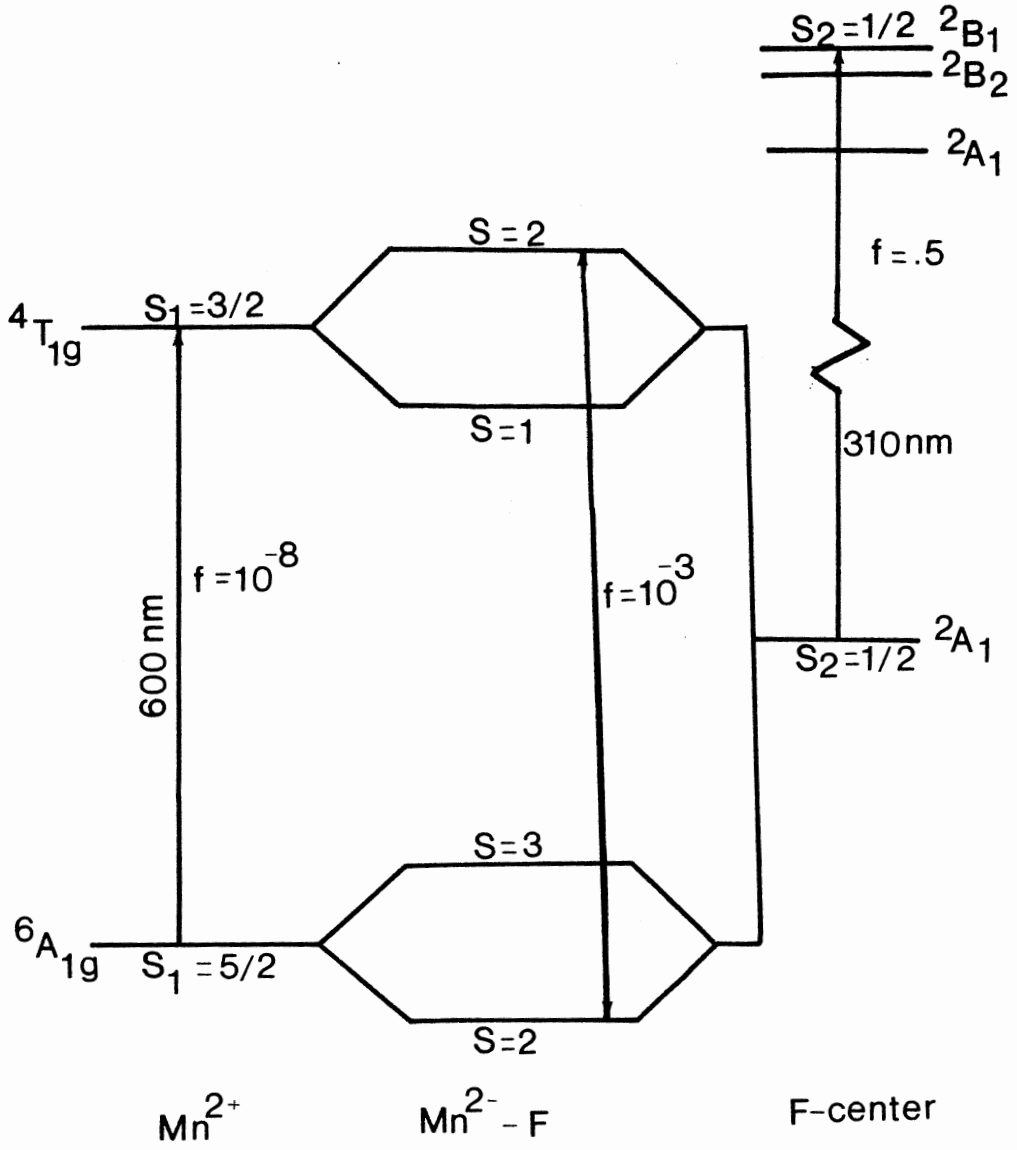

Figure 79. Schematic diagram for spin coupling between the ground and first excited states of isolated Mn^{2+} and F centers. (After Sardar et al[83]).

ions. Furthermore, they noted that 564nm bleaching resulted in a decrease in all of the absorption bands. Hence, it is not possible to reconcile these facts with the view that the bands are due to internal transitions in Mn^{2+} ions. Instead, they suggest that the spectrum is due to perturbed F center absorption in (Mn-F) complex(es) (i.e. a C_{3v} defect consisting of a body-centered Mn^{2+} with a nn F center along <111>).

This model is possible as is discussed in what follows. The presence of an analogous center, namely, the PC center (RE^{2+}-F) complex, has already been confirmed in $CaF_2:RE^{3+}$, both experimentally[14] and theoretically.[41] It has been suggested that the observed spectrum due to these latter centers can be explained by using the energy levels of the F_A-center (perturbed F center). The F center in CaF_2 has dT symmetry with respect to the Ca^{2+} ions. The optical absorption of this center (at ~375nm) corresponds to the transition from the orbitally-singlet s-like ground state to the orbitally-triplet p-like excited state. The presence of an impurity cation on a lattice site nearest the F center reduces the potential acting on it to C_{3v}. This symmetry reduction results in the splitting of the triplet excited state (see figure 14b). The optical absorption associated with these new energy levels will consist of bands polarized in the plane perpendicular to the impurity (impurity-F) complex axis and along the (impurity-F) complex axis.

Alig [41] arrived at the calculation of the energy levels for the PC center, in a manner similar to that for the F_A-center in alkali halides. He did so by substituting a Na^+ ion for a RE ion. He suggested that the analogy with the F_A-center will be complete if the impurity

ion was divalent and was of smaller size than the Ca^{2+} ion. Mn^{2+} is such an ion having a smaller ionic size (.80Å) compared with Ca^{2+} (.99Å). Thus from the point of view of both valency and size it fits very well with the above calculation.

The observation which indirectly supports the presence of the (Mn^{2+}-F) complex was the enhancement of the Mn-related absorption bands and a decrease in the "four-band" spectrum during heating (RT-200°C). We recall from chapter 5 that heating to ~150°C released electrons from Ce^{2+} (O_h). Capturing of the electrons by PC^{+} centers formed PC centers. This consequently gave rise to an enhancement of the PC bands. In an analogous manner to this, what we may be observing in CaF_2:Mn is the thermal release of the electrons from the trace RE^{2+} ions and their capture by $(Mn^{2+}\text{-}F)^{+}$ (an ionized (Mn^{2+}-F) complex) to form (Mn^{2+}-F) center, thus increasing the Mn-related absorption bands (viz. figure 68).

Photoluminescence

In order to understand the absorption and emission processes involved in the production of TL from Mn^{2+}-doped CaF_2, the emission properties of Mn^{2+} in CaF_2 have been extensively studied.[15] Earlier, in figure (3), we showed the 490nm emission from CaF_2:Mn (0.5%) for excitation at 390nm. This emission corresponds to a transition from the first excited $^4T_{1g}(^4G)$ level to the $^6A_{1g}(^6S)$ ground state within Mn^{2+} ions.[15,87] However, it should be mentioned that from the point of view of the point symmetry of Mn^{2+}, which is O_h and possesses eigthfold coordination with the surrounding F^- ions, the emission from these ions is normally expected in the orange-red, not green (495nm).[15] The

green emission normally corresponds to Mn^{2+} with fourfold coordination.[15]

The excitation spectrum for 490nm emission from CaF_2:Mn (0.5%) is displayed in figure (80). We have labeled the observed bands according to the assignments of these bands made by Alonso and Alcala[87] using the Tanabe-Sugano diagram of Mn^{2+} in O_h symmetry (figure 81).[87] The required crystal field (Dq) calculated by Alonso and Alcala[87] is 425cm^{-1}. The assignment of these excitation bands are in agreement with the McKeever et al[15] assignment of the absorption spectra for Mn^{2+} in CaF_2 using an Orgel diagram (figure 82). They estimated a Dq value of 420cm^{-1}.

Thermoluminescence

Earlier, we observed in figure (76) that the TL from high Mn concentration (3%) is a single, composite peak at ~280°C. This glow peak appears in the temperature range over which Mn-related absorption bands disappear.[82] We concluded earlier (Section A) that the center(s) responsible for these Mn-related absorption bands are (Mn^{2+}-F) complex(es). We now attempt to suggest our model for the production of this TL glow peak.

During ionizing irradiation electrons and holes are generated. Capturing of holes by two nearest-neighbor F^- ions forms the self-trapped hole (V_k) center (see chapter 2, section B). The V_k center is then stabilized at Mn^{2+} sites forming stable perturbed-V_k centers (the presence of stable hole centers at room temperature was already confirmed by other authors).[35-37] Recombination of the electrons wandering around in the crystal with these perturbed V_k centers forms

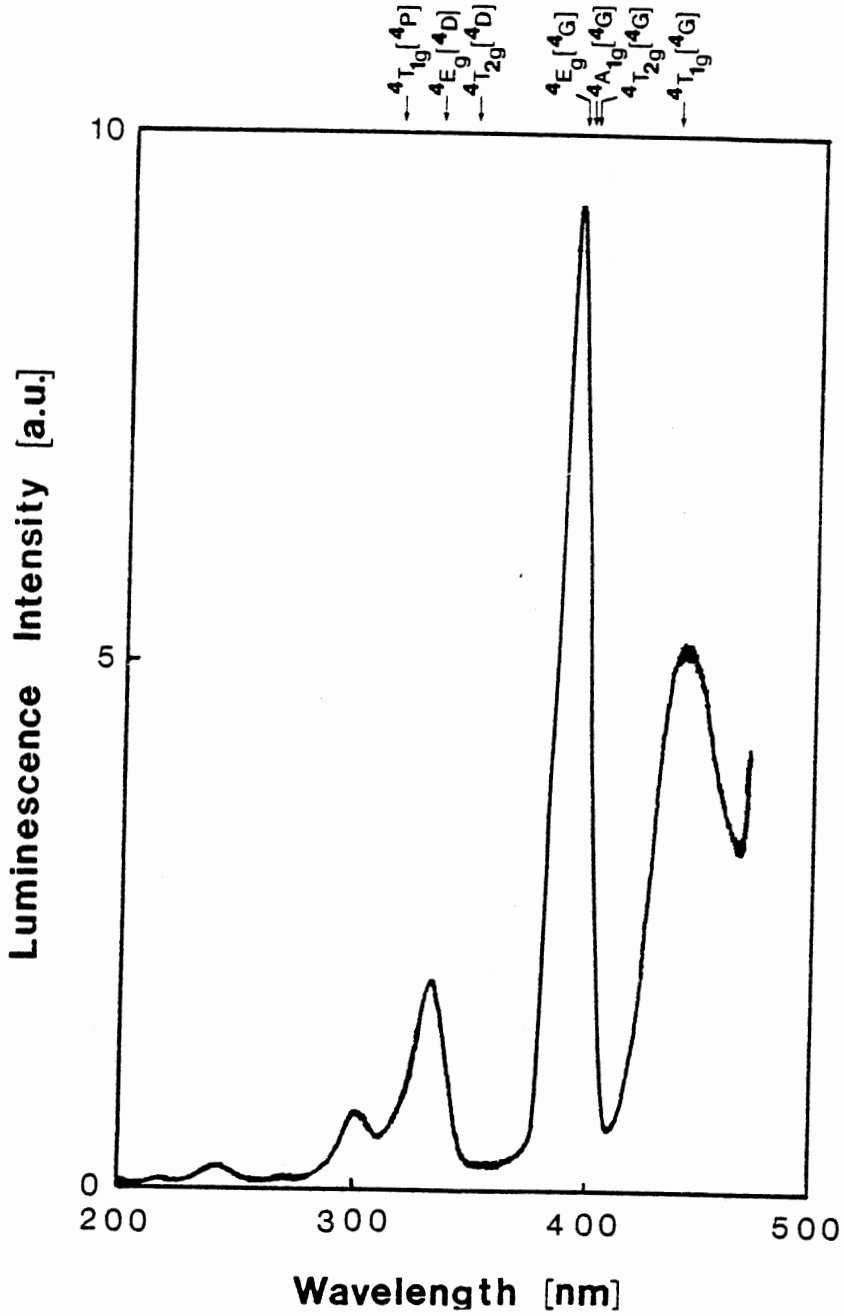

Figure 80. Excitation spectrum for the 490nm emission from CaF_2:Mn (0.5%) at room temperature. The bands are characteristic of Mn^{2+} absorption.

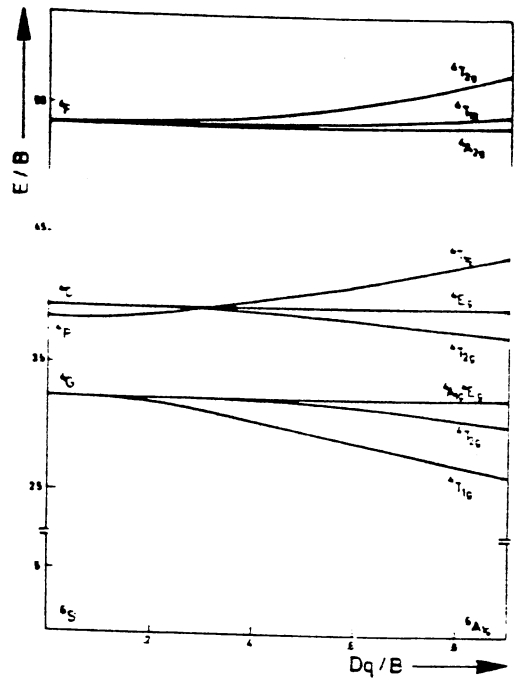

Figure 81. Tanabe-Sugano diagram for Mn^{2+} in O_h symmetry with C/B= 4.48. (After Alonso and Alcala[87]).

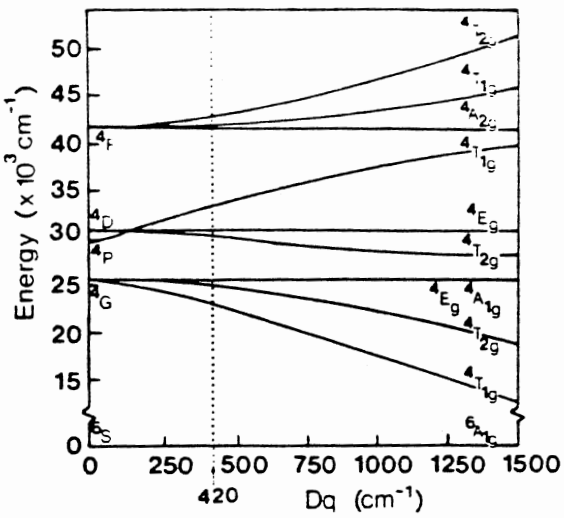

Figure 82. Orgel diagram for Mn^{2+} in CaF_2, showing the estimated value of Dq (After McKeever[15]).

self-trapped excitons, i.e. F-H pair in fluorites (see chapter 2, section B). Since the recombination occurs near Mn^{2+}, the F center and the Mn^{2+} form (Mn^{2+}-F) complex(es). Heating results in F-H pair recombination. (Such recombination mechanisms were proposed for TL production in alkali halides.)[13,77] This yields 290nm emission.[78] Absorption of this emission by Mn^{2+} ions (which possess a weak absorption band at 290nm) may then produce 490nm emission. This TL mechanism may be represented as follows:

$$\text{crystal} + \gamma\text{-ray} \rightarrow e^- + h \qquad (7.1)$$

$$2F^- + h \rightarrow V_k \qquad (7.2)$$

$$V_k + Mn^{2+} \rightarrow V_{KA}(\text{perturbed } V_k) \qquad (7.3)$$

$$V_{KA} + e^- \rightarrow (F\text{-}Mn^{2+}) + \text{H center} \xrightarrow{\text{heat}} 290\text{nm light} \qquad (7.4)$$

$$Mn^{2+} + 290\text{nm} \rightarrow Mn^{2+*} \rightarrow Mn^{2+} + 490\text{nm light (TL)}. \qquad (7.5)$$

Thus, based on this model, the TL emission (490nm) from CaF_2 doped with high Mn concentration (3%) is certainly not a result of energy transfer from rare-earth ions to Mn^{2+} ions. Thus, we believe the claim by Sunta[8] (see chapter 1) is unfounded.

Section C

Summary and Conclusions

The presence of trace rare-earth impurities influences the TL and optical absorption from CaF_2:Mn (viz. figures 70,77). This thus affects the thermal stability and sensitivity of TL from these materials. This effect was observed in the TL from CaF_2:Mn from two different batches but from the same manufacturer (figure 78). The 490nm TL light from CaF_2 doped with high Mn concentrations (3%) is certainly not a result of energy transfer from rare-earth ions to Mn^{2+} ions. Instead we

believe it was produced via reactions (7.1-7.5). From indirect experimental evidence (figure 68) and analogy with the work of other authors[4,41] on RE doped CaF_2 we conclude that the (Mn-F) complex(es) are formed in CaF_2:Mn. However, it is important to provide more-direct experimental and theoretical evidence for formation of these centers.

CHAPTER VIII

FUTURE WORK

In chapter 7 we presented indirect evidence for the formation of (Mn^{2+}-$\underline{F}$) complexes in CaF_2:Mn. The further work which may provide more direct experimental and theoretical evidence for the formation of these complexes are as follows: (A) Optical dichroism (linear and circular dichroism). The (Mn^{2+}-$\underline{F}$) complex consists of Mn^{2+} at O_h site with a nn $\underline{F}$ center along the <111>. Since this aggregate (now with C_{3v} symmetry) is made up of two defects at definite lattice sites, it can exhibit optical anisotropy. That is, optical absorption by the complex is dependent on the direction of linear polarization of the absorbing light (linear dichroism). Thus, by a study of the anisotropic absorption we can obtain information about the alignment of the complexes within the lattice and the orientation of the absorption dipoles relative to the defect axis.[39] From these, one may determine models for the center and its energy levels.[39] The application of circular dichroism provides information regarding the orbitally degenerate states.[39]

(B) Theoretical calculation of the energy level of this complex (using LCAO methods) could be used to compare with the obtained experimental data.

(C) The lifetime measurement of 495nm emission from Mn^{2+}, both before and after irradiation would tell us if the symmetry of Mn^{2+} is

altered by the F center. This provides evidence for the formation of the F centers near the Mn^{2+} ions.

BIBLIOGRAPHY

1. Kitts, E.L. and Crawford, J.H., Phys. Rev. B 9 5264 (1974).

2. Anderson, C.H., In Crystals with the Fluorite structure ed. Hayes, W. (Clarendon Press: Oxford, 1974).

3. McKeever, S.W.S., In Thermoluminescence of solids (Cambridge University Press: Cambridge, 1985).

4. Staebler, D.L. and Schnatterly, S.E., Phys. Rev. B 3 516 (1971).

5. Bangert, U., Theil, K., Ahmed, K. and Townsend, P.D., Radiat. Eff. 64 143 (1982)

6. Sunta, C.M., Radiat. Eff. 79 149 (1983).

7. Merz, J.L. and Pershan, P.S., Phys. Rev. 162 217 (1967).

8. Sunta, C.M., Radiat. Prot. Dosim., 8 25 (1984).

9. Ginther, R.J., J. Electrochem. Soc., 101 246 (1954).

10. Sen, S.C. and Bose, H.N., Z. Physik, 201 246 (1967).

11. Schulman, J.H., Proc. Symp. Sol. St. and Chem. Radiat. Dosim. Med. Biol. IAEA, Vienna, 3. (1967).

12. Alcala, R., Alonso, P.J., Lalinde, G. and Carretero, A., Phys. Stat. Sol. (b) 98 315 (1980).

13. Alonso, P.J. and Alcala, R., J. Lumin. 21 (1980).

14. Wagner, J. and Mascarenhas, S., Phys. Rev. Letts, 27 1514 (1971).

15. McKeever, S.W.S., Jassemnejad, B., Landreth, J.F., and Brown, M.D., J. Appl. Phys. 3 60 (1986).

16. Rhodes, J.F., Abbundi, R.J., Cook, D.W., Mathur, V.K. and Brown, M.D., Phys. Rev. B. 31 5393 (1985).

17. Manthey, W.J., Phys. Rev. B. 8 4086 (1973).

18. Loh, E., Phys. Rev. 154 270 (1967).

19. McKeever, S.W.S., Brown, M.D., Abbundi, R.J., Chen, H. and Mathur, V.K., J. Appl. Phys. 7 60 (1986).

20. Alig. R.C.,Kiss, Z. J., Brown, J.P. and McClure, D.S., Phys. Rev. 186 276 (1969).

21. Pooley, D., Proc. Phys. Soc. 87 245 (1966).

22. Hersh, H.N., Phys. Rev. 148 928 (1966).

23. Itoh, N., Advances in Physics 3 491 (1982).

24. Aguilo-Lopez,F., Lopez, F.L. and Jaque, F., Cryst. Latt. Def. and Amorph. Mat. 9 227 (1982).

25. Hayes, W. and Stoneham, A.M. In Defects and Defect Processes in Nonmetallic Solids (John Wiley and Sons: New York).

26. Hayes, W. and Lambourn, R.F., J. Phys. C6 11 (1973).

27. Hayes, W. and Lambourn, R.F., Phys. Stat. Sol. (6) 57 693 (1973).

28. Arends, J., Sol. St. Commun. 6 421 (1968).

29. Williams,R.J., Kabler, M.N., Hayes, W. and Stott, J.P., Phys. Rev. B. 14 725 (1976).

30. Eshita, T., Tanimura, K. and Itoh, N., Phys. Stat. Sol. (b) 122 489 (1984).

31. Adair, M.,Leung, C.H. and Song, K.S., J. Phys. C: Sol. St. Phys. 18 L909 (1985).

32. Parker, S., Song, K.S., Catlow, C.R. and Stoneham, A.M., J. Phys. 14 4009 (1981).

33. Mukerji, A., Tanton, G.A., and Williams, J.B., Phys. Stat. Sol. 22 K19 (1967).

34. Hayes, W. and Stoneham, A.M. In Crystals with the Fluorite Structure ed. Hayes, W. (Clarendon Press: Oxford, 1974) 185.

35. Hall, T.P.P., Leggeat, A. and Twidell, J.W., J. Phys. C: Sol. St. Phys. 2 1590 (1969).

36. Hall, T.P.P. and Twidell, T.W., J. Phys. C: Sol. St. Phys. 3 2352 (1970).

37. Beaumont, V.H., Hayes, W., Kirk, D.L. and Summers, G.P., Proc. Roy. Soc. Lond. A., 315 69 (1970).

38. Hayes,W.and Stoneham, A. M. In Crystals with the Fluorite Structure ed. Hayes, W. (Clarendon Press: Oxford, 1974) 239.

39. Staebler, D.L., Thesis, Princeton University (1970).

40. Hayes,W. and Staebler,D.L. In Crystals with the Fluorite

Structure, ed. Hayes, W. (Clarendon Press: Oxford, 1974).

41. Alig, R., Phys. Rev. B. 3 536 (1971).

42. Randall, J.T. and Wilkins, M.H.F., Proc. Roy. Soc. Lond., 184 366 (1945).

43. Randall, J. T. and Wilkins, M.H.F., Proc. Roy. Soc. Lond., 184 390 (1945).

44. Garlick, G.F.J. and Gibson, A.F., Proc. Phys. Soc., 60 574 (1948).

45. Cook, D.W., Gavathas, E.P. and Brown, M.D., J. Appl. Phys. 54 1165 (1983).

46. Hornyak, N.F., Levy, P.W. and Kierstead, J.A., Nucl. Tracks, 10 557 (1985).

47. Bräunlich, P. and Scharmann, A., Phys. Status Solidi 18 307 (1966).

48. McKeever, S.W.S., Rhodes, J.F., Mathur, V.K., Chen, R., Brown, M.D. and Bull, R.K., Phys. Rev. B. 32 3835 (1983).

49. Ginther, R.J. and Kirk, R.D., J. Electrochem. Soc. 104 365 (1957).

50. Steinfeld, J.I., In An Introduction to Modern Molecular Spectroscopy (MIT Press: Cambridge; London, 1985).

51. Schiff, L.I., In Quantum Mechanics (McGraw Hill Book Company, Inc: New York, 1949).

52. Curie, D., In Luminescence in Crystals (Dunod: Paris, 1960).

53. Dexter, D.L., The Journal of Chemical Physics, 21 836 (1952).

54. Föster, Th., Ann. Physik, 22 55 (1948).

55. Föster, Th., Z. Naturforschy. 49 321 (1949).

56. Leach, R., J. Electrochem. Soc. 105 27 (1958).

57. McKeever, S.W.S., Jassemnejad, B., Brown, M.D., Mathur, V.K., Abbundi, R.J. and Chen, H., Radiat. Eff. 99 15 (1986).

58. Bucci, C. and Fieschi, R., Phys. Rev. Lett. 12 16 (1964).

59. Vanderscheren, J. and Gasiot, J., In Thermally Stimulated Relaxation in Solids, ed. Braunlich, P. (Springer-Verlag: New York, 1979).

60. Weperen, W., Lenting, B.P.M., Bijvansk, E.J. and Den Hartog,

H.W., Phys. Rev. B. 16 2953 (1977).

61. Den Hartog, H.W., J. de Physique. C6 275 (1980).

62. Van Weperen,W. and Den Hartog,H.W., Phys. Rev. B. 18 2857 (1978).

63. Laredo, E., Puma, M., Suarez, N. and Figueroa, D.R., Phys. Rev. B. 23 3009 (1981).

64. Den Hartog, H.W. and Nauta. Letters, Z.C., Phys. Rev. B 14 4162 (1979).

65. Wagner, J. and Mascarenhas, S., Phys. Rev. B. 6 4867 (1972).

66. Royce, B.S.H. and Mascarenhas, S., Phys. Rev. Let. 24 98 (1970).

67. Campos, V.B., Leal Ferreira, G.F., J. Phys. Chem. Solids 35 905 (1974).

68. Andeen, C.G., Fontanella, J.J., Wintersgill, M.C., Welcher, P.J. Kimble, R.J. and Matthews,G.E., J. Phys. C: Sol. St. Phys. 14 3557 (1981).

69. Wintersgill,M.C., Fontanella, J.J., Welcher, P., Kimber, R.J. and Andeen, C.G., J. Phys. C: Sol. St. Phys. 13 L661 (1980).

70. Capelletti, R., Okuno, E., Matthews, G.E., Crawford, J.H., Phys. Stat. Sol. 47 617 (1978).

71. Andeen,C., Matthews, G.E., Smith, M.K., Fontanella, J., Phys. Rev. B. 19 5293 (1979).

72. Capelletti, R., Radiat. Eff. 74 119 (1983).

73. Barrow,G.M., In Physical Chemistry (McGraw Hill: New York, 1961).

74. Dorenbos, P. and Hartog, H.W., Phys. Rev. B., 31 3932 (1985).

75. Staebler, D.L.and Schnatterly, S.E., Phys. Rev. B. 3 516, (1971).

76. Hayes, W. and Twidell, J.W., J. Chem. Phys. 35 1521 (1961).

77. Alvarez, R.J.L., J. Physique 41 353 (1980).

78. Williams, R.T., Kabler, M.N., Hayes, W. and Stott, J.P., Phys. Rev. B. 14 725 (1976).

79. McKeever, S.W.S. and Halliburton,L. E.,In Report # NSWC/1 prepared under contract number N60921-84-M-2714 for the N.S.W.C. (1985).

80. McKeever, S.W.S., unpublished (1986).

81. McClure, D.S. and Kiss, Z.J., J. Chem. Phys., 39 3251 (1963).

82. McKeever, S.W.S., in Report # NSWC/3 prepared under contract number N60921-85-M-7416 for the N.S.W.C. (1986).

83. Sardar, D.K., Shinn, M.D. and Sibley, W.A., Phys. Rev. B. 26 2382 (1982).

84. Yun, S.I., Kappers, L.A. and Sibley, W.A., Phys. Rev. B. 8 773 (1973).

85. Sibley, W.A. and Koumvakalis, N., Phys. Rev. B. 14 35 (1976).

86. Lee, K.H. and Sibley, W.A., Phys. Rev. B. 12 3392 (1975).

87. Alonso, P.J. and Alcala, R., J. Lumin. 22 321 (1981).

VITA

Bahaeddin Jassemnejad

Candidate for the Degree of

Doctor of Philosophy

Thesis: THERMOLUMINESCENCE PROCESSES IN CaF_2 DOPED WITH Ce AND Mn.

Major Field: Physics

Biographical:

Personal Data: Born at Sanandaj, Iran, May 10, 1958, the son of Muhammed A. Jassemnejad and Kobra Sarmary.

Education: Graduated from Hashtroody High School in 1976; received Bachelor of Science degree in Computer Science/ Mathematics (May, 1981) and Master of Science degree in Industrial and Applied Physics (Jan, 1984) from Central State University, Edmond, Oklahoma; completed the requirements for the degree of Doctor of Philosophy at Oklahoma State University, Stillwater, Oklahoma in May, 1987.

Professional Experience: Graduate Teaching Assistant, Central State University, May, 1981 to Jan., 1984. Graduate Teaching Assistant, Oklahoma State University, Jan., 1984 to Summer, 1985. Graduate Research Assistant, Oklahoma State University, Summer, 1985 to present. Member of the American Physical Society.